WIMPs and sterile neutrinos as dark matter

Master's Thesis of

Carlos Fabian Jaramillo Gracia

at the Department of Physics,
Institute for Nuclear Physics
and
Max-Planck-Institute for Nuclear Physics (Heidelberg)

Reviewer:	Prof. Dr. T. Schwetz-Mangold
Second reviewer:	Prof. Dr. Dr. h.c. M. Lindner
Advisor:	Dr. Werner Rodejohann

08. January 2018 – 08. March 2019

Karlsruher Institut für Technologie
Fakultät für Physik
Postfach 6980
76128 Karlsruhe

Ich versichere wahrheitsgemäß, die vorliegende Arbeit selbstständig verfasst, alle benutzten Hilfsmittel vollständig und genau angegeben und alles kenntlich gemacht zu haben, was aus Arbeiten anderer unverändert oder mit Abänderungen entnommen wurde sowie die Satzung des KIT zur Sicherung guter wissenschaftlicher Praxis in der jeweils gültigen Fassung beachtet zu haben.

I declare that I have developed and written the enclosed thesis completely by myself, and have not used sources or means without declaration in the text.

.....

(Carlos Fabian Jaramillo Gracia)

Heidelberg, 08.03.2019

Abstract

This thesis deals with some aspects concerning the fascinating nature of the dark matter of the Universe. After an overview of the solid body of observational evidence in favour of the existence of dark matter, both from astrophysical and cosmological sources, we concentrate our attention on two of the most prominent dark matter particle candidates: the generic *Weakly Interacting Massive Particle* (WIMP) and the sterile neutrino. We study the most common production mechanism of WIMPs in the early Universe (freeze-out from thermal equilibrium), and derive carefully the analytical solution to the Boltzmann equation, mentioning every approximation and assumption along the way.

We then motivate the sterile neutrino as a dark matter candidate by elaborating on the observation of neutrino oscillations and the problem of generating neutrino masses in the Standard Model. The most prominent production mechanisms of sterile neutrino dark matter and their experimental constrains are discussed.

Finally, we show that within the minimal seesaw type I model, the introduction of a varying neutrino Yukawa coupling opens the possibility of producing sterile neutrinos by freeze-out from thermal equilibrium in the early Universe. Until now, this has been ruled out due to the stringent bounds on the active-sterile neutrino mixing angle. Furthermore, we show that there is a thin region in the parameter space in which the resulting relic abundance can account for 100% or a fraction of the observed dark matter density. This possibility is open at all masses investigated, i.e. $1\,\mathrm{GeV} \sim 10^5\,\mathrm{GeV}$, but potentially even further.

Zusammenfassung

Diese Arbeit befasst sich mit einigen theoretischen Aspekten über die Natur der Dunklen Materie im Universum. Nach einem Überblick über die vielfältigen und unabhängigen Evidenzen astrophysikalischen sowie kosmologischen Ursprungs, die für die Existenz von Dunkler Materie sprechen, konzentrieren wir uns auf zwei der beliebtesten Kandidaten zu Dunklen Materie Teilchen: das *schwach wechselwirkende massive Teilchen*, kurz WIMP, und das sterile Neutrino. Wir diskutieren den gängigen Produktionsmechanismus von WIMPs - das Ausfrieren vom thermischen Gleichgewicht - und leiten die analytische Lösung der entsprechenden Boltzmann Gleichung her. Dabei sprechen wir jede Näherung und Annahme an.

Um das sterile Neutrino als Dunkle Materie Teilchen zu motivieren, gehen wir auf das Phänomen von Neutrino Oszillationen und das Problem der Neutrino Massen ein. Die wichtigsten Produktionsmechanismen steriler Neutrinos werden ebenso diskutiert, wie ihre experimentellen Einschränkungen.

Zum Schluss zeigen wir, dass durch die Einführung einer variablen Yukawa Kopplung in dem einfachsten Seesaw Model erster Art, die Produktion von sterilen Neutrinos durch Ausfrieren aus dem thermischen Gleichgewicht im frühen Universum erfolgen kann. Dieser Mechanismus war bislang für sterile Neutrinos ausgeschlossen, und zwar aufgrund der strengen Einschränkungen auf den Mischungswinkel für aktive-sterile-Neutrino Oszillationen. Weiterhin wird gezeigt, dass innerhalb eines schmalen Bandes, das sich über den kompletten Parameterraum ausbreitet, die durch thermisches Ausfrieren erzeugte Energiedichte mit der beobachteten Energiedichte der Dunklen Materie im Einklang ist. Dies bedeutet, dass die so produzierten sterilen Neutrinos als Dunkle Materie Kandidaten gut geeignet sind.

Contents

1. Introduction

Since the Copernican revolution, physics has been all about the quest for answers to the most profund questions one can formulate. Questions like "What is everything in the Universe made of?" or "Why is there anything instead of nothing?" have lead physicists to truly fascinating insights about the inner workings of Nature at the most fundamental level. With the Standard Model of particle physics, the theory General Relativity and the Standard Model of Cosmology, we have come a long way to unfolding the secrets of the Universe. It is truly remarkable that our cognitive capabilities, the scientific method, and the mathematical language have allowed us to come this far. And yet, both questions mentioned above remain without answer.

Most of the people my age or older learned in science class at school about atoms and their constituent - subatomic - particles, the electron, the proton and the neutron. We were taught about the different chemical elements and molecules, and were told that everything we know to exist is made of these objects. Today, we know that this is not true.

Since the studies on the dynamics of galaxy clusters by the Swiss astronomer Fritz Zwicky [1, 2], it has been known that the interstellar space is filled with a mysterious, massive substance, which does not interact electromagnetically with ordinary matter. Zwicky dubbed this substance *dark matter*. The discovery [3, 4] and study [5, 6] of the Cosmic Microwave Background radiation (CMB) has convincingly led us to the conclusion that only a small fraction of about 5% of the content of the Universe consists of atoms. The vast majority of it is in the form of the so-called *dark energy* (which we know nothing about, but is probably related to the accelerated expansion of the Universe) and dark matter (which we know very little about). Thus, in relation to that which we do not understand, our achievements in the field of fundamental physics seem a bit more modest. Nevertheless, extraordinary efforts are being undertaken in the search for answers to these questions. The construction of the Large Hadron Collider at CERN, which has been labeled the largest and most complex machine ever built by mankind [7], has the sole purpose of investigating the fundamental interactions of matter at energies similar to those in the early universe in order to shed light on the most profund mysteries in physics. The discovery of the Higgs boson [8, 9] was a huge milestone, but the nature of dark energy and dark matter, and the origin of the neutrino masses and the matter-antimatter asymmetry of the Universe remain unanswered. Many other international collaborations are also working hard on the resolutions of these problems, e.g. the *XENON dark matter project* which uses cutting edge technology and 3.5 tons of liquid xenon to search for dark matter particles and currently sets world-leading constrains on its parameter space [10], or the *LIGO scientific collaboration*, which has for the first time detected gravitational waves [11], just to name a few.

Today, the nature of dark matter is one of the most fascinating, open problems in physics and drives the imagination of many of the most talented and brilliant theoreticians, who formulate mathematical models to explain the observations, and experimentalists, who build experiments with impressive technology and unprecedented precision to actually detect dark matter particles. Since the 1930s multiple independent astrophysical and cosmological observations point to the existence of electrically neutral and almost decoupled matter in the Cosmos, that interacts gravitationally with the ordinary matter in the Cosmos. Discovering what exactly the dark matter is, and which role it plays in cosmology and particle physics, is crucial to our understanding of the history and fate of the Universe. This thesis hopes to make a modest contribution to this quest.

In the course of this work, we will review two of the most popular and promising dark matter candidates: the Weakly Interacting Massive Particle (WIMP) and the sterile neutrino, which could also be involved in the solution to other problems in the frontier of physics. Inspired by the WIMP and by solutions to the problems of baryogenesis and neutrino masses, we propose to adapt the most common production mechanism of WIMP dark matter (thermal freeze-out) to sterile neutrino dark matter. We will see that this newly adapted, old concept is capable of producing the correct amount of sterile neutrinos for them to be a suitable dark matter candidate.

2. Evidence for dark matter

The presence of dark matter in the cosmos was first proposed in 1933 by the Swiss astrophysicist Fritz Zwicky, who is the father of the term “dark matter" [2]. The evidence comes from the analysis of the dynamics of galaxies and clusters, observations of gravitational lensing effects (particularly weak lensing), our models of structure formation in the Universe, the analysis of the Cosmic Microwave Background radiation (CMB), and the analysis of the large-scale structures. One peculiar piece of evidence (which will be discussed later in this chapter) is the Bullet cluster (cluster 1E 0657-558), which is actually a pair of colliding clusters that display a mismatch between the distribution of hot intergalactic gas and the gravitational potential. This behaviour can be best explained by the presence of dissipationless dark matter [12]. Modified theories of gravity, which aim to explain these observations without invoking dark matter, have difficulty addressing all arguments simultaneously [13, 14].

In this introductory chapter, the most important pieces of evidence for dark matter will be briefly discussed: the dynamics of galaxies and clusters, observations of gravitational lensing effects, arguments from cosmic structure formation and the analysis of the anisotropies of the CMB.

2.1. Evidence from the dynamics of galaxies and clusters

For a gravitationally bound many particle system, the virial theorem relates the mean kinetic energy of the particles $\langle T \rangle$ to their mean gravitational potential energy $\langle U \rangle$ as follows:

$$\langle T \rangle = \frac{1}{2} \langle U \rangle.$$

In a galaxy cluster, the velocities of galaxies can be calculated by measuring their redshift and, prior to the postulation of dark matter, the mass of a cluster could be estimated simply by observing the amount of visible matter. When F. Zwicky was studying the dynamics of the Coma cluster in 1933 as a virialized system, he noticed that the kinetic energy of the galaxies within the cluster was much larger than expected by the virial theorem [1]. Unless there was additional, invisible matter in large amounts in the cluster, it would be unstable, expand, and eventually blow apart. Zwicky estimated that the amount of invisible matter in the cluster, which he then called *dark matter*, should be about 10 times larger than the amount of common matter. Later studies confirmed the problem of missing mass in other clusters [15]. This was the first hint for the existence of large amounts of non-baryonic matter in the Universe.

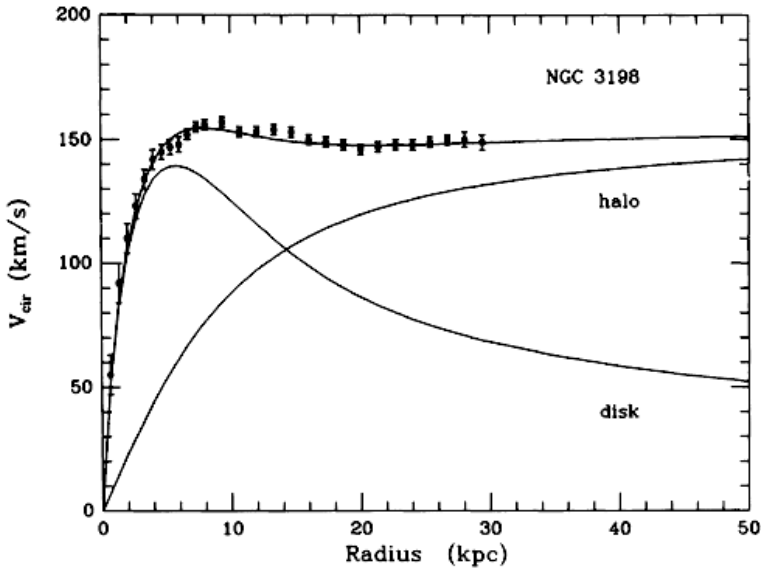

Figure 2.1.: Rotation curve of the Andromeda galaxy. Figure from [17].

The dynamics of spiral and elliptical galaxies delivered additional hints for the presence of dark matter. By measuring the Doppler shift of the 21-cm Hydrogen line from different regions of a galaxy, one can compute the rotational velocity of the stars in the galaxy as a function of their distance to the galactic center. This is the so called *rotation curve*. By Kepler's third law, at large distances from the galactic center, the rotation velocity should fall off as $v \propto 1/\sqrt{r}$. However, this is not what was observed [15]; instead, observations of multiple galaxies showed that v stays constant even at very large distances. This behaviour is easily explained, if galaxies are embedded in much larger halos of dark matter, thus extending the mass distribution far beyond the visible galactic disc [16].

2.2. Evidence from gravitational lensing effects

From Einstein's theory of general relativity, we know that, in the presence of a mass distribution, the space around it will be curved as described by Einstein's equations. We also know that light always travels through space along (null-)geodesics, which in Euclidian space are just straight lines. As a consequence, if light traveling from a source to an observer goes through the vicinity of a mass distribution, where space is deformed, the observer will receive a distorted image. This effect (which manifests itself with different strengths depending on the size of the mass distribution) was actually used by astronomer Arthur Eddington in 1919 during a solar eclipse to prove the validity of Einstein's theory by measuring the apparent displacement of stars behind the sun [18]. The most spectacular form of gravitational lensing is called *strong lensing* and is generated by extremely massive clusters and galaxies producing ring-images, multiple images, or clearly distorted images of background objects which are favourably aligned along the line of sight.

Figure 2.2.: Strong gravitational lensing. Right: Einstein ring induced by luminous red galaxy LRG 3-757. Left: galaxy cluster CL0024+1654. Images by: ESA/Hubble & NASA, H. Lee & H. Ford (Johns Hopkins U.).

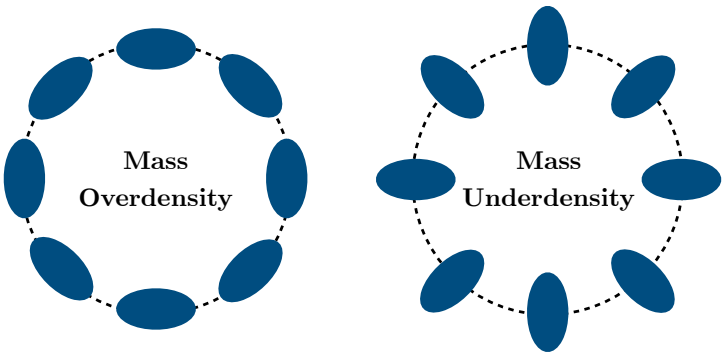

Figure 2.3.: Diagrammatic depiction of the weak gravitational lensing effect of the images of galaxies induced by a region of mass overdensity (left) and mass underdensity (right).

Using strong gravitational lensing, it has been possible to confirm the results from the virial theorem (which use X-ray data to estimate the amoung of luminous mass in a cluster) that baryonic matter amounts to only a portion of the total mass of a galaxy cluster [15].

Perhaps more importantly, the analysis of weak gravitational lensing allows us to reconstruct the mass distribution in some regions of the Universe. The effect of weak gravitational lensing is not immediately visible in optical telescope images, like strong gravitational lensing, which produces clear rings and arcs (see Figure 2.2). This only occurs when very large mass distributions are at the right distance and perfectly aligned with a background galaxy and the observer. However, most of the time the mass distribution acting as a lens is not so densely concentrated and the background galaxies are neither perfectly aligned nor at the correct distance to produce strong lensing effects. Nevertheless, the light from distant galaxies can still be modestly affected when propagating through a gravitational field. This is effect

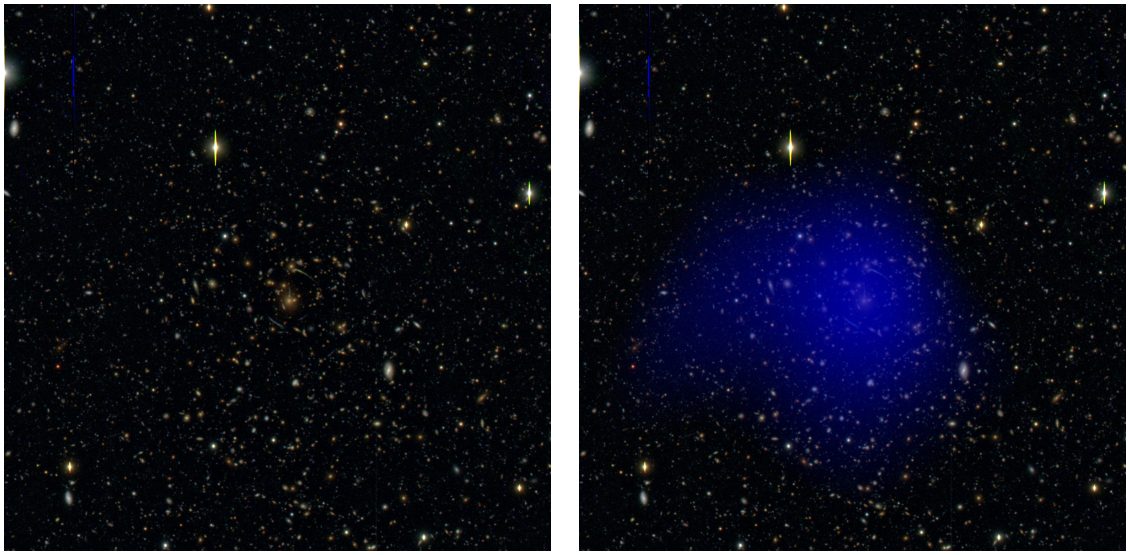

Figure 2.4.: Weak gravitational lensing. Right: Optical image of Cluster $SDSSJ1050 + 0017$. Left: The same cluster superposed with the dark matter mass distribution, shown as a transparent blue cloud [20].

of weak gravitational lensing, which is more subtle than strong lensing. The result is that the images of background galaxies get slightly distorted and elongated when traveling through over- or under dense regions, as shown in Figure 2.3.

By applying sophisticated statistical analysis tools on optical images, weak gravitational lensing allows not only a mapping of the dark matter distribution, but also a good estimate for the amount of dark matter on a wide range of physical scales [19]. This adds to the evidence from dynamical analysis for the existence of dark matter in the Universe and that it is roughly four to five times more common than baryonic matter[1]. An example for the mapping of the dark matter distribution in a galaxy cluster by analysing weak gravitational lensing effects can be seen in Figure 2.4.

A further remarkable piece of evidence for dark matter comes from the combined analysis of weak gravitational lensing and X-ray emission from the Bullet cluster, Figure 2.5. The analysis of weak gravitational lensing allows the mapping of the dark matter distribution in the cluster while the observation of X-rays allows the mapping of the distribution of baryonic matter. The measurements show that the distributions of baryonic and dark matter are displaced with respect to each other in a very peculiar manner. The explanation for this configuration is that the Bullet cluster is actually a pair of clusters that have experienced a head-on collision. During the collision, the huge clouds of interstellar gas from both clusters (which account for most of the baryonic mass of the clusters) are heated up by friction to the point of radiating X-rays. However, the dark matter, which is responsible for the bulk of the gravitational potential, just goes its way through undisturbed without experiencing any friction.

[1]Originally, it was estimated that dark matter was roughly ten times more abundant in clusters than ordinary matter; this overestimation was caused by large uncertainties in astronomical observations.

Figure 2.5.: The Bullet cluster. X-ray emission is shown in red while the bulk of the gravitational potential, as reconstructed by weak gravitational lensing, is shown in blue. Image credit: X-ray: NASA/CXC/CfA/M.Markevitch et al.; Optical: NASA/STScI; Magellan/U.Arizona/D.Clowe et al.; Lensing Map: NASA/STScI; ESO WFI; Magellan/U.Arizona/D.Clowe et al.

The original reference publishing these findings is [12]. Today, after comparing the observations from the Bullet cluster with realistic simulations of cluster mergers that take into account the influence of magnetic fields and plasma cooling, most experts agree that dark matter is the best explanation for the misalignment between the X-ray emitting matter and the gravitational potential.

2.3. Evidence from structure formation

Dark matter is also necessary to explain the way structures in the Universe have formed starting from primordial density fluctuations right after the big bang [21]. The generally accepted picture is that directly after the big bang, quantum fluctuations were dramatically expanded by the process of cosmic inflation, during which the Universe grew exponentially in size by many orders of magnitude. This allowed the initial quantum fluctuations to turn into real (mass-)density fluctuations and grow by gravitational attraction depending on their size.

Let us assume for a moment that 100% of the matter content of the Universe were composed of common baryonic matter and consider a (not too large) density fluctuation. Baryonic matter couples strongly to radiation, which was the dominating component of the Universe until the time of matter-radiation-equality, roughly 50 000 years after the big bang. During this epoch, gravity pulls more and more matter to-

gether, allowing the fluctuation to grow. Photons are also pulled in by their coupling to baryons, which increases the radiation pressure in the fluctuation. At some point the radiation pressure overcomes the gravitational attraction and drives the density fluctuation apart until it is so diluted that the radiation pressure no longer dominates. Then, the density fluctuation can start to grow again. This process of growth (by gravitational attraction) and expansion/dilution (by radiation pressure) is called *acoustic oscillation*, and is responsible for the damping of matter density fluctuations of a size smaller than a characteristic size scale called the *Jeans length* λ_{J}. The Jeans length is a measure for the distance an acoustic wave would travel through a cloud of matter in the time available before the cloud (i.e. the density fluctuation) collapses on itself because of its own gravitational pull. During the radiation-dominated epoch, the Jeans length almost coincides with the causal horizon. This implies that during this epoch, all causally connected density fluctuations would undergo oscillations and their growth would be impeded. This continues until the coupling between baryons and photons, which generates radiation pressure in the fluctuations, was *broken* when the cosmic plasma became nuetral in an event called *recombination* [22, 21]. Recombination occurred when the temperature of the Universe had dropped enough that protons could bind electrons to form (neutral) hydrogen atoms without being immediately reionized by high energy photons (see also section 2.5). This occurred when the Universe was about 380 000 years old and its temperature was about $T \sim 0.39\,\mathrm{eV}$ [5]. After recombination, the matter in the Universe is neutral and thus no longer coupled to photons; therefore, the density fluctuations are also no longer subject to radiation pressure and there is nothing to prevent their gravitational growth.

Let us estimate the evolution of a density fluctuation from the earliest time at which it can begin to grow, the time of recombination, to more recent times. The dynamics of the Universe are governed by the *Friedmann equation* [22], which relates the expansion rate of the Universe to its content and geometry; it reads

$$H^2 = \frac{8\pi}{3} G\,\rho - \frac{k}{a^2}, \tag{2.1}$$

where a is the scale factor (i.e. a measure for the size of the Universe), H is called *the Hubble rate* and gives the expansion rate of the Universe - it is defined as $H = \dot{a}/a$ -, G is Newtons gravitational constant, ρ is the energy density of the Universe (which can be in the form of matter, radiation, or vacuum energy) and k stands for the curvature of the Universe - it can have values $k = -1, 0, 1$ for an open-, flat- and closed-curvature geometry respectively. Current measurements suggest that $k = 0$ [5]. For our example, let us assume that these measurements are correct and the Universe is flat at very large scales and its energy content is 100% in the form of conventional matter. Then the Friedmann equation reads

$$H^2 - \frac{8}{3}\pi G\rho = -\frac{k}{a^2} = 0. \tag{2.2}$$

In a small overdense region of the Universe, the expansion rate stays the same, but the matter density ρ' and the curvature k are different. Thus we would have

$$H^2 - \frac{8}{3}\pi G\rho' = -\frac{k}{a^2}. \tag{2.3}$$

Subtracting both of these equations and diving by the average density ρ, we get the following definition for a density fluctuation:

$$\delta \equiv \frac{\rho' - \rho}{\rho} = \frac{3k}{8\pi G a^2 \rho}. \tag{2.4}$$

In cosmology, a measurable proxy for the scale factor a (but also for the age and temperature of the Universe) is the so-called redshift factor z, which is defined as $1 + z = a_{\text{today}}/a(t)$ (so the redshift z of very recent events is very small, while events that took place in the early Universe have very large values of z). Since in the matter dominated epoch, the density evolves as $\rho \sim a^{-3}$, and $a \sim (1+z)^{-1}$, this implies

$$\delta \sim a \sim \frac{1}{1+z}. \tag{2.5}$$

Now we can build the ratio of δ at the time of recombination, for which the redshift factor had a value of $z_{\text{rec}} \approx 1000$ [22], to δ at a much more recent redshift, e.g. $z = 5$. We know from the analysis of the CMB, that the density fluctuations at the time of the recombination were of scale of 10^{-5} [5]. Therefore, we estimate

$$\delta(z=5) = \delta_{\text{rec}} \frac{1+z_{\text{rec}}}{1+z|_{=5}} = 10^{-5} \frac{1+1100}{1+5} \approx 0.002. \tag{2.6}$$

However, this is at least two orders of magnitude smaller than what we observe [23] (today we have $\delta \gg 1$). The solution to this problem is delivered by dark matter! Because dark matter does not interact electromagnetically, it does not couple to photons. Therefore, it is immune to the radiation pressure that counteracts gravity and prevents the baryon density fluctuations from growing. Dark matter can fall into the primordial density fluctuations and begin to grow already at the time of matter-radiation equality, more than 300 000 years before recombination. This means that if the Universe contains sufficient amounts of dark matter, it would have plenty of time to built deep gravitational potential wells on top of the primordial density fluctuations, where the baryons will quickly cluster as soon as recombination is over. As one can see in Figure 2.6, dark matter offers the most compelling explanation to the question of how the structures of the Universe have grown to the scale we observe today [21]. Modified theories of gravity, e.g. the TeVeS-theory [24], fail at the attempt to reproduce the density fluctuation power spectrum [16].

2.4. Evidence from the large scale structures in the Universe

In the decades since the 1980's, remarkable theoretical and observational progress on the matter of *large-scale structures* in the Universe has been made [27]. Today, galaxy redshift surveys have mapped the galaxy distribution over larges portions of the sky and revealed a distinctive structure on the largest scales; walls and filaments made of galaxies and galaxy clusters span all over the Universe together with huge voids [28]. According to our current understanding, these structures are the product of

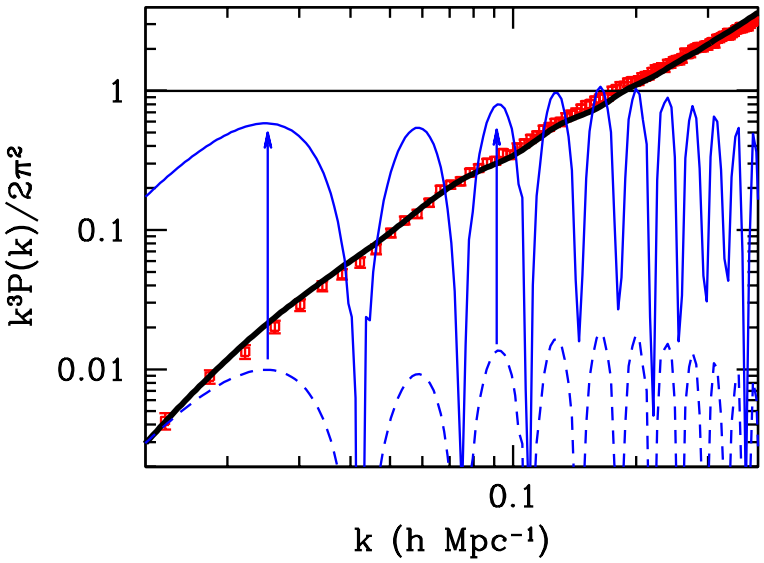

Figure 2.6.: Figure taken from [25]. The plot shows the power spectrum of density fluctuations as a function of the inverse size of the density fluctuations. The red points are real measurements taken by SDSS [26], the dashed blue line is the prediction in a baryonic-matter-only Universe, the solid oscillating blue line is the prediction of a relativistic theory of modified gravity [24], which actually reaches the non-linear amplitude of $k^3P(k) \sim 1$ but still displays the wrong behaviour. In contrast to that, the solid black line, which corresponds to the ΛCDM model (which includes cold dark matter and dark energy) matches the observations remarkably well.

primordial quantum fluctuations which, after inflation, were populated by the infall of dark matter (see section 2.3).

The careful analysis of the results of galaxy surveys like the 2dF and the *Sloan Digital Sky Survey* (SDSS) also allows the fitting of the cosmological model and the extraction of model parameters. Both 2dF and SDSS conclude that [28]

$$\Omega_\mathrm{M} \neq \Omega_\mathrm{b},$$

and the 2001 results from 2dF [29] give us

$$\Omega_\mathrm{M} h = 0.2 \pm 0.03, \qquad \frac{\Omega_\mathrm{b}}{\Omega_\mathrm{M}} = 0.15 \pm 0.07 \tag{2.7}$$

with 1 σ error bars. Here, h is defined by the Hubble rate as $H = 100\,h\,\mathrm{km\,s^{-1}Mpc^{-1}}$. This implies $\Omega_\mathrm{b} \approx 4.3$, which is in excellent agreement with the predictions from *Big Bang nucleosynthesis* (BBN) [22].

Nowadays it is possible no run very large and complex simulations of the evolution of the Universe to test different cosmological models. The so called *Millennium Simulation* by the *Virgo consortium* received much attention. The millennium simulation, which is based on the standard model of cosmology (ΛCDM), computes the evolution

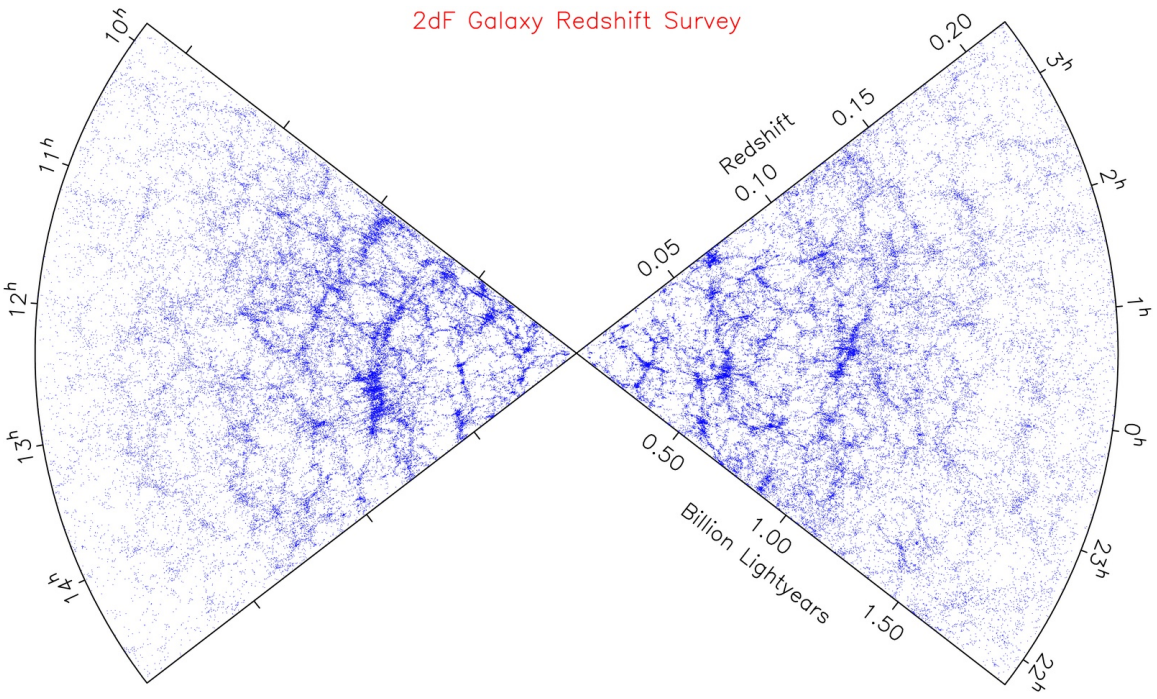

Figure 2.7.: The z cone of distribution of galaxies by the 2dF redshift galaxy survey. Image from [28].

of the Universe taking into account the contributions to its content from dark energy and cold dark matter[2]. The results show astonishing resemblance with the galaxy distributions obtained from redshift surveys, see [30].

2.5. Evidence from the cosmic microwave background radiation

The cosmic microwave background (CMB) is an invaluable source of information about the early history of the Universe. Its existence was first predicted in 1948 by Gamow, Alpher and Herman [31, 3]. They understood that, after big bang nucleosynthesis (which is also based on early work by Gamow and Alpher [32, 33]), the Universe primarily consisted of a thermal bath of atomic nuclei, free electrons, and photons. During this time the photons were coupled to the rest of the plasma by frequent scattering processes. However, as the Universe expanded, it cooled down, such that at some point the temperature was low enough for the nuclei to capture electrons without being reionized by high energy photons. This event is called *recombination* and it marks the moment in the history of the Universe, where it became electrically neutral and transparent to photons. From this point on, the photons

[2]The largest simulations ignore the contributions from baryonic matter and radiation because taking those into account would require immense amounts of additional computational power.

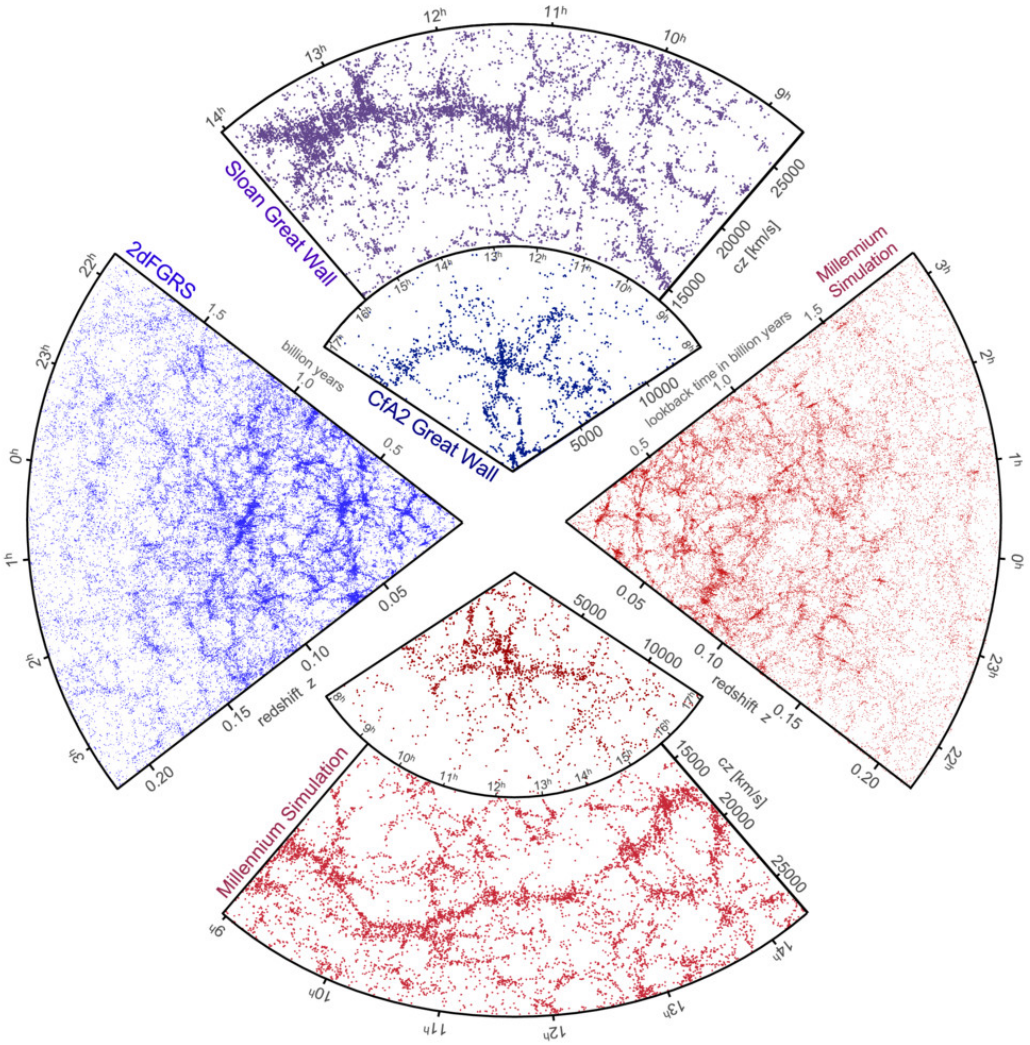

Figure 2.8.: Comparison of the galaxy distribution between 2dF/SDSS (in blue) and the Millennium simulations (in red). Even peculiar features, like filaments and voids are reproduced. Image: [30].

of the big bang are propagating (mostly) freely and can be detected today as the photons of the CMB. Since right up to the moment of recombination the plasma was in thermal equilibrium, the later expansion of the Universe conserves the thermal form of the spectrum while only redshifting its temperature. Alpher and Herman first predicted an energy spectrum with $T = 5\,\mathrm{K}$ [3], while modern measurements reveal that $T = 2.275\,\mathrm{K}$ [5], and its matching of the thermal Planck distribution is truly remarkable. One may safely say that the Universe itself is a perfect black-body radiator. It was also revealed that the CMB radiation is isotropic and homogeneous, i.e. the Universe has the same temperature everywhere and in all observing directions.

The first satellite to measure the CMB with high precision was *COBE* (Cosmic Background explorer), launched in 1989. It demonstrated that the CMB is isotropic up to $\delta T/T \sim 10^{-5}$. Beyond that, the CMB is anisotropic and a sophisticated analysis

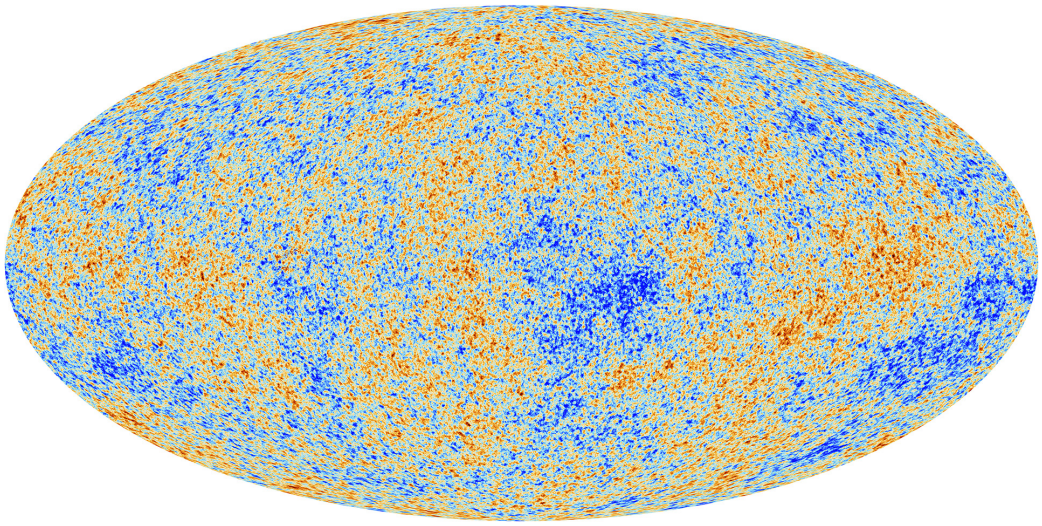

Figure 2.9.: A full-sky map of the anisotropies of the CMB as measured by the Planck satellite. Image credit: ESA, Planck Collaboration, `http://sci.esa.int/jump.cfm?oid=51553`

of the anisotropies reveals a large amount of very precise information about the early Universe.

After measuring the full-sky map of the CMB (see Figure 2.9), the analysis requires to expand the anisotropies into spherical harmonics and compute correlation functions. The result is a power spectrum of temperature fluctuations, which depends sensitively on the parameters of the cosmological model. The latest plot of the CMB power spectrum, from the 2018 results released by the Planck collaboration, can be seen on Figure 2.10. From the data, one can fit a cosmological model and extract the model parameters. The position of the first peak and the amplitude of all peaks depends crucially on the total matter density Ω_{M}. At the same time, the ratio of the amplitudes of the even to the odd peaks is highly sensitive to the density of baryonic matter Ω_{b}. The best fit results are [6]

$$\begin{aligned} \Omega_{\mathrm{M}}\, h^2 &= 0.022383 \\ \Omega_{\mathrm{b}}\, h^2 &= 0.14314 \end{aligned}$$

which clearly shows that there is more matter than just baryonic matter.

As we have seen, the evidence for the existence of dark matter is very solid; it comes from different and independent astrophysical and cosmological observations and is consistent. That there is something out there worthy of the name *dark matter* is not controversial. Nevertheless, the nature of this strange but vital substance still eludes us. In the remainder of this work, we will investigate some of the most prominent candidates to solve the mystery.

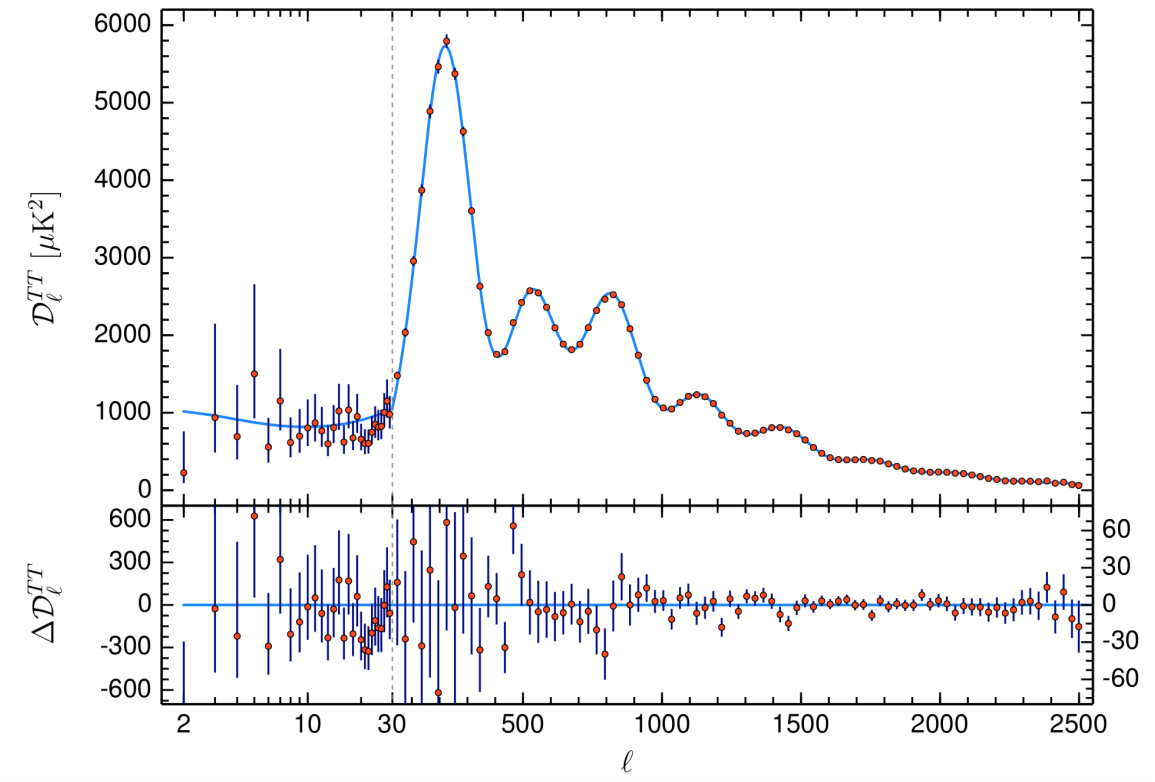

Figure 2.10.: The temperature power spectrum of the CMB as measured by the Planck mission. [6]

3. WIMP Dark Matter

One of the most prominent candidates for particle dark matter is the *Weakly Interacting Massive Particle*, or WIMP, for short. This candidate is a generic massive particle that aside from interacting gravitationally is only weakly coupled to the standard model (SM) [34]. When physicist first theoretized the WIMP, they thought of a particle that actually featured an interaction with the SM of the same strength as the SM-weak interaction [35]. This was because the assumption of a massive particle with a thermal relic abundance and an interaction cross section of the size of the SM-weak interaction would naturally yield the right order of magnitude for the relic abundance. This coincidence was called *The WIMP Miracle*. Today, the "weakly interacting" part of the name is taken more generally, i.e. it refers to interactions of a strength equal to, or smaller than the $SU(2)$ interactions of the SM.

In this Chapter we will introduce the WIMP paradigm and go a bit beyond it.

3.1. Thermal equilibrium and the Boltzmann equation

What keeps a particle species in equilibrium with a thermal bath? Thermal equilibrium is established and maintained by particle reactions between the species in question and the particles of the plasma. The rate with which these reactions take place is

$$\Gamma = \langle \sigma v \rangle \cdot n, \tag{3.1}$$

where $\langle \sigma v \rangle$ is the thermally averaged total cross section and n is the particle number density. The expansion of the Universe has the effect of diluting n and thus decreasing Γ. Therefore, the condition for thermal equilibrium is that the reaction rate be larger that the expansion rate,

$$\Gamma \gtrsim H, \tag{3.2}$$

where H ist the expansion rate of the Universe, also called *the Hubble rate*. Since Γ falls off more rapidly with temperature than the Hubble rate, even if the equilibrium condition is satisfied at high temperatures, at some point the temperature will have decrease enough that (3.2) will be violated. Therefore, for a particle species that was initially in equilibrium, the temperature for which the relation

$$\Gamma \approx H \tag{3.3}$$

is satisfied, is called the freeze-out temperature T_{fo}. This is a good approximation for the temperature at which the particle species drops out of equilibrium and its comoving number density stays constant, i.e. its density is only diluted by the expansion of the Universe but otherwise not modified.

Since the number density n (and also Γ) have a different functional form for relativistic and non-relativistic species, the decoupling process occurs differently for both cases.

3.2. Relativistic species

In the case of a relativistic fermion species, the number density is

$$n = \frac{3\,\zeta(3)\,g}{4\pi^2} T^3, \tag{3.4}$$

where g is the number of internal degrees of freedom of the species and ζ is the Riemann-Zeta function with $\zeta(3) = 1.20\ldots$. For spin-1/2 particles, we set $g = 2$. Furthermore, the Friedmann equation, which governs the expansion rate of the Universe, is

$$\left(\frac{\dot{a}}{a}\right)^2 = H^2 = \frac{8\pi G}{3}\rho = \frac{1}{3\,M_{\mathrm{Pl}}^2}\,\rho, \tag{3.5}$$

where $a = a(t)$ is the scale factor, G is Newton's gravitational constant, M_{Pl} is the reduced Plank mass and ρ is the energy density. During the early ages of the Universe, the energy density was dominated by the radiation component, so that we have

$$\rho \approx \rho_{\mathrm{R}} = \frac{\pi^2}{30}\,g_\rho\,T^4, \tag{3.6}$$

where g_ρ stands for the effective number of relativistic degrees of freedom in a plasma of temperature T and is defined by

$$g_\rho(T) = \sum_{i=\text{bosons}} g_i \left(\frac{T_i}{T}\right)^4 + \frac{7}{8} \sum_{i=\text{fermions}} g_i \left(\frac{T_i}{T}\right)^4. \tag{3.7}$$

We will refer to g_ρ as *the energetic degrees of freedom*. Thus, the equilibrium condition (3.2) gives us the following expression for the freeze-out temperature:

$$T_{\mathrm{fo}} = \frac{4\pi^3}{3\zeta(3)} \sqrt{\frac{g_\rho(T_{\mathrm{fo}})}{90 \cdot g^2}} \frac{1}{M_{\mathrm{Pl}}\,\langle\sigma v\rangle}, \tag{3.8}$$

plugging in the numbers we get

$$T_{\mathrm{fo}} \approx 1.8 \frac{\sqrt{g_\rho(T_{\mathrm{fo}})}}{M_{\mathrm{Pl}}\,\langle\sigma v\rangle}. \tag{3.9}$$

After specifying a particle physics model for this thermal relic, $\langle\sigma v\rangle$ can be specified. A good approximation for $g_\rho(T_{\mathrm{fo}})$ is obtained by setting $g_\rho(T_{\mathrm{fo}}) \approx g_\rho(T = m_\chi)$, where m_χ stands for the mass of the relic.

What would the relic density of such a particle be? As is customary, we introduce the new variable $y = n/s$, where s is the entropy density. The advantage of doing so

is that in an adiabatically expanding Universe (as we assume ours to be) the total entropy $S = s \cdot a^3$ is conserved and thus the entropy density scales as $s \sim a^{-3}$. Thus, $y = n/s$ is a measure for the comoving particle number density, and, as we have already recognised in the previous section, the comoving number density will stay constant after freeze-out, i.e. $y_{\text{today}} := y_0 = y(T_{\text{fo}})$. The entropy density given by $s = (2\,\pi^2/45)\, g_s\, T^3$, where g_s is, similarly to g_ρ, defined as

$$g_s(T) = \sum_{i=\text{bosons}} g_i \left(\frac{T_i}{T}\right)^3 + \frac{7}{8} \sum_{i=\text{fermions}} g_i \left(\frac{T_i}{T}\right)^3 . \tag{3.10}$$

We will refer to g_s as *the effective number of entropic degrees of freedom*. Then, we get the following expression for the frozen-out comoving density of any thermal relic that was relativistic at freeze-out:

$$y(T_{\text{fo}}) := y_{\text{fo}} = \frac{45}{2\pi^2} \frac{3\zeta(3)}{4\pi^2} \cdot \frac{1}{g_s(T_{\text{fo}})}. \tag{3.11}$$

When this type of particles, i.e. those that are relativistic at freeze-out, are hypothesised to be the dark matter, they get the name of ***hot dark matter***. Notice that y_{fo} is not only independent of T, but it's also independent of m_χ. It only depends on the freeze-out temperature through g_s.

Now we can easily calculate the relic abundance. The abundance of a given species is defined as the ratio of its energy density to the critical density of the Universe,

$$\Omega_i = \frac{\rho_i}{\rho_{\text{crit}}}. \tag{3.12}$$

The critical density is defined as the total energy density in a flat Universe as measured today,

$$\rho_{\text{crit}} = \frac{8\pi G}{3\, H_0^2} = \frac{1}{3\, M_{\text{Pl}}^2\, H_0^2}, \tag{3.13}$$

where H_0 stands for the Hubble parameter today. For a species that was relativistic at freeze-out and non-relativistic at present times[1] we obtain the following expression for the relic abundance:

$$\Omega_\chi\, h^2 = \frac{\rho_{\chi,0}}{\rho_{\text{crit}}}\, h^2 = \frac{n_{\chi,0} \cdot m_\chi}{\rho_{\text{crit}}}\, h^2 = \frac{s_0\, y_{\text{fo}}\, m_\chi}{\rho_{\text{crit}}}\, h^2, \tag{3.14}$$

where $s_0 \approx 2900\,\text{cm}^{-3}$ [5] is the entropy density today[2] and the numerical value of the critical density is $\rho_{\text{crit}} = 8.08\, h^2\, 10^{-47}\,\text{GeV}^4$ [5], with h defined through the Hubble rate: $H = h \cdot 100\,\text{Km}\,\text{s}^{-1}\,\text{Mpc}^{-1}$. Inserting the values of ρ_0, s_0, y_{fo} we get

$$\begin{aligned} \Omega_\chi\, h^2 &= \frac{10^{47}\,\text{GeV}^{-4}}{8.08} \frac{3\zeta(3)}{2\pi^2} \frac{g_s(T_0)}{g_s(T_{\text{fo}})}\, T_0^3\, m_\chi \\ &\approx \frac{0.115}{g_s(T_{\text{fo}})} \left(\frac{m_\chi}{\text{eV}}\right). \end{aligned} \tag{3.15}$$

[1] The energy density of a non-relativistic species i is $\rho_i = m_i \cdot n_i$.
[2] $T_0 = 2.73\,\text{K}$ [5].

In this last equation the only variables are the freeze-out Temperature and the mass of the particle. By demanding that the relic abundance does not exceed the observed dark matter abundance of $\Omega_\chi h^2 = 0.12$ [6], we can obtain an upper bound on the mass of this hot WIMP. Notice from (3.11), (3.14) and (3.15) that, because y_{fo} is constant and independent of m_χ, the relic abundance is proportional to the mass of the dark matter candidate

$$\Omega_\chi \propto m_\chi. \tag{3.16}$$

This behaviour is typical for hot thermal relics.

For a concrete example, let us consider a fourth heavy $SU(2)$ neutrino. We can approximate $\langle \sigma v \rangle \approx G_F^2 T^2/2\pi$ and if the freeze-out temperature lies between 1-100 MeV (as we should expect for a fourth heavy $SU(2)$ neutrino) we can set $g_\rho = g_s \approx 10$ [22]. Then, equation (3.9) gives us $T_{\text{fo}} \approx 7\,\text{MeV}$ (confirming the validity of setting $g_\rho = g_s \approx 10$) and the mass bound described in the previous paragraph from Equation (3.15) is

$$m_\chi \lesssim 9.65\,\text{eV}. \tag{3.17}$$

The bound in (3.17) is an updated version of the Cowsik-McClelland-bound [36].

3.3. The Boltzmann equation and non-relativistic relics

We want to treat the non-relativistic case with more precision. This requires solving a Boltzmann equation[3]. The Boltzmann equation governs the evolution of the particle momentum distribution $f_\chi(t, \vec{p})$ for a particle species χ and is given by

$$L[f_\chi] = C[f_\chi], \tag{3.18}$$

where L is the Liouville operator which describes the change in time of f_χ and C is the collision operator. For the Friedmann-Robertson-Walker metric, the left hand side of (3.18) is given by

$$L[f_\chi] = E\,\frac{\partial f_\chi}{\partial t} - \frac{\dot{a}}{a}\,|\vec{p}|^2\,\frac{\partial f_\chi}{\partial E}, \tag{3.19}$$

Before considering the r.h.s. of (3.18), let us divide (3.18) by E and integrate over $g_\chi d^3p_\chi/(2\pi)^3$:

$$\frac{\partial}{\partial t}\int \frac{d^3p_\chi g_\chi}{(2\pi)^3} f_\chi - H\int \frac{d^3p_\chi g_\chi}{(2\pi)^3}\frac{|\vec{p}|^2}{E}\,\frac{\partial f_\chi}{\partial E} = \int \frac{d^3p_\chi g_\chi}{(2\pi)^3}\,\frac{C[f_\chi]}{E} \tag{3.20}$$

$$\dot{n}_\chi + 3Hn_\chi = \int \frac{d^3p_\chi g_\chi}{(2\pi)^3}\,\frac{C[f_\chi]}{E}, \tag{3.21}$$

where for the second integral in the l.h.s. we transformed the integration variables and used partial integration. As always, $\dot{n}$ stands for $\partial n/\partial t$. The integral over the collision operator on the r.h.s. is a bit more intricate and contains the particle

[3] We will be following the treatment by Kolb and Turner [22] and Gondolo and Gelmini [37].

physics information about the processes that can affect the distribution function of the species χ we are interested in. In its general form and for the generic process $\chi + a + b + \cdots \leftrightharpoons i + j + \ldots$, and with f_i for the momentum distribution of the species i, it reads [22]

$$\begin{aligned}
\dot{n}_\chi + 3Hn_\chi &= \int \frac{d^3p_\chi g_\chi}{(2\pi)^3}\frac{C[f_\chi]}{E} \\
&= -\int d\pi_\chi d\pi_a d\pi_b \ldots d\pi_i d\pi_j \ldots (2\pi)^4\delta^{(4)}(p_\chi + p_a + p_b + \cdots - p_i - p_j - \ldots) \\
\times \sum_{\text{spins}} &\Big[|\mathcal{M}|^2_{\chi+a+b+\cdots\to i+j+\ldots} f_\chi\, f_a\, f_b \ldots (1 \pm f_i)(1 \pm f_j)\ldots \\
&- |\mathcal{M}|^2_{i+j+\cdots\to\chi+a+b+\ldots} f_i\, f_j \ldots (1 \pm f_\chi)(1 \pm f_a)(1 \pm f_b)\ldots \Big]. \qquad (3.22)
\end{aligned}$$

Here we have introduced the definition $d\pi_i := g_i d^3p_i/[(2\pi)^3 2E_i]$. Furthermore, $\mathcal{M}$ stands for the matrix elements of the corresponding process and the delta function ensures four-momentum conservation. Also, the $(+)$ sign applies to bosons while the $(-)$ sign applies to fermions. As we can now see, the Boltzmann equation is generally a set of coupled differential equations for the particle distribution functions of all species involved. However, if we **assume that all particles involved in the relevant processes are in thermal equilibrium and only the WIMPs χ will undergo freeze-out**, the system reduces to a single integro-differential equation for $f_\chi(p,t)$.

For concreteness, let us consider the annihilation and pair creation processes of the type $\chi + \overline{\chi} \leftrightharpoons 1 + 2$. Then, the collision term on the r.h.s. simplifies to [22]

$$\begin{aligned}
\int \frac{d^3p_\chi g_\chi}{(2\pi)^3}\frac{C[f_\chi]}{E} = -\int d\pi_\chi d\pi_{\overline{\chi}} d\pi_1 d\pi_2 (2\pi)^4\delta^{(4)}(p_\chi + p_{\overline{\chi}} - p_1 - p_2) \\
\times \sum_{\text{spins}} \Big[|\mathcal{M}|^2_{\chi+\overline{\chi}\to 1+2} f_\chi\, f_{\overline{\chi}} (1 \pm f_1)(1 \pm f_2) \\
- |\mathcal{M}|^2_{1+2\to\chi+\overline{\chi}} f_1\, f_2 (1 \pm f_\chi)(1 \pm f_{\overline{\chi}}) \Big]. \qquad (3.23)
\end{aligned}$$

Now let us implement a couple of simplifications:

- Assuming that the WIMPs χ are non-relativistic and the distribution functions for the SM particles are small, we can be satisfied with using Boltzmann statistics and thus ignoring the blocking/stimulating factors, $(1 \pm f_i) \approx 1$.
- We assume that the process $\chi + \overline{\chi} \leftrightharpoons 1 + 2$ is CP or T invariant, such that

$$|\mathcal{M}|^2 := |\mathcal{M}|^2_{\chi+\overline{\chi}\to 1+2} = |\mathcal{M}|^2_{1+2\to\chi+\overline{\chi}}.$$

Then, Equation (3.23) can be written in the simpler form

$$\begin{aligned}
\int \frac{d^3p_\chi g_\chi}{(2\pi)^3}\frac{C[f_\chi]}{E} = -\int d\pi_\chi d\pi_{\overline{\chi}} d\pi_1 d\pi_2 (2\pi)^4\delta^{(4)}(p_\chi + p_{\overline{\chi}} - p_1 - p_2) \\
\times \sum_{\text{spins}} |\mathcal{M}|^2 \Big[f_\chi\, f_{\overline{\chi}} - f_1\, f_2 \Big]. \qquad (3.24)
\end{aligned}$$

- Next, we recall the fact that species 1 and 2 are always in thermal equilibrium, i.e. $f_i = f_i^{\mathrm{eq}} = e^{-E_i/T}$, $i = 1, 2$. Also, thanks to the energy component of the delta function, it holds that $E_\chi + E_{\overline{\chi}} = E_1 + E_2$. Therefore, we can substitute

$$f_1 f_2 = f_1^{\mathrm{eq}} f_2^{\mathrm{eq}} = e^{-(E_1+E_2)/T} = e^{-(E_\chi+E_{\overline{\chi}})/T} = f_\chi^{\mathrm{eq}} f_{\overline{\chi}}^{\mathrm{eq}}.$$

- Furthermore, if the species $\chi, \overline{\chi}$ stay in kinetic equilibrium with the plasma even after chemical decoupling, the principle of detailed balance implies that [37]

$$\frac{f_\chi f_{\overline{\chi}}}{n_\chi n_{\overline{\chi}}} = \frac{f_\chi^{\mathrm{eq}} f_{\overline{\chi}}^{\mathrm{eq}}}{n_\chi^{\mathrm{eq}} n_{\overline{\chi}}^{\mathrm{eq}}}.$$

Then, the Boltzmann Equation (3.24) can be reformulated as follows:

$$\begin{aligned}
\dot{n}_\chi + 3Hn_\chi &= \int \frac{d^3p_\chi g_\chi}{(2\pi)^3} \frac{C[f_\chi]}{E} \\
&= -\int d\pi_\chi d\pi_{\overline{\chi}} d\pi_1 d\pi_2 (2\pi)^4 \delta^{(4)}(p_\chi + p_{\overline{\chi}} - p_1 - p_2) \sum_{\text{spins}} |\mathcal{M}|^2 \Big[f_\chi \, f_{\overline{\chi}} - \, f_1 \, f_2 \Big] \\
&= -\int d\pi_\chi d\pi_{\overline{\chi}} d\pi_1 d\pi_2 (2\pi)^4 \delta^{(4)}(\dots) \sum_{\text{spins}} |\mathcal{M}|^2 f_\chi^{\mathrm{eq}} \, f_{\overline{\chi}}^{\mathrm{eq}} \left(\frac{n_\chi \, n_{\overline{\chi}}}{n_\chi^{\mathrm{eq}} \, n_{\overline{\chi}}^{\mathrm{eq}}} - 1 \right) \\
&= -\int d\pi_\chi d\pi_{\overline{\chi}} d\pi_1 d\pi_2 (2\pi)^4 \delta^{(4)}(\dots) \sum_{\text{spins}} |\mathcal{M}|^2 \, \frac{f_\chi^{\mathrm{eq}} f_{\overline{\chi}}^{\mathrm{eq}}}{n_\chi^{\mathrm{eq}} \, n_{\overline{\chi}}^{\mathrm{eq}}} \left(n_\chi \, n_{\overline{\chi}} - n_\chi^{\mathrm{eq}} \, n_{\overline{\chi}}^{\mathrm{eq}} \right) \\
&= -\left\{ \int d\pi_\chi d\pi_{\overline{\chi}} \left[\int d\pi_1 d\pi_2 (2\pi)^4 \delta^{(4)}(\dots) \sum_{\text{spins}} |\mathcal{M}|^2 \right] \frac{f_\chi^{\mathrm{eq}} f_{\overline{\chi}}^{\mathrm{eq}}}{n_\chi^{\mathrm{eq}} \, n_{\overline{\chi}}^{\mathrm{eq}}} \right\} \left(n_\chi \, n_{\overline{\chi}} - n_\chi^{\mathrm{eq}} \, n_{\overline{\chi}}^{\mathrm{eq}} \right) \\
&= -\left\{ \int d\pi_\chi d\pi_{\overline{\chi}} \left[4 \, F \, \sigma \right] \frac{f_\chi^{\mathrm{eq}} f_{\overline{\chi}}^{\mathrm{eq}}}{n_\chi^{\mathrm{eq}} \, n_{\overline{\chi}}^{\mathrm{eq}}} \right\} \left(n_\chi \, n_{\overline{\chi}} - n_\chi^{\mathrm{eq}} \, n_{\overline{\chi}}^{\mathrm{eq}} \right) \\
&= -\left\{ \int \frac{g_\chi \, d^3p_\chi}{(2\pi)^3} \frac{g_{\overline{\chi}} \, d^3p_{\overline{\chi}}}{(2\pi)^3} [v_{\mathrm{mol}} \sigma] \frac{f_\chi^{\mathrm{eq}} f_{\overline{\chi}}^{\mathrm{eq}}}{n_\chi^{\mathrm{eq}} \, n_{\overline{\chi}}^{\mathrm{eq}}} \right\} \left(n_\chi \, n_{\overline{\chi}} - n_\chi^{\mathrm{eq}} \, n_{\overline{\chi}}^{\mathrm{eq}} \right). \qquad (3.25)
\end{aligned}$$

The result of the square brackets from the fifth to the sixth line is $4F\sigma$, where σ is the cross section for the annihilation reaction and $F = [(p_\chi \cdot p_{\overline{\chi}})^2 - m_\chi^2 m_{\overline{\chi}}^2]^{1/2}$. In the last equality, we define the *Moller velocity*, $v_{\mathrm{mol}} = F/E_\chi E_{\overline{\chi}}$ [37]. The expression in the curly braces in the last line of (3.25) is defined as the thermal average of σv_{mol}, which we write as $\langle \sigma v_{\mathrm{mol}} \rangle$. Thus, we finally arrive at the common expression for the Boltzmann equation for a particle χ that is initially kept in equilibrium by its annihilation (and pair-creation) reaction until it freezes out:

$$\dot{n}_\chi + 3Hn_\chi = -\langle \sigma v_{\mathrm{mol}} \rangle \left(n_\chi \, n_{\overline{\chi}} - n_\chi^{\mathrm{eq}} \, n_{\overline{\chi}}^{\mathrm{eq}} \right). \qquad (3.26)$$

If the WIMPs are Majorana particles, i.e. $\chi = \overline{\chi}$, or if there is no particle-antiparticle asymmetry in the WIMP sector, this reduces to

$$\dot{n}_\chi + 3Hn_\chi = -\langle \sigma v_{\mathrm{mol}} \rangle \left(n_\chi^2 - n_{\chi,\mathrm{eq}}^2 \right). \qquad (3.27)$$

3.3.1. The Boltzmann equation for a cold relic

If we solve the differential equation (3.27), we will be able to compute the relic abundance of the WIMP and compare it to the observed value of dark matter abundance $\Omega_\chi h^2 = 0.12$ [6]. As we did in section 3.2, we define the comoving particle number density $y = n_\chi/s$. Remember that for y to actually represent a comoving density, the total entropy of the Universe has to remain constant $S = s\,a^3 = \text{const.}$, so that the entropy density scales as $s \sim a^{-3}$. This also means that

$$\frac{d}{dt}S = \frac{d}{dt}(s\,a^3) = \dot{s}\,a^3 + 3\,s\,a^2\,\dot{a} \stackrel{!}{=} 0 \qquad \Rightarrow \qquad \dot{s} = -3sH. \tag{3.28}$$

With this, we can write the time derivative of y as follows:

$$\frac{d}{dt}\,y = \frac{d}{dt}(n_\chi/s) = \frac{\dot{n}_\chi}{s} - \frac{n_\chi}{s^2}\,\dot{s} = \frac{1}{s}\left(\dot{n}_\chi + 3\,H\,n_\chi\right). \tag{3.29}$$

We immediately see that the last parenthesis here is identical to the l.h.s. of Eq. (3.27). Thus, Eq. (3.27) can be rewritten as

$$\dot{y} = -\langle\sigma v_{\text{mol}}\rangle\; s\left(y^2 - y_{\text{eq}}^2\right). \tag{3.30}$$

It is convenient to use derivatives with respect to a dimensionless variable instead of time derivatives; the common choice is to define the dimensionless inverse temperature $x = m_\chi/T$ and rewrite Eq. (3.30) as a differential equation in $y(x)$ (one can think of x as a proxy for time t)[4]. Now we have to translate $d/dt \to d/dx$:

$$\begin{aligned}\frac{d}{dt} &= \frac{da}{dt}\frac{dx}{da}\frac{d}{dx} \\ &= \dot{a}\;\;\frac{dx}{da}\frac{d}{dx}.\end{aligned} \tag{3.31}$$

Noticing that Eq. (3.28) implies that $ds = -3s\,da/a$, we can replace $da = -(a/3s)\,ds$ and get

$$\begin{aligned}\frac{d}{dt} &= \dot{a}\,\frac{dx}{-(a/3s)\,ds}\,\frac{d}{dx} \\ &= -3sH\,\frac{dx}{ds}\,\frac{d}{dx} = -3sH\left(\frac{ds}{dx}\right)^{-1}\frac{d}{dx}.\end{aligned} \tag{3.32}$$

With this result, we can now write Eq. (3.30) as

$$\frac{dy}{dx} = \frac{1}{3\,H}\,\frac{ds}{dx}\,\langle\sigma v_{\text{mol}}\rangle\,\left(y^2 - y_{\text{eq}}^2\right). \tag{3.33}$$

[4]The evolution of $x = m_\chi/T$ is monotonically equivalent to time: in the epoch of radiation domination, time and temperature are related as $t \propto 1/T^2 \propto x^2$, i.e. the temperature of the Universe decreases with time.

Computing the derivative of s with respect to x we have

$$\begin{aligned}\frac{ds}{dx} &= \frac{dT}{dx}\frac{d}{dT}\left(\frac{2\pi^2}{45}\, g_s(T)\, T^3\right) \\ &= -\frac{T^2}{m}\,\frac{2\pi^2}{45}\Big(g_s'(T)T^3 + 3\, g_s(T)\, T^2\Big) \\ &= -3\frac{T}{m}\,\frac{2\pi^2}{45}\, g_s(T)\, T^3\left(\frac{T\, g_s'(T)}{3\, g_s(T)} + 1\right) \\ &= -3\, x^{-1}\, s\left(\frac{1}{3}\frac{d\,\ln g_s(T)}{d\ln T} + 1\right). \end{aligned} \tag{3.34}$$

Inserting this into (3.33) we finally obtain a differential equation for the comoving density $y(x)$:

$$\frac{dy}{dx} = -\sqrt{\frac{8\pi^2}{45}}\frac{M_{\rm Pl}\, m_\chi\, g_*^{1/2}}{x^2}\,\langle\sigma v_{\rm mol}\rangle\,\left(y^2 - y_{\rm eq}^2\right), \tag{3.35}$$

where we have defined

$$g_*^{1/2} := \frac{g_s(T)}{\sqrt{g_\rho(T)}}\cdot\left(\frac{1}{3}\frac{d\,\ln g_s(T)}{d\ln T} + 1\right). \tag{3.36}$$

The differential equation (3.35) can be numerically solved if we know $\langle\sigma v_{\rm mol}\rangle$. An approximative analytical solution is also possible. A couple of remarks are appropriate at this point:

- Although the energetic and entropic degrees of freedom of the plasma, g_ρ and g_s, are temperature dependent, there are large intervals of temperature in the thermal history of the Universe where they are not only equal but also nearly constant. The thermal evolution of g_ρ and g_s is shown in Figure 3.1. It is clear that g_ρ and g_s are only different at temperatures below the 0.1 MeV level. Furthermore, we recognise that, with the exception of the QCD phase transition at $T \sim 150 - 200\,\text{MeV}$, the slope of both curves is rather moderate or near zero. Above $T \sim 1\,\text{GeV}$, g_ρ and g_s go from ~ 100 to ~ 80, but only over a range of 3 orders of magnitude in temperature. Above $T \sim 100\,\text{GeV}$ all of the degrees of freedom of the SM are available and exist in the thermal soup, i.e. $g_\rho = g_s \approx 107$ are constant. In such intervals we can approximate $g_s'(T) = 0$ and therefore

$$g_*^{1/2} = \frac{g_s}{\sqrt{g_\rho}} = \frac{g_\rho}{\sqrt{g_\rho}} = \sqrt{g_\rho} \approx 10.3, \qquad \text{for } T \gtrsim 1\,\text{GeV}.$$

- Besides y, other objects in (3.35) that are also temperature dependent (or equivalently, x-dependent) are $\langle\sigma v_{\rm mol}\rangle$, $y_{\rm eq}$ and in general (as mentioned above) $g_*^{1/2}$.

- If there are no thresholds or resonances in the relevant temperature region, it is possible to expand $\langle\sigma v_{\rm mol}\rangle$ in powers of the relative velocity of the annihilating particles, or equivalently x^{-1}. Up to first order, the result is [37]

$$\langle\sigma v_{\rm mol}\rangle \approx a + \frac{3}{2}b\, x^{-1}. \tag{3.37}$$

- Of course, the thermally averaged cross section in (3.35) musst be summed over all final states, i.e.

$$\langle \sigma v_{\mathrm{mol}} \rangle = \sum_{1,2} \langle \sigma_{\chi\bar{\chi}\to 12}\, v_{\mathrm{mol}} \rangle \tag{3.38}$$

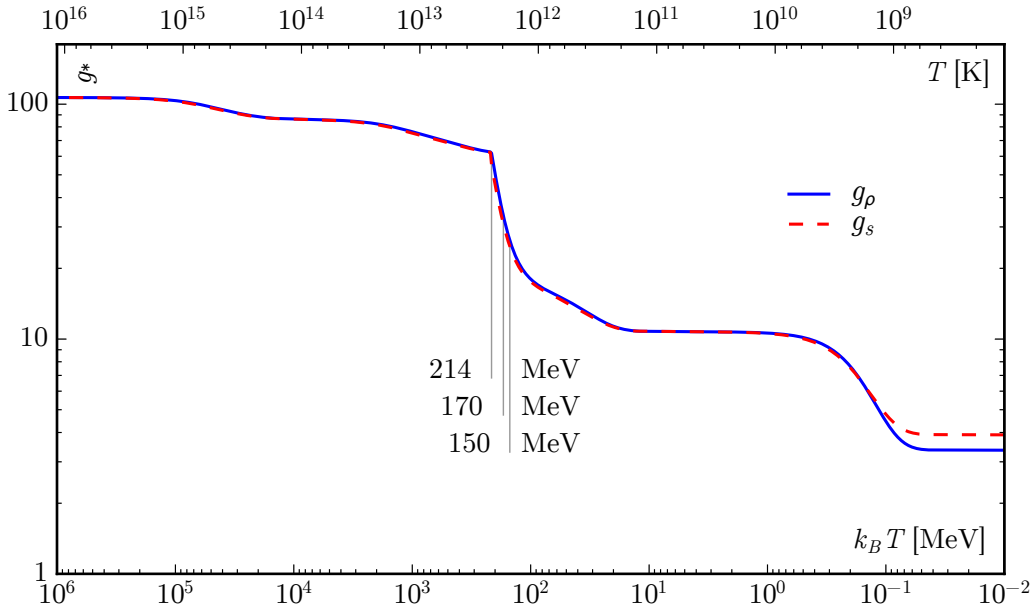

Figure 3.1.: The thermal evolution of the energetic and entropic effective number of degrees of freedom, g_ρ and g_s respectively, modified from [38].

3.3.2. Solving the Boltzmann equation: The comoving density and the relic abundance

Now, we want to solve Eq. (3.35) in order to obtain the relic abundance of the WIMP χ and compare it to the measured dark matter relic abundance. As is, Eq. (3.35) has no closed-form analytical solution; it is a special form of the *Riccati differential equation*, which can only be solved numerically (see subsection 3.3.3). However, we can find an approximative analytical solution for the limiting case we are interested in. For that, we will proceed in the following way:

1. Solve the equation in the late time limit, for which $x = m_\chi/T \to \infty$. In this case, the equilibrium term y_{eq} in Eq. (3.35), which is proportional to $\exp(-x)$ can be neglected and the differential equation turns homogeneous. Then we can simply integrate it from $x = x_*$ to $x = x_0 \to \infty$, where x_* stands for the value of x, for which $y(x)$ starts departing from its equilibrium value. The result of this step will be the comoving WIMP density today $y(x_0)$ with x_* as a parameter.

2. Determine the value of x_* by considering Eq. (3.35) in the early time regime, where $y(x)$ closely tracks $y_{\mathrm{eq}}(x)$.

3. Insert x_* from the second step into $y(x_0)$ from the first step. Then, calculate the relic abundance $\Omega_\chi = \rho_\chi/\rho_{\rm crit} = n_{\chi,0}\, m_\chi/\rho_{\rm crit} = y(x_0)\, s_0\, m_\chi/\rho_{\rm crit}$ and compare it to the measured dark matter relic abundance $\Omega_{\rm DM}$.

Beware that in the literature the value that we here call x_* ist often referred to as $x_{\rm fo}$, meaning x at the time of freeze out. The difference lies in the meaning that one ascribes to the statement "x at the time of freeze out": our convention here is to call $x_{\rm fo}$ the value of x for which the comoving density $y(x)$ has frozen out and remains constant, i.e. for which we have $y_0 = y(x_{\rm fo}) = y(x_{\rm today})$. By x_* we mean the value of x for which the comoving density starts deviating *significantly* from the equilibrium value $y_{\rm eq}(x)$ (we will quantify the word "significantly" later). In this sense, $x_* \neq x_{\rm fo}$, because even after the freeze out process has started and y has departed noticeably from $y_{\rm eq}$, annihilations may still occur and thus further deplete y. Let us now beginn with the first step to solve the Eq. (3.35).

1. Late time-/low temperature- regime.

For convenience, we remind ourselves of the differential equation (3.35):

$$\frac{dy}{dx} = -\sqrt{\frac{8\pi^2}{45}}\frac{M_{\rm Pl}\, m_\chi\, g_*^{1/2}}{x^2}\,\langle\sigma v_{\rm mol}\rangle\,\left(y^2 - y_{\rm eq}^2\right). \tag{3.35}$$

At late times we can neglect the production term in the Boltzmann equation (i.e. the one proportional to $y_{\rm eq}$), because at low temperatures $y_{\rm eq}$ is exponentially suppressed. Then, we are left with

$$\begin{aligned}
\frac{dy}{dx} &= -\sqrt{\frac{8\pi^2}{45}}\frac{M_{\rm Pl}\, m_\chi\, g_*^{1/2}}{x^2}\,\langle\sigma v_{\rm mol}\rangle\, y^2 \\
\int_{y_*}^{y_0}\frac{dy}{y^2} &= -\sqrt{\frac{8\pi^2}{45}}\, M_{\rm Pl}\, m_\chi \int_{x_*}^{\infty}\frac{g_*^{1/2}}{x^2}\,\langle\sigma v_{\rm mol}\rangle\, dx \\
\frac{1}{y_0} - \frac{1}{y_*} &= \sqrt{\frac{8\pi^2}{45}}\, M_{\rm Pl}\, m_\chi \int_{x_*}^{\infty}\frac{g_*^{1/2}}{x^2}\,\langle\sigma v_{\rm mol}\rangle\, dx.
\end{aligned} \tag{3.39}$$

For an approximative analytical solution of the integral in the r.h.s. we make the following assumptions:

- Since $g_*^{1/2}(x)$ is much larger for high temperatures than for lower temperatures and it is being divided by x^2, we may approximate the contribution of $g_*^{1/2}(x)$ to the integral by evaluating it at $x = x_*$, which allows us to pull it out of the integral.

- For $\langle\sigma v_{\rm mol}\rangle$ we use its partial wave expansion in powers of x, which allows us to perform the integration over x. This is only valid when σ has no resonances or thresholds in the relevant parameter region; in case this does not hold, see Ref. [37]. Instead of using (3.37), we use the more compact form

$$\langle\sigma v_{\rm mol}\rangle = c_n\, x^{-n}, \tag{3.40}$$

  with $n = 0$ for the s-wave, and $n = 1$ for the p-wave. Then the integral in the r.h.s. is solved trivially.

- Lastly, since $y_0 \ll y_*$ (because y_0 has been further diminished by annihilations after it depleted from its equilibrium value at x_*), we can neglect $1/y_*$ in favour of $1/y_0$.

In the end we find the following expression for the frozen-out comoving density of WIMPs today:

$$y_0 = \frac{x_*}{1.32\, M_{\rm Pl}\, m_\chi\, g_*^{1/2}\, \langle \sigma v_{\rm mol} \rangle}, \tag{3.41}$$

where $g_*^{1/2}$ and $\langle \sigma v_{\rm mol} \rangle$ are evaluated at $x = x_*$. With this, the only thing left to do before calculating the relic abundance of the WIMPs, is to determine x_*.

2. Late time-/low temperature- regime.

To determine the value of x_* we consider Eq. (3.35) in the early time-/high temperature range. It is useful to define the departure from equilibrium Δ (departure, for short):

$$\Delta = y - y_{\rm eq}.$$

Now, we reformulate the Boltzmann equation (3.35) using Δ:

$$\frac{d\Delta}{dx} = -\frac{dy_{\rm eq}}{dx} - \sqrt{\frac{8\pi^2}{45}} M_{\rm Pl}\, m_\chi\, g_*^{1/2}\, \frac{\langle \sigma v_{\rm mol} \rangle}{x^2}\, \Delta\, (2 y_{\rm eq} + \Delta)\,. \tag{3.42}$$

In this regime, the comoving WIMP density y closely follows the equilibrium function $y_{\rm eq}$, which also means that Δ and its derivative are small. Therefore, we may neglect Δ^2 and $d\Delta/dx$ and obtain

$$\begin{aligned} \frac{dy_{\rm eq}}{dx} &= -\lambda\, \frac{\langle \sigma v_{\rm mol} \rangle}{x^2}\, 2 y_{\rm eq} \Delta, \\ \Rightarrow \Delta &= -\frac{x^2}{2\,\lambda\, \langle \sigma v_{\rm mol} \rangle} \cdot \frac{dy_{\rm eq}/dx}{y_{\rm eq}}, \end{aligned} \tag{3.43}$$

where we have introduced $\lambda = \sqrt{8\pi^2/45}\, M_{\rm Pl}\, m_\chi\, g_*^{1/2}$ simply for convenience. Notice that λ is strictly speaking temperature dependent through $g_*^{1/2}$, but as we have already discussed, its temperature dependence above the QCD scale may be neglected (see Figure 3.1). Remember that

$$y_{\rm eq} = \frac{n_{\rm eq}}{s}\,, \qquad n_{\rm eq} = \frac{2}{(2\pi)^{3/2}} m_\chi^3\, x^{-3/2}\, e^{-x}\,, \qquad \text{and} \qquad s = \frac{2\pi^2}{45} g_s m^3\, x^{-3}, \tag{3.44}$$

$$\Rightarrow y_{\rm eq} = \underbrace{\frac{45}{\pi^2 (2\pi)^{3/2} g_s}}_{\alpha}\, x^{3/2}\, e^{-x} = \alpha\, x^{3/2}\, e^{-x}, \tag{3.45}$$

where we have introduced α. With this, the derivative of $y_{\rm eq}$ with respect to x is readily calculated and we get $dy_{\rm eq}/dx = y_{\rm eq}\,(3/2 \cdot x^{-1} - 1)$ and Eq. (3.43) reduces to

$$\Delta = \frac{x^2}{2\,\lambda\, \langle \sigma v_{\rm mol} \rangle} \left(1 - \frac{3}{2\,x}\right). \tag{3.46}$$

Next, we define the temperature of decoupling x_* by the equation

$$\Delta(x_*) = \xi \cdot y_{\mathrm{eq}}(x_*) \qquad \text{with} \qquad \xi \sim \mathcal{O}(1). \tag{3.47}$$

The numerical value assigned to ξ is somewhat arbitrary; by comparing the result of the approximative analytical solution that we are trying to derive here with the numerical solution of the Boltzmann equation, one assigns *a posteriori* an appropriate value to ξ so that that the numerical and analytical solutions agree. A good fit is obtained with $\xi = \sqrt{2}-1 \approx 0.41$ [39]. Inserting this into (3.46) we obtain an equation for x_*:

$$\begin{aligned}
\xi\,\alpha\, x_*^{3/2}\, e^{-x_*} &= \frac{x_*^2}{2\,\lambda\,\langle\sigma v_{\mathrm{mol}}\rangle}\left(1-\frac{3}{2\,x_*}\right) \\
e^{x_*} &= 2\,\xi\,\alpha\,\lambda\,\langle\sigma v_{\mathrm{mol}}\rangle x_*^{-1/2}\left(1-\frac{3}{2\,x_*}\right)^{-1} \\
x_* &= \ln(2\,\xi\,\alpha\,\lambda) + \ln\Big(\underbrace{\langle\sigma v_{\mathrm{mol}}\rangle_*}_{c_n x_*^{-n}}\, x_*^{-1/2}\Big) - \ln\left(1-\frac{3}{2\,x_*}\right) \\
x_* &= \ln(2\,\xi\,\alpha\,\lambda\,c_n) - \left(\frac{1}{2}+n\right)\ln(x_*) - \ln\left(1-\frac{3}{2\,x_*}\right).
\end{aligned} \tag{3.48}$$

Here we used (3.40) for the expansion of $\langle\sigma v_{\mathrm{mol}}\rangle$; for s-wave annihilation we have $n = 0$, and for p-wave annihilation $n = 1$. Equation (3.48) can be solved for x_* iteratively or by expanding the logarithms. By the later method and assuming s-wave annihilation with weak strength, i.e. $\langle\sigma v_{\mathrm{mol}}\rangle \approx c_0 = 10^{-10}\,\mathrm{GeV}^{-2}$ we find

$$x_* \approx 19.02 \qquad \text{for } n = 0, \tag{3.49}$$

$$x_* \approx 16.75 \qquad \text{for } n = 1. \tag{3.50}$$

Note that x_* depends on m_χ and $\langle\sigma v_{\mathrm{mol}}\rangle$ only logarithmically.

This means that, with our definition of when freeze-out occurs (see (3.47)), the WIMP decouples from equilibrium when the temperature is approximately 5% the WIMP mass.

3. The relic abundance

The last step is, now that we have an expression for the frozen-out comoving WIMP density, to compute the relic abundance and compare it to the measured dark matter abundance. Remember that the abundance of a given species is defined as the ratio of its energy density to the critical density of the Universe.

$$\Omega_i = \frac{\rho_i}{\rho_{\mathrm{crit}}}. \tag{3.51}$$

The observable actually measured by Planck and WMAP is $\Omega_{\mathrm{dm}}h^2$ rather than just Ω_{dm}; therefore (and because h^2 it will cancel out with the h^2 in ρ_{crit}, see (3.13)) it is more convenient to calculate $\Omega_\chi\, h^2$. Since the WIMP we are considering is non-relativistic, its energy density today is $\rho_\chi = m_\chi\, n_{\chi,0}$. In step 1., we calculated the

comoving density today $y_0 = n_{\chi,0}/s_0$. Thus, with (3.41) we obtain the relic abundance by computing

$$\begin{aligned}\Omega_\chi h^2 &= \frac{\rho_\chi}{\rho_{\text{crit}}} h^2 = \frac{m_\chi\, s_0\, y_0}{\rho_{\text{crit}}} h^2 \\ &= \frac{m_\chi\, s_0\, x_*\, h^2}{1.32\, M_{\text{Pl}}\, m_\chi\, g_*^{1/2} \langle\sigma v_{\text{mol}}\rangle\, 1.05 \cdot 10^{-5}\, h^2\, \text{GeV}\, \text{cm}^{-3}} \\ &= \frac{(s_0/\text{cm}^{-3})\, x_*}{1.39 \cdot 10^{-5}\, M_{\text{Pl}}\, g_*^{1/2} \langle\sigma v_{\text{mol}}\rangle\, \text{GeV}}. \end{aligned} \tag{3.52}$$

Plugging in the numerical values $s_0 = 2900\,\text{cm}^{-3}$ [22] and $M_{\text{Pl}} = 2.44 \cdot 10^{18}\,\text{GeV}$ [40] we get

$$\Omega_\chi h^2 = 8.57 \cdot 10^{-11} \frac{x_*}{g_*^{1/2}} \left(\frac{\text{GeV}^{-2}}{\langle\sigma v_{\text{mol}}\rangle}\right). \tag{3.53}$$

As we can see from Eq. (3.53), it is remarkable that the relic abundance of our WIMP does not depend explicitly on its mass. The inverse decoupling temperature x_* does depend on the WIMP mass, but only logarithmically, as we saw in Eq. (3.48). Also, when computing y_0, we simplified the integral in (3.39) by taking the value of $g_*^{1/2}$ at $T = T_*$ to pull it out of the integral. And as we can see from Figure 3.1, as long as the decoupling temperature T_* lies above 100 GeV, $g_*^{1/2}(T)$ has the constant value of $g_*^{1/2}(T_*) \approx \sqrt{107}$ and is independent of the WIMP mass.[5] Inserting this value for $g_*^{1/2}$ and (3.49) for x_* in (3.53), we obtain the final expression for the WIMP relic density

$$\Omega_\chi h^2 = 1.59 \cdot 10^{-10} \left(\frac{\text{GeV}^{-2}}{\langle\sigma v_{\text{mol}}\rangle}\right) \tag{3.54}$$

$$= 1.84 \cdot 10^{-27} \left(\frac{\text{cm}^3\,\text{s}^{-1}}{\langle\sigma v_{\text{mol}}\rangle}\right). \tag{3.55}$$

In the literature (e.g. [34]) one often finds the value $\Omega_\chi h^2 = 3 \cdot 10^{-27} \langle\sigma v_{\text{mol}}\rangle^{-1} (\text{cm}^3\,\text{s}^{-1})$, whose precise origin is unclear but is probably the result of multiple approximations and rounding-off to one significant figure [41]. Steigman et al. compute the relic abundance through a slightly more intricate but also more precise treatment in [41] and find that x_* increases slowly with m_χ from $x_* = 17$ at $m_\chi = 0.1\,\text{GeV}$ to $x_* = 27$ at $m_\chi = 10^4\,\text{GeV}$, leading to a relic abundance for WIMP masses above $m_\chi \sim 10\,\text{GeV}$ of $\Omega_\chi h^2 \approx 2.3 \cdot 10^{-27} \langle\sigma v_{\text{mol}}\rangle^{-1} (\text{cm}^3\,\text{s}^{-1})$.

Now we can compare our result (3.55) with the measured dark matter abundance [6]

$$\Omega_{\text{dm}} h^2 = 0.1206 \pm 0.0021. \tag{3.56}$$

[5] Since $x_* \approx 20$, the decoupling temperature T_* will be above 100 GeV if $m_\chi \gtrsim 5\,\text{GeV}$.

By requiring the WIMP to account for the total of the dark matter, we can write the WIMP abundance in the following way

$$\Omega_\chi h^2 = 0.12 \left(\frac{1.53 \cdot 10^{-26}\,\mathrm{cm}^3\,\mathrm{s}^{-1}}{\langle \sigma v_{\mathrm{mol}} \rangle} \right) \tag{3.57}$$

$$= 0.12 \left(\frac{1.31 \cdot 10^{-9}\,\mathrm{GeV}^{-2}}{\langle \sigma v_{\mathrm{mol}} \rangle} \right). \tag{3.58}$$

If we were to simply require that the WIMP abundance does not exceed the observed cold matter abundance (3.56), we get a bound on the thermally averaged annihilation cross section. Of course, $\langle \sigma v_{\mathrm{mol}} \rangle$ will depend on some way on the WIMP mass m_χ; the specific relationship will be given by a concrete WIMP dark matter model.

3.3.3. A numerical solution to the Boltzmann equation for a cold WIMP

The approximative solution (3.41) to the Boltzmann equation (3.35) and the resulting expression for the relic abundance (3.55) enable us to understand the relationship between the comoving density y, the mass m_χ, the cross section $\langle \sigma v_{\mathrm{mol}} \rangle$ and the relic

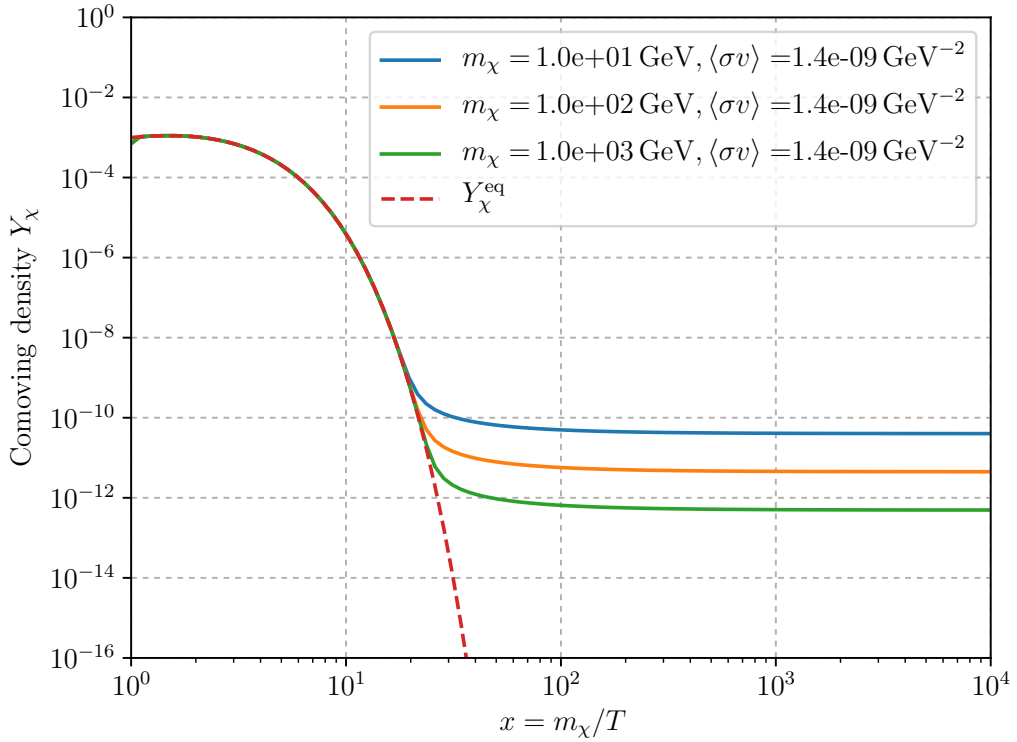

Figure 3.2.: Numerical solution to the Boltzmann equation for the comoving density of WIMPs in the standard paradigm, i.e. initial equilibrium by annihilation interactions.

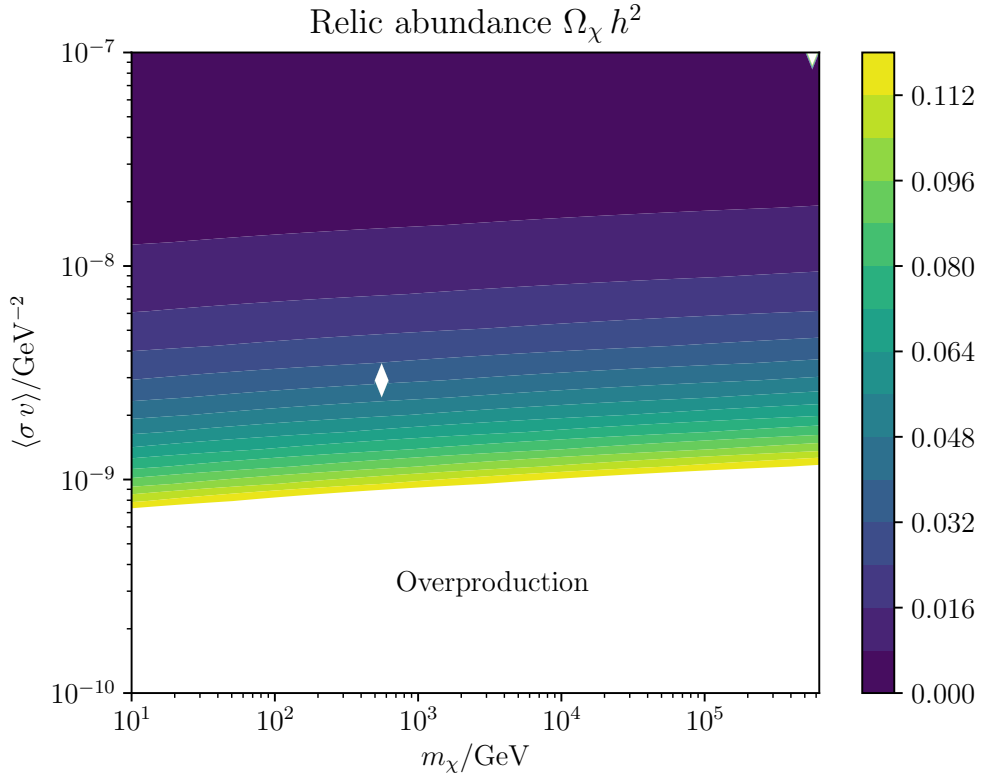

Figure 3.3.: WIMP abundance produced by freeze out from thermal equilibrium. The yellow stripes right on the edge before overproduction represent the region of the parameter space where the WIMPs account for 100% of the observed dark matter density. In the blue regions the WIMPs make a contribution of less than 100% to the dark matter density.

abundance Ω_χ. But we can also compute a more exact numerical solution to the Boltzmann equation as it is formulated in Eq. (3.35); for convenience, we reprint it here:

$$\frac{dy}{dx} = -\sqrt{\frac{8\pi^2}{45}}\frac{M_{\mathrm{Pl}}\, m_\chi\, g_*^{1/2}}{x^2}\,\langle\sigma v_{\mathrm{mol}}\rangle\,\left(y^2 - y_{\mathrm{eq}}^2\right). \tag{3.35}$$

The numerical solution is shown in Figure 3.2. From Eq. (3.41) we see that $y_0 \propto \langle\sigma v_{\mathrm{mol}}\rangle^{-1}$ and $y_0 \propto m_\chi^{-1}$, as we see in Figure 3.2. However, for the abundance Ω_χ the explicit mass dependence gets cancelled; Ω_χ depends on m_χ only logarithmycaly through x_* (see (3.53)). Therefore, we expect that the different curves in Figure 3.2 give us roughly the same relic abundance $\Omega_\chi\, h^2 = m_\chi\, s_0\, y_0\, h^2/\rho_{\mathrm{crit}}$. Indeed, this is the result that we obtain from the computation. Clearly, a WIMP with these parameters ($\langle\sigma v_{\mathrm{mol}}\rangle = 1.4 \cdot 10^{-9}\,\mathrm{GeV}$) is a viable dark matter candidate.

m_χ in GeV	10	100	1000
$\Omega_\chi h^2$	0.11	0.12	0.13

3.4. The Lee-Weinberg curve

In section 3.2 and section 3.3 we investigated two classes of dark matter candidates: *cold* WIMPs and *hot* WIMPs. The difference between these two types of WIMPs is that hot WIMPs are relativistic at freeze-out while cold WIMPs are non-relativistic at freeze-out. This means that the relationship between their abundance, annihilation cross section and mass is different in both cases. As we saw in (3.15), for hot dark matter the relic abundance is proportional to the WIMP mass, $\Omega_\chi \propto m_\chi$. In contrast to this, we saw in Equation (3.55) that for cold dark matter the relic abundance is proportional to the inverse of the cross section, which itself is often proportional to the square of the WIMP mass (and the inverse of the mediator's mass to the fourth power), i.e. $\Omega_\chi \propto \langle \sigma v_{\text{mol}} \rangle^{-1} \propto m_\chi^{-2}$. The turning point between this two very different behaviours of Ω_χ lies at $m_\chi \sim T_{\text{fo}}$. The famous *Lee-Weinberg curve* shows the dependence of the relic abundance on the mass of the WIMP and identifies mass intervals where cold- and hot dark matter match the observed relic abundance, assuming that the interactions of the WIMPs are of the same strength as the weak interactions of the Standard Model (this could be the case if a massive fourth neutrino existed, as was speculated in the 70's [36, 35]). Hot dark matter has been excluded as a feasible dark matter candidate by structure formation arguments [16].

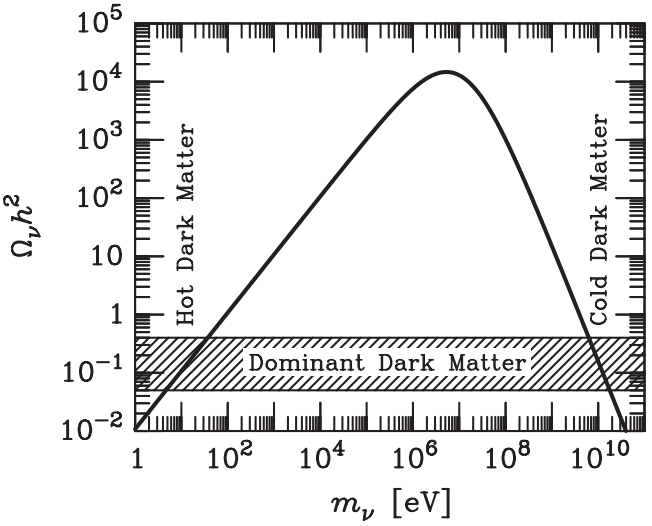

Figure 3.4.: The Lee-Weinberg curve. Requiring that the relic abundance of *weakly interacting WIMPs* does not exceed the measured dark matter abundance and taking into account some uncertainty with respect to the value of the Hubble parameter (originally $0.05 \lesssim \Omega_{\text{dm}} h^2 \lesssim 0.4$, which today is outdated, of course) one can determine mass intervals in which hot or cold WIMPs are viable dark matter candidates. Figure from: [42].

3.5. The unitarity bound

An important question one might ask is, how heavy can a WIMP be in order for it to be the dark matter, i.e. is there a model-independent upper bound on its mass? The answer is, under certain circumstances, yes! In 1990 Griest and Kamionkowski published a paper in which they derived an upper limit on the mass of a dark matter particle of the class that we have been discussing in this charter, i.e. particles that were in full thermal equilibrium in the early Universe by annihilation and pair-creation reactions with the cosmic plasma [43]. This is the so called *unitarity bound*. The argument is that the unitarity condition on the scattering matrix for the annihilation and pair-creation interactions of the dark matter particles implies an upper bound on the annihilation cross section. The authors estimate that

$$(\sigma\, v_{\rm rel}) \lesssim (\sigma\, v_{\rm rel})_{\rm max} \equiv \frac{4\pi}{m_\chi^2\, v_{\rm rel}}, \tag{3.59}$$

where $v_{\rm rel}$ stands for the relative velocity of the annihilating particles. This condition is valid for s-wave annihilation. If annihilations also occur into other partial waves, those contributions should be added to (3.59), but they are usually much smaller, because each partial wave index comes with an additional factor of $v_{\rm rel}^2/4$, which is small for non-relativistic particles. The thermal average of (3.59) is

$$\langle \sigma\, v_{\rm rel} \rangle_{\rm max} = \frac{4\sqrt{\pi}}{m_\chi^2}\, \sqrt{x}. \tag{3.60}$$

Notice that this expression corresponds to $\langle \sigma\, v_{\rm rel} \rangle = c_n\, x^n$ with $n = 1/2$ (instead of $n = 0, 1$ for s- or p-wave annihilation). In the integral in (3.39) this causes an additional factor of $1/2$ which is carried along all the way to the expression for the abundance (3.53). Inserting (3.60) into (3.53) and taking into account the aforementioned additional factor of $1/2$ we get

$$\Omega_\chi h^2 \approx 6 \cdot 10^{-13}\, x_*^{1/2} \left(\frac{m_\chi}{\rm GeV}\right)^2. \tag{3.61}$$

In the original paper, Griest and Kamionkowski demand that the dark matter abundance does not overclose the Universe, i.e. $\Omega_\chi h^2 \leqslant 1$ and set $x_* = 28$. This delivers a conservative bound on the mass of the WIMP dark matter:

$$m_\chi \leqslant 560 \text{ TeV}. \tag{3.62}$$

We can now update this bound by requiring that that the WIMP abundance does not exceed the dark matter abundance as measured by the Planck satellite [6] (as opposed to simply requiring that it do not overclose the Universe) and using our own result for the decoupling temperature (3.49) $x_* = 19.02$. The resulting upper bound for s-wave annihilation is

$$m_\chi \leqslant 75 \text{ TeV}. \tag{3.63}$$

It is important to keep in mind that this bound holds only for dark matter particles that were once in full thermal equilibrium through annihilation interactions. Also, it is not free of exceptions, e.g. if in some region of the parameter space the partial wave expansion is not valid (because it does not converge), then the derivation of this bound is not valid either. Also, there might be annihilation processes, such as some t-channel annihilations, in which the p-wave and even higher order terms from the partial wave expansion contribute in the same order as the s-wave and may therefore not be neglected with respect to the s-wave. In this case, the cross section for each contributing partial wave must be added.

With this, we conclude this chapter on WIMP dark matter. As we have seen, WIMPs are a very appealing class of dark matter candidates, partly because their production mechanism, thermal freeze-out in the early Universe, is able to naturally produce the correct order of magnitude of dark matter abundance.

4. Neutrino Phenomenology

Like dark matter, the true, fundamental nature of neutrinos in particle physics is one of the most pressing issues modern physics. The neutrino was first proposed almost 90 years ago by Wolfgang Pauli, as a way to explain the continuous energy spectrum of β-decay experiments [44]. Its existence was confirmed 26 years later by Cowan et al. in 1957 [45]. Since then, a lot has been learned about the physics of neutrinos and their role not only in particle physics, but also in astrophysics and cosmology. Today, we know that there are three types of neutrinos (called flavours), all of which are electrically neutral, interact with other matter particles only through the weak interaction and constitute the most abundant fermionic particle in the Universe. Until recently, it was thought that neutrinos were also massless. This is because it is not possible to consistently write down neutrino-mass terms in the SM-Lagrangian using only the known matter fields and without violating the gauge invariance of theory [46]. However, in 1999 and 2002 the phenomena of neutrino oscillations was finally confirmed as a solution to the atmospheric and solar neutrino problem by the Super-Kamiokande [47] and SNO [48] collaborations respectively. This discovery was rewarded with the 2015 Nobel prize and counts as a definitive proof of the incompleteness of the SM, because neutrino flavour oscillations necessarily require neutrinos to have a none-zero mass. Thus, we are bound to look *beyond the Standard Model* (BSM) to explain the origin of the neutrino masses. One very appealing possibility, is that the same extension of the SM that solves this problem, might also deliver a solution to the dark matter problem (and maybe even other problems in the frontiers of physics, e.g. *baryogenesis*).

In this chapter, we will explore the basics of neutrino physics with the aim of understanding how sterile neutrinos might not only explain the generation of mass for the SM neutrinos, but also the dark matter problem.

4.1. Neutrinos in the Standard Model

In the SM, the force carrier particles have an integer spin and are called bosons; bosons with spin 1 are called vector bosons, those with spin 0 are called scalar bosons (like the Higgs particle). The fundamental matter particles have all spin 1/2 and are called fermions. They are further divided into two groups: those which interact through the strong force (i.e. those that have color charge) are called quarks, and those that do not, which are called leptons. There are 6 quarks and 6 leptons in the SM, plus their antiparticles.

The gauge interactions in the SM arise because of the requirement of gauge invariance of the Lagrangian under certain symmetry groups; the group responsible for

the electroweak interactions is $SU(2)_L \times U(1)_Y$. With respect to the $SU(2)_L$ group, quarks and leptons are also grouped, according to their $SU(2)_L$ transformation properties, in *isospin*[1] singlets (also referred to as *right-handed* fields, see section 4.2 and equation (4.9)) and isospin doublets (or *left-handed* fields). In the quark and lepton sector, there are three doublets, also called *generations*. The three quark $SU(2)_L$ generations are

$$\begin{pmatrix} u \\ d \end{pmatrix}_L, \begin{pmatrix} c \\ s \end{pmatrix}_L, \begin{pmatrix} t \\ b \end{pmatrix}_L. \tag{4.1}$$

Each element in each generation is a Weyl spinor. The upper spinors have an electric charge of $Q_u = 2/3$, while the lower spinors have $Q_d = -1/3$. The quark singlets are

$$u_R^i = \{u_R, c_R, t_R\}, \qquad d_R^i = \{d_R, s_R, b_R\}. \tag{4.2}$$

In the same fashion, the 6 leptons, to which the neutrinos belong, are also organised in 3 doublets, or generations

$$\begin{pmatrix} \nu_e \\ e \end{pmatrix}_L, \begin{pmatrix} \nu_\mu \\ \mu \end{pmatrix}_L, \begin{pmatrix} \nu_\tau \\ \tau \end{pmatrix}_L. \tag{4.3}$$

As for the $SU(2)_L$ leptonic singlets, only the right-handed partners to the charged leptons have been observed. These are:

$$e_R^i = \{e_R, \mu_R, \tau_r\}. \tag{4.4}$$

No right-handed neutrinos have been observed yet, but it is possible that they do exist. We will examine this possibility throughout this work. While the charged leptons, e, μ, τ have all an electric charge of $Q_e = -1$, neutrinos have no electric and no color charge, i.e. they do not interact through the electromagnetic nor through the strong force. However, they are charged with respect to the weak force and can thus interact with the charged leptons of the SM through the exchange of vector bosons W^+, W^- in a charged current (CC) or Z^0 in a neutral current. The weak interaction is a short range interaction. This has to do with the fact that the vector bosons which are exchanged are massive, with $m_W \approx 80\,\text{GeV}$ and $m_Z \approx 90\,\text{GeV}$. A measure for the range R of the interaction is given by $R = \hbar/m_V c$ [49], where m_V stands for the vector boson's mass. For the weak force, this gives us roughly $R \approx 2 \cdot 10^{-3}\,\text{fm}$, which is much smaller than a hydrogen nucleous.

One can define the generation lepton number L_α, with $\alpha = e, \mu, \tau$. Particles of the lepton generation α (both the charged lepton and the neutrino) have $L_\alpha = 1$ and $L_\beta = 0$ for $\alpha \neq \beta$. Similarly, the antiparticles of generation α are assigned the same lepton number but with opposite sign. In the SM, the weak interactions in which the neutrinos are involved, are *diagonal*, meaning that they occur only within a generation and not across generations. In other words, the SM weak interaction

[1] The isospin I is the name of the $SU(2)_L$ charge a particle may have. Left-handed particles have $I = 1/2$ and right-handed particles have $I = 0$.

conserves the lepton number of each flavour[2]. The interaction vertices relevant for neutrinos are shown below in Eq. (4.5). The charged currents mediated by the $W^{\pm}$ bosons, are shown in the first two columns; the neutral currents, mediated by the Z^0 boson are shown in the third and last column.

$$\begin{array}{lll} W^+ \to e^+ + \nu_e, & W^- \to e^- + \bar{\nu}_e, & Z^0 \to \nu_e + \bar{\nu}_e, \\ W^+ \to \mu^+ + \nu_\mu, & W^- \to \mu^- + \bar{\nu}_\mu, & Z^0 \to \nu_\mu + \bar{\nu}_\mu, \\ W^+ \to \tau^+ + \nu_\tau, & W^- \to \tau^- + \bar{\nu}_\tau, & Z^0 \to \nu_\tau + \bar{\nu}_\tau. \end{array} \tag{4.5}$$

A very important process for neutrinos is β-decay, which occurs when a neutron, which is composed two d-quarks and one u-quark, turns into a proton by emitting an electron and an electron antineutrino. In terms of fundamental particles, one of the d-quarks transforms into an u-quark and a W^- boson, which then produces an electron and an electron antineutrino:

$$\begin{aligned} n &\to p + e^- + \bar{\nu}_e, \\ d \to u + W^- &\to u + e^- + \bar{\nu}_e. \end{aligned} \tag{4.6}$$

Other common reactions involving electron neutrinos are *electron capture* (4.7) and *positron capture* (4.8):

$$p + e^- \to n + \nu_e \tag{4.7}$$

$$n + e^+ \to p + \bar{\nu}_e \tag{4.8}$$

By these and other similar reactions huge amounts of neutrinos are produced everr second, both artificially as well as naturally. The Sun, which gets its energy by the nuclear fusion of hydrogen to helium, is one of our most prominent natural sources of neutrinos; from the processes depicted in Figure 4.1, neutrinos are produced at a rate of $2 \cdot 10^{38}\,\mathrm{s}^{-1}$ [50]. Natural radioactivity from the Earths inner material also produces neutrinos, called *geoneutrinos*, with a flux of $\sim 6 \cdot 10^6\,\mathrm{cm}^{-2}\,\mathrm{s}^{-1}$. Cosmic rays routinely produce charged $\mu^{\pm}$ leptons and their corresponding neutrinos ν_μ, $\bar{\nu}_\mu$ in collisions with gas in our atmosphere. Along the cascade induced by the cosmic rays, many ν_e, $\bar{\nu}_e$ are also produced. The total atmospheric neutrino flux at the earths surface is $\sim 10^{-1}\,\mathrm{cm}^{-2}\,\mathrm{s}^{-1}$. Another fascinating natural source of neutrinos are Supernova explosions of type II (SNII). Neutrinos carry $\sim 99\%$ of the energy liberated in such violent explosions, where $\sim 6 \cdot 10^{58}$ neutrinos are emitted in a period of time as short as 10 s [50]. Then there is also the Cosmic Neutrino Background (CνB), which consists of left over neutrinos from the big bang, much like the photons of the CMB, which we discussed earlier (see section 2.5). The cosmic neutrinos decoupled much earlier than the CMB photons, when the Universe had a temperature of $\sim 1\,\mathrm{MeV}$. Since these neutrinos would have an extremely low energy and do not interact electromagnetically, detecting then remains and extremely difficult and yet unachieved challenge. The current CνB number density is calculated to be $\sim$

[2]Not so in the quark sector, where weak transitions across quark generations are possible due to quark-mixing.

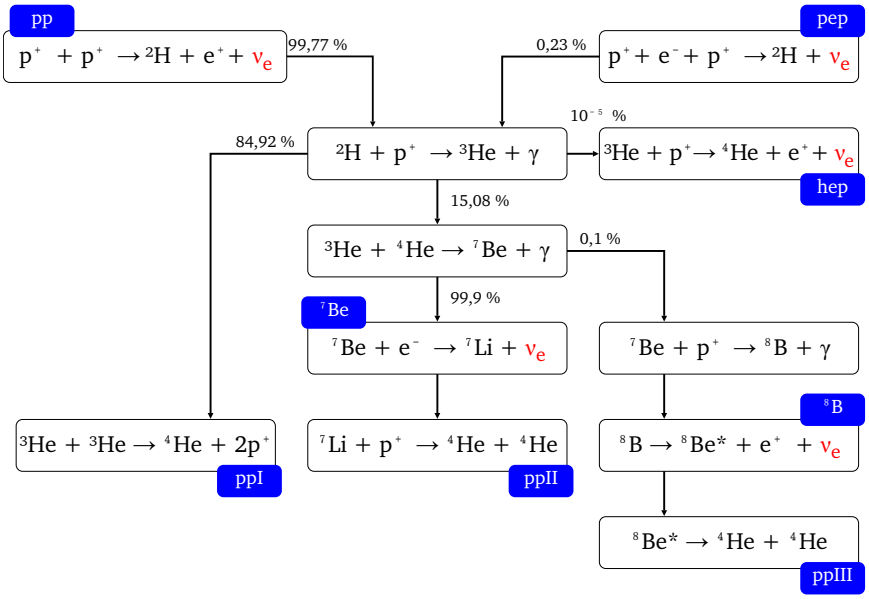

Figure 4.1.: Nuclear reaction taken place in our Sun. Image modified from [51].

$110\,\mathrm{cm}^{-3}$. As for artificial sources, nuclear power plants and particle accelerators can be used as very reliable and controllable neutrino factories. A 3 GW nuclear plant will emit $8 \cdot 10^{20}\,\mathrm{s}^{-1}$ antineutrinos [50], while particle accelerators can produced high energy beams of neutrinos to experiment with.

As we can already see, neutrinos not only can feed us with invaluable information about cosmology, astrophysics, nuclear physics and geology, but are fascinating entities on their own, still hiding mysteries about their fundamental nature.

4.2. Chirality and the fermionic nature of neutrinos

The question of whether neutrinos are Dirac or Majorana particles is profound and has far-reaching consequences. As opposed to Dirac fermions, Majorana fermions are identical to their anti-particles, which opens up many phenomenological possibilities, from the violation of certain symmetries to the feasibility of mass generating mechanisms. All known matter particles in the SM are known to be Dirac fermions, except for neutrinos, which could be Majorana particles. That we are unsure about this, hast to do with the fact that neutrinos are only observed with helicity $h = -1$ and anti-neutrinos with $h = +1$. This is a necessary but not a sufficient requirement for neutrinos to be Majorana particles. In the massless limit (and in the SM neutrinos are massless), helicity and chirality are identical. Chirality is a property a particle has; a particle can be of *left-handed* (LH) or *right-handed* (RH) chirality or a combination of both. The chirality projection operators P_L and P_R are defined as

$$P_L = \frac{1 - \gamma_5}{2}, \qquad P_R = \frac{1 + \gamma_5}{2}, \tag{4.9}$$

with $\gamma_5 = i\gamma_0\gamma_2\gamma_2\gamma_3$ and γ_i as the gamma matrices[3]. P_L and P_R form a complete set of projection operators, which means that $P_L + P_R = 1$ and $P_L P_R = P_R P_L = 0$. Therefore, it is possible to decompose any fermion ψ into its chiral left- and right-handed components,

$$\psi = P_L\psi + P_R\psi = \psi_L + \psi_R. \tag{4.10}$$

The CC interactions of the weak force, see Eq. (4.5), which we discussed in the previous section, couple only to the LH component of weakly charged particles (and to the RH component of their antiparticles). In general, the NC interactions in (4.5) couple also to the RH components of **electrically charged fermions**. However, since neutrinos are electrically neutral, a RH neutrino (or a LH anti-neutrino) would not couple to NC weak interactions either. This means that RH neutrinos (or LH anti-neutrinos) are totally decoupled from SM interactions[4], which is why they are also called *sterile neutrinos*. In other words, RH neutrinos are SM singlets.

Ignoring the experiments which have demonstrated that neutrino oscillations exist, there is no other experimental observation requiring the existence of RH neutrinos; all other known physical phenomena observed in the lab can be explained with only LH neutrinos. Therefore, in the current formulation of the SM, neutrinos only appear in the LH isospin doublets introduced in (4.3), and the anti-neutrinos in the Dirac adjoints of the doublets are also strictly RH. RH neutrinos (and LH anit-neutrinos) are not contained in the SM.

To understand the difference between Dirac and Majorana neutrinos, we need the *particle-antiparticle conjugation* operator $\hat{C}$, which we define by its action on a spinor ψ:

$$\hat{C}\,\psi = \psi^c = C\,\bar{\psi}^T, \tag{4.11}$$

where C is a new matrix that satisfies the relations $C^\dagger = C^T = C^{-1} = -C$. In the Dirac representation of the gamma matrices, $C = i\gamma_0\gamma_2$. Using this representation and the definition for the chiral projectors (4.9) we quickly see that

$$\hat{C}\,\psi_L = (\psi_L)^c = (\psi^c)_R, \qquad \hat{C}\,\psi_R = (\psi_R)^c = (\psi^c)_L, \tag{4.12}$$

i.e. the antiparticle of a left-handed particle is right-handed and vice versa. With this, let us consider the decomposition of ψ^c into its chiral components. From Eq. (4.10), we see that

$$\psi \xrightarrow{\hat{C}} \psi^c = (\psi_L)^c + (\psi_R)^c \tag{4.13}$$

$$= (\psi^c)_R + (\psi^c)_L. \tag{4.14}$$

For a Majorana particle, we further have $\psi = \eta\psi^c$, with the phase factor $\eta = e^{i\varphi}$ and the arbitrary phase φ. Together with (4.10) and (4.13), this implies that $\psi_R = (\psi_L)^c$

[3]The gamma matrices are the four-dimensional generators of the *Clifford algebra*.

[4]If RH neutrinos exist, a Yukawa interaction is possible, which then allows for active-sterile neutrino mixing. More on this in section 4.3.

and vice versa. This means that, for a Majorana particle, the RH component is not independent but can be constructed from the LH component of the spinor, and we can write

$$\psi = \psi_L + \eta(\psi_L)^c = \psi_L + \eta C(\bar{\psi}_L)^T. \tag{4.15}$$

With this knowledge, we can now turn to a discussion about the difficulties of generating mass terms for neutrinos within and beyond the SM.

4.3. The problem of neutrino masses and the seesaw mechanism

As we have already mentioned multiple times, neutrinos in the SM are massless. However, the neutrino observatories Super-Kamiokande [47] and SNO [48] have shown, that neutrinos undergo flavour oscillations, indicating that in reality, they have a tiny, non-vanishing mass.

Let us begin this discussion by investigating the implications of regular mass terms in the Lagrange density of a gauge theory. For a fermion ψ, the mass term in the Lagrangian has the form

$$\mathcal{L}_m = -m\bar{\psi}\psi. \tag{4.16}$$

Decomposing ψ into its chiral parts we have

$$\mathcal{L}_m = -m\,\bar{\psi}_L\psi_R - m\,\bar{\psi}_R\psi_L. \tag{4.17}$$

This equation shows us immediately that if ψ is a Dirac fermion, then it is mandatory for this type of mass term, that ψ has both LH and RH components. There is another problem with this mass term (which is usually refered to as a *Dirac mass term*), and it has to do with the gauge transformation properties of the chiral components of ψ. As we discussed in the previous section, ψ_L and ψ_R do not couple in the same way to the vector bosons of the weak interaction. In the language of group theory, we say that ψ_L transforms as a $SU(2)_L$ doublet, while ψ_R transforms as a $SU(2)_L$ singlet. Since the Lagrangian is required to be invariant under $SU(2)_L$ transformations, we conclude that the Dirac mass term from (4.17) cannot be included in the SM Lagrangian, as this invariance would be violated by (4.17) due to the different transformation properties of ψ_L and ψ_R. This is the reason why the Higgs mechanism and spontaneous symmetry breaking is needed to generate masses for all SM particles. After spontaneous symmetry breaking by the Higgs mechanism, Dirac mass terms of the same structure as in (4.17) are generated. However, this is of no use in the case of neutrinos because, as there are no RH neutrinos in the SM. And even if we expanded the SM to accommodate for RH neutrinos, we would still have to explain why their mass is so many orders of magnitude smaller than all other masses in the SM.

What about the case in which neutrinos are Majorana particles? Recalling Eq. (4.15), we see that for a Majorana neutrino (using now ν_L instead of ψ) the mass term in the Lagrangian would be

$$\mathcal{L}_m = -\frac{m}{2}\left[\overline{(\nu_L)^c}\nu_L - \overline{\nu_L}(\psi_L)^c\right] = -\frac{m}{2}\left[(\nu_L)^T C\nu_L + h.c.\right] \tag{4.18}$$

This Majorana mass term does not require the existence of RH neutrinos. Yet this does not mean that Majorana masses for neutrinos can be included trivially within the SM. The problem is that a $SU(2)_L$ transformation of ν_L would not leave (4.18) invariant. Therefore, we would need something similar to the Higgs mechanism or an effective operator to generate (4.18). However, it turns out that none of these options can be implemented within the SM without violating gauge invariance, Lorentz invariance, or renormalizability [50]. The conclusion is that it is not possible to consistently introduce neutrino mass terms under the rules of the SM.

One simple and very appealing BSM solution is the introduction of RH neutrinos ν_R and the seesaw mechanism. With ν_R, Dirac mass terms can be generated by the Higgs mechanism just like for all other particles, and with the seesaw mechanism we explain the smallness of the neutrino masses. Since the RH neutrinos are singlets with respect to all SM gauge groups, Majorana mass terms are allowed with no restrictions. For the LH neutrinos, Majorana mass terms stay forbidden as they violate gauge invariance. For simplicity, we will consider only one single neutrino flavour. The part of the Lagrangian containing the mass terms for neutrinos can be written as

$$\mathcal{L}_m = -\bar{\nu}_L m_D \nu_R - \frac{1}{2}\,\nu_R^T\, C\, m_R\, \nu_R + h.c. \tag{4.19}$$

Here we refer to m_D as the *Dirac mass* and m_R as the *right-handed Majorana mass*. Now we define $\nu := (\nu_L, (\nu_R)^c)^T$, and using $(\nu_{R,L})^c = (\nu^c)_{L,R}$ we can rewrite Eq. (4.19) in a matrix form as follows:

$$\mathcal{L}_m = -\frac{1}{2}\,\overline{\nu^c}\,\mathcal{M}\,\nu + h.c. = -\frac{1}{2}\,\nu^T C\,\mathcal{M}\,\nu + h.c., \tag{4.20}$$

where $\mathcal{M}$ is the neutrino mass matrix, defined as

$$\mathcal{M} = \begin{pmatrix} 0 & m_D \\ m_D & m_R \end{pmatrix}. \tag{4.21}$$

With an appropriate rotation of the neutrino vectors we can change to a basis in which the mass matrix is diagonal. Let us call the orthogonal rotation matrix U. We can parametrize it with an angle θ:

$$U = \begin{pmatrix} \cos\theta & \sin\theta \\ -\sin\theta & \cos\theta \end{pmatrix} \tag{4.22}$$

Since U is orthogonal, we can introduce $U\,U^T$ in both sides of the mass matrix in Eq. (4.20) to get

$$\mathcal{L}_m = -\frac{1}{2}\,\nu^T U\, C\, U^T \mathcal{M} U\, U^T \nu + h.c. \tag{4.23}$$

$$= -\frac{1}{2}\,(U^T\nu)^T\, C\, U^T \mathcal{M} U\, (U^T\nu) + h.c. \tag{4.24}$$

We immediately recognise the diagonalized mass matrix $\mathcal{M}_d = U^T \mathcal{M} U$ and the neutrino mass eigenstates $N = U^T \nu$. For U to be the correct diagonalizing matrix, θ must satisfy

$$\tan(2\theta) = \frac{2m_D}{m_R}. \tag{4.25}$$

The mass eigenvalues are

$$\tilde{m}_{1,2} = \frac{m_R}{2} \mp \sqrt{\frac{m_R^2}{4} + m_D^2}. \tag{4.26}$$

If we consider the case in which $m_R \gg m_D$ (or equivalently $\theta \ll 1$) we finally obtain the neutrino *seesaw*:

$$\tilde{m}_1 \simeq -\frac{m_D^2}{m_R}, \qquad \tilde{m}_2 \simeq m_R. \tag{4.27}$$

The unexpected (-) sign in $\tilde{m}_1$ is actually the $\hat{C}$-conjugation phase factor $\eta = \pm 1$. The physical masses are of course positive, $m_i = \tilde{m}_i \cdot \eta_i$, so we have

$$m_1 \simeq \frac{m_D^2}{m_R}, \qquad m_2 \simeq m_R. \tag{4.28}$$

Now we see how the seesaw mechanism easily explains the smallness of the (active) neutrino masses. The natural thing to expect is the Dirac mass m_D, which arises through the Higgs mechanism by spontaneous symmetry breaking, to be within the same range as the rest of the fermion masses. At the same time, there is no restriction on the Majorana mass of the RH neutrino at all [5]; m_R can be as high as the Planck scale. Equation (4.28) tells us that, in the seesaw limit, we have one very light neutrino mass eigenstate, and one very heavy mass eigenstate. For example, for a Majorana mass in the GUT scale $m_R = 10^{15}\,\text{GeV}$ and a Dirac mass in the electroweak (EW) scale $m_D = 10^2\,\text{GeV}$, the active neutrino mass would be $m_1 \sim 10^{-9}\,\text{GeV} \sim 1\,\text{eV}$.

As for the neutrino mass eigenstates $N = (N_1,\, N_2)^T$, we see that they are a linear combination of the interaction eigenstates $\nu = (\nu_L,\, (\nu_R)^c)^T$.

$$\begin{aligned} N_1 &= +\cos(\theta)\,\nu_L + \sin(\theta)\,\nu_R^c, \\ N_2 &= -\sin(\theta)\,\nu_L + \cos(\theta)\,\nu_R^c. \end{aligned} \tag{4.29}$$

This is similar to the phenomena of light neutrino oscillations. Neutrinos are created in weak interactions as eigenstates of the interaction operator, but they propagate as mass eigenstates. From Eq. (4.29) it is clear that the neutrino interaction eigenstates can be written as a linear combination of the mass eigenstates ($\nu = U \cdot N$), whose time evolution is given by a factor of $\exp(-iE(m_i)t)$. Thus, if we try to detect a neutrino of flavour α after a certain propagation length, there is a non-zero

[5] Usually, m_R is generated at the GUT scale due to the breaking of the GUT symmetry

probability that we will find it as a different interaction eigenstate as it was created, $P(\nu_\alpha \to \nu_\beta) \neq 0$ (we will discuss this in more detail in the next section).

Notice that since we are assuming $\theta \ll 1$, we have $N_1 \simeq \nu_L$ and $N_2 \simeq \nu_R^c$. So we have a very light mass eigenstate, that is mostly composed of ν_L and a very heavy mass eigenstate mostly composed of ν_R^c.

In this section, we have worked out the simple case of only one neutrino generation, and (4.29) describes oscillations between one LH and one RH neutrinos. In reality there are three active neutrinos in the SM and the most natural extension for RH neutrinos would include three of these[6]. This would mean that $\nu = (\nu_L,\, (\nu_R)^c)^T$ has actually 6 components, where ν_L contains all three LH flavours and $(\nu_R)^c$ respectively. The Dirac and Majorana masses in $\mathcal{M}$ would actually be themselves 3×3 matrices, and the diagonal matrix $\mathcal{M}_d$ computed here would be only block-diagonal, with eigenvalues $\tilde{m}_{1,2}$ also being 3×3 matrices, nameley

$$\tilde{m}_1 \simeq -m_D\, m_R^{-1}\, m_D^T, \qquad \tilde{m}_2 \simeq m_R. \tag{4.30}$$

So clearly, further diagonalization of $\tilde{m}_{1,2}$ would lead to oscillations between the three LH (active) neutrinos among themselves. These are the oscillations that have been observed in [47, 48].

4.4. Neutrino oscillations - a quick overview

In this section we want to continue the discussion we motivated at the end of the last section and review the basics about neutrino oscillations. This phenomena arises if the flavour eigenstates, in which neutrinos are created and detected, are not identical to the mass eigenstates. Thus, a necessary condition for this to occur, is that the neutrino masses are not allowed to vanish (more precisely, not all neutrino masses are allowed to be degenerate). Also, a consequence of neutrino oscillations is that only the total lepton number L will still be conserved, but the individual flavour-lepton number L_α will not [49]. Therefore, the observation of neutrino oscillations in the atmospheric and solar neutrino fluxes [47, 48] is the first indisputable laboratory evidence for BSM physics. For us, this is relevant because some of the most simple and appealing BSM models that have been developed to explain the origin of the neutrino masses (and with that, neutrino oscillations), also suggest viable dark matter candidates.

For the phenomenological description that we will discuss in this section, a quantum mechanical treatment is sufficient. We will be using neutrino flavour eigenstates $|\nu_\alpha\rangle$ and mass eigenstates $|N_i\rangle$ instead of field operators. For a detailed comparison of the quantum mechanical approach and the full quantum field theoretical treatment, see [52] and references therein.

As we will see, neutrino oscillations occur differently for neutrinos propagating in vacuum and through matter, because in the presence of a background medium, the neutrinos can undergo interactions which affect the oscillatory behaviour. We will first concern ourselves with oscillations in vacuum.

[6]This would establish a quark-lepton symmetry, where every LH fermion has a RH partner.

4.4.1. Neutrino oscillations in vacuum

In this section we will be following a similar treatment to that by Zuber, [53].

We begin by considering the general case of n generations of LH neutrinos, leading to a set of n flavour and another set of n mass eigenstates, which we will refer to as $|\nu_\alpha\rangle$ and $|N_i\rangle$ respectively. Each set constitutes a complete basis of the Hilbert space. The mapping between them is given the unitary transformation matrix U as follows:

$$|\nu\rangle = U \cdot |N\rangle = \sum_{i=1}^{n} U_{\alpha i}|N_i\rangle. \tag{4.31}$$

Here, $|\nu\rangle$ and $|N\rangle$ are n dimensional vectors containing the individual states $|\nu_\alpha\rangle$ and $|N_i\rangle$ respectivly. The number of independent variables of such a unitary $n \times n$ matrix differs for Dirac and Majorana neutrinos by the number of CP violating phases. There are $n\,(n-1)/2$ mixing angles and $(n-1)(n-2)/2$ phases in the Dirac case, and $n\,(n-1)/2$ in the Majorana case. So in the simplest case of $n = 2$, which is also the most frequently discussed, there is only one mixing angle and no CP phase for Dirac neutrinos (and one CP phase for Majorana neutrinos); for $n = 3$ we would have three mixing angles and one Dirac CP phase and two possible Majorana CP phases.

The time evolution of a neutrino state is given by the multiplying factor of $e^{-iE\,t}$, where the energy $E = \sqrt{p^2 + m^2}$ depends on the mass. Therefore, in order to properly describe the time evolution of an arbitrary neutrino state, it is best to express that state in terms of mass eigenstates. Lets assume that, in an electroweak interaction, a neutrino of flavour α is created at time-space coordinates $(t_0, x_0) = (0, 0)$. At a later time and place we would have

$$|\nu_\alpha\rangle \overset{t,x}{\rightarrow} |\nu(t,x)\rangle = \sum_{i=1}^{n} U_{\alpha i} e^{-i(E_i t - p_i x)}|N_i\rangle. \tag{4.32}$$

Now we want to calculate the probability of measuring and finding this neutrino in a different flavour state as it was created, say in flavour $\beta \neq \alpha$. For that, the first step would be to expand $|N_i\rangle$ in flavour eigenstates, after which we are left with

$$|\nu(t)\rangle = \sum_{i,\gamma} U_{\alpha i} U^*_{\gamma i} e^{-i(E_i t - p_i x)}|\nu_\gamma\rangle. \tag{4.33}$$

Then, using $\langle\nu_\beta|\nu_\gamma\rangle = \delta_{\beta\gamma}$, the probability amplitude is

$$A_{\alpha\to\beta}(t) = \langle\nu_\beta|\nu(t)\rangle = \sum_{i,\gamma} U_{\alpha i} U^*_{\gamma i} e^{-i(E_i t - p_i x)}\langle\nu_\beta|\nu_\gamma\rangle \tag{4.34}$$

$$= \sum_{i} U_{\alpha i} U^*_{\beta i} e^{-i(E_i t - p_i x)}. \tag{4.35}$$

Since we know that the mass of the neutrinos is extremely small, it is safe to use a relativistic approximation for the momentum p, namely

$$p_i \approx E_i + \frac{m_i^2}{2E_i}. \tag{4.36}$$

For relativistic particles and using natural units, we can replace $t = x =: L$, defining the *baseline* L. Also, since the energy is much larger than the mass for all neutrinos, it is customary to replace E_i by a neutrino energy independent of the mass eigenstate, $E_i \to E$. With this changes, the oscillation amplitude reduces to

$$A_{\alpha\to\beta}(t) = \sum_i U_{\alpha i} U^*_{\beta i} e^{-i(m_i^2\, L/2E)}, \tag{4.37}$$

and the oscillation probability

$$\begin{aligned} P_{\alpha\to\beta}(t) &= |A_{\alpha\to\beta}|^2 = A^*_{\alpha\to\beta} A_{\alpha\to\beta} \\ &= \sum_{i,j} U_{\alpha i} U^*_{\beta i} U_{\beta j} U^*_{\alpha j} e^{-i(\Delta m^2_{ij}\, L/2E)} \\ &= \sum_i |U_{\alpha i} U^*_{\beta i}|^2 + 2\mathrm{Re} \sum_{i<j} U_{\alpha i} U^*_{\beta i} U_{\beta j} U^*_{\alpha j} e^{-i(\Delta m^2_{ij}\, L/2E)}. \end{aligned} \tag{4.38}$$

Where in the second line we have defined $\Delta m^2_{ij} = m^2_i - m^2_j$. The first term in (4.38), which is time-independent, is actually the time (or energy averaged) oscillation probability (i.e. the second term vanishes when averaging); it is just the transition probability from flavour α to β without taking propagation effects into account. The second term, which varies in time through the propagation length L, is responsible for the oscillatory behaviour. The oscillation phase is $\Delta m^2_{ij} \frac{L}{2E}$. Let us note the following important points:

- Oscillations only take place if $\Delta m^2_{ij} \neq 0$, i.e. if not all masses are degenerate.
- Observing neutrino oscillations will tell us nothing about the absolut masses of the neutrinos.
- The factor L/E in the oscillation frequency can be used to investigate the features of the oscillations in experiments.

Let us now take a closer look at the special cases with $n = 2$ and $n = 3$ neutrino generations, which are of high practical relevance.

The case of $n = 2$ generations

The case of $n = 2$ is still widely used in the literature and is of high pedagogical value. As we stated above, here there is only one mixing angle and no Majorana phase; the transformation matrix is (4.22). The oscillation probability reduces to

$$P_{\alpha\to\beta} = \sin^2(2\theta) \cdot \sin^2\left(\frac{\Delta m^2_{ij} L}{4E}\right). \tag{4.39}$$

The first factor $\sin^2(2\theta)$ sets the amplitude of the oscillations and the second factor drives the oscillations. The survival probability is

$$P_{\alpha\to\alpha} = 1 - \sin^2(2\theta) \cdot \sin^2\left(\frac{\Delta m^2_{ij} L}{4E}\right). \tag{4.40}$$

It is easy to validate the points mentioned above.

The case of $n = 3$ generations

The case of $n = 3$, which is of course much more realistic, is unfortunately also more intricate. Here we have three mixing angles θ_i with $i = 12, 23, 13$ and, in the case of Dirac neutrinos, one Dirac CP phase δ. One possible parametrization for the unitary matrix U is

$$U = \begin{pmatrix} 1 & 0 & 0 \\ 0 & c_{23} & s_{23} \\ 0 & -s_{23} & c_{23} \end{pmatrix} \cdot \begin{pmatrix} c_{13} & 0 & s_{13}e^{-i\delta} \\ 0 & 1 & 0 \\ -s_{13}e^{i\delta} & 0 & c_{13} \end{pmatrix} \cdot \begin{pmatrix} c_{12} & s_{12} & 0 \\ -s_{12} & c_{12} & 0 \\ 0 & 0 & 1 \end{pmatrix}, \tag{4.41}$$

where we have defined

$$s_{ij} = \sin(\theta_{ij}), \qquad c_{ij} = \cos(\theta_{ij}). \tag{4.42}$$

For Majorana neutrinos we have two additional CP Majorana phases φ_1 and φ_2, which come in by multiplying (4.41) with $\mathrm{diag}(1, \exp(i\varphi_1/2), \exp(i\varphi_2/2))$ from the right. The resulting mixing matrix in (4.41) is called the *PMNS matrix* and is analogue to the CKM matrix for quark mixing (which can be found in any QFT book and will not be needed in the course of this work). The general form of the oscillation probabilities in this scenario is rather complicated and will not be needed here; approximations for limiting cases, e.g. a quasi mass degeneracy and specific mass ordering, can be made, see e.g. [53].

4.4.2. Neutrino oscillations in matter

For neutrinos propagating through a matter background instead of vacuum, the oscillation behaviour is modified, which can be quiet drastic in some situations. As we will see, under certain conditions a resonance effect may drive the probability for neutrino flavour oscillations to a maximal value even if the vacuum mixing angle is very tiny. This resonance is due to the so-called *Mikheyev-Smirnov-Wolfenstein effect* (MSW effect), named in honour its discoverers [54, 55]. It probably plays a decisive role in the propagation and flavour conversion of neutrinos in the Sun and, in the context of active-sterile neutrino oscillations and sterile neutrino dark matter, it also may be involved in the production of sterile neutrinos in the early Universe [56, 57]. In this section we want to qualitatively understand the effects of matter in the propagation and flavour oscillations of neutrinos. For a more detailed description see [49, 53, 50].

For simplicity, we will be discussing only two neutrino generations. As we learned in the previous section, the origin of the oscillations is the fact that the flavour eigenstates are a linear combination of the mass eigenstates which, having non-degenerate masses, evolve differently with time, namely by the factor e^{-iE_it}. In the quantum mechanical approximation, this factor for the time evolution is a result of the Schrödinger equation of motion

$$i\frac{d\nu}{dt} = \hat{H}(t)\nu, \tag{4.43}$$

with $\hat{H}$ as the Hamilton operator (or *Hamiltonian*). In the presence of matter, propagating neutrinos may be subject to interactions with the neutrinos present in the background medium (see equation (4.5)). This interactions would generate mean potentials which would contribute to the Hamiltonian for neutrinos in matter $\hat{H}_m$, such that it would differ from the case in vacuum. The most relevant reactions are coherent forward scatterings of the type $\nu_\alpha + f \to \nu_\alpha + f$, which can occur through Z^0 or $W^\pm$ exchange, i.e. in NC or CC interactions respectively. All neutrino flavours scatter of electrons in NC processes with the same cross section, which means that the potential induced by the NC interactions is the same for all flavours. Therefore, the NC potential has no effect on flavour oscillations, because it treats all neutrino flavours democratically. However, since electrons are the only charged leptons available in large quantities in normal matter, the CC interactions are only available for ν_e, while $\nu_{\mu,\tau}$ can only participate in NC processes. Therefore, only ν_e induces an additional CC-potential in $\hat{H}_m$. Thus, the neutrino mass eigenstates for the propagation in vacuum are not eigenstates for the propagation in matter.

Since we are now dealing with interactions, it is better to start in the interaction basis. The vacuum Hamiltonian, which was diagonal in the mass basis, is transformed into the interaction basis by the unitary matrix U,

$$\hat{H}_{\mathrm{v}}^{\alpha} = U\, \hat{H}_{\mathrm{v}}^{m}\, U^{\dagger}, \tag{4.44}$$

where $\hat{H}_{\mathrm{v}}^{\alpha}$ stands for the vacuum Hamiltonian in the flavour basis, and $\hat{H}_{\mathrm{v}}^{m}$ is the vacuum Hamiltonian in the mass basis. Adding the CC-potential $V_{CC} = \sqrt{2} G_F\, N_e$ (N_e stands for the electron number density) in the appropriate position to $\hat{H}_{\mathrm{v}}^{\alpha}$, we obtain the matter Hamiltonian in the flavour basis[7] $\hat{H}_{\mathrm{m}}^{\alpha}$ [50]. Considering only two neutrino generations, it reads

$$\hat{H}_{\mathrm{m}}^{\alpha} = \begin{pmatrix} -\frac{\Delta m^2}{4E}\cos(2\theta) + \sqrt{2} G_F\, N_e & \frac{\Delta m^2}{4E}\sin(2\theta) \\ \frac{\Delta m^2}{4E}\sin(2\theta) & \frac{\Delta m^2}{4E}\cos(2\theta) \end{pmatrix}, \tag{4.45}$$

where θ is the vacuum mixing angle. The effective Hamiltonian $\hat{H}_{\mathrm{m}}^{\alpha}$ can be diagonalized with a new unitary matrix $\tilde{U}$ which has the same structure as U but a different mixing angle, which we name θ_m. The mass eigenstates in matter $\nu_{1,m}$, $\nu_{2,m}$ are different to those in vacuum. The transition probability has the same structure as in vacuum, except we replace $\theta \to \theta_m$. The oscillation amplitude (see equation (4.39)) $\sin^2(2\theta_m)$ can be written as a function of θ, N_e and $\Delta m^2/2E$:

$$\sin^2(\theta_m) = \frac{(\Delta m^2/2E)^2 \sin^2(2\theta)}{[(\Delta m^2/2E)^2 \cos(2\theta) - \sqrt{2} G_F N_e]^2 + (\Delta m^2/2E)^2 \sin^2(2\theta)}. \tag{4.46}$$

This equation as a function of N_e has the form of a *Breit-Wigner resonance*. If the condition

$$\left(\frac{\Delta m^2}{2E}\right)^2 \cos(2\theta) = \sqrt{2} G_F N_e \tag{4.47}$$

[7] We do not include the mean potentials induced by the NC interactions in the matter Hamiltonian, because they do not contribute to neutrino oscillations.

is satisfied, then Eq. (4.46) equals $\sin^2(2\theta_m) = 1$, i.e. maximal oscillation amplitude for all values of $\theta \neq 0$, regardless how tiny. This is the MSW resonance. It tells us that propagating in matter, even if the vacuum mixing angle is extremely small, neutrino flavour oscillations may still occur to a significant degree if the electron neutrino density in the medium is such that the MSW condition (4.47) holds. It might seem that this would require fine tuning, yet for matter with an adiabatically varying electron density that is not necessarily the case. If the neutrinos are created in a region of high electron density $N_{e,i}$ which adiabatically decreases along the propagation line of the neutrinos, it is possible that along the way they encounter a layer where the local density $N_{e,\mathrm{loc}} = N_{e,\mathrm{MSW}} \ll N_{e,i}$ suits the MSW condition (4.47). In that case the MSW resonance acts to efficiently drive flavour oscillations. Whether the density gradient is adiabatic or not is quantified by the adiabaticity parameter, which is defined as [50]

$$\gamma := \frac{|E_{1,m} - E_{2,m}|^3}{(\Delta m^2/2E)\sin(2\theta) \cdot |\dot{V}_{CC}|}, \tag{4.48}$$

where $E_{i,m}$ is the energy of the i'th mass eigenstate in matter and $\dot{V}_{CC}$ is the time derivative of the effective matter CC potential. The adiabaticity requirement is fulfilled if $\gamma \gg 1$, which, in practical terms, means that the thickness of the layer of matter where Eq. (4.47) is satisfied is at least as large as one oscillation length in matter [50]. It is assumed that this is the case in matter [49].

With this, we conclude this chapter on neutrinos and return to our core business: dark matter.

5. Sterile neutrinos as Dark Matter

Now that we have discussed the phenomenology of active neutrinos in the SM and understand how neutrino oscillations point to the existence of BSM physics by demanding a mass-generation mechanism, we can finally return to the problem of the identity of dark matter. As we have learned in the previous chapter, one of the most appealing mechanisms to generate neutrino masses is the seesaw mechanism, in which RH neutrinos are introduced. These are SM gauge singlets which, by the quality of being neutral particles, are allowed to have a Majorana mass without violating the gauge invariance of the theory. If RH neutrino exists and are responsible for the masses of the active neutrinos, could they also be related to dark matter? The RH neutrino would be massive, electrically neutral and interact even more feebly with the rest of the SM than active neutrinos (which is why they are also called sterile neutrinos). These are already three indispensable properties of a dark matter candidate. The requirements left to be fulfilled are, in rough terms:

1. Particle longevity. Since dark matter has to be around since the very early Universe and still exist today, a good dark matter candidate should be stable on cosmological time scales, i.e. its lifetime should be at least as long as the age of the Universe.

2. Correct abundance. As we discussed in chapter 2, we know rather well from the CMB analysis how much dark matter exists. Therefore, a good dark matter candidate must be produced in the early Universe to the right amount if is to make up 100% of the dark matter mass density[1]. However, it is possible that the dark matter density gets contributions from multiple components, i.e. there is not one single dark matter particle species, but many. In this case, the dark matter candidate still may not be over-produced in the early Universe unless its density is reduced to the correct amount before recombination (see section 2.5).

3. Comply with experimental constrains. There exist many experiments and observations that constrain the allowed parameter space for many dark matter models. Obviously, a good dark matter candidate may not be already ruled out by experiments.

Since RH neutrino are almost decoupled from the SM, producing them by interactions in the early Universe is non-trivial. In the most conservative models in which

[1]Indeed, there is a number of known objects that certainly contribute to the dark matter density, e.g. active neutrinos, black holes, MACHOS (massive astrophysical halo object). However, the contribution from these objects is estimated to be very small.

RH neutrinos are the only new particles introduced to implement the seesaw mechanism, they only couple through their Yukawa couplings with the Higgs boson and the LH leptons before symmetry breaking, and through their mass mixing with active neutrinos after symmetry breaking. Therefore, establishing and maintaining thermal equilibrium might not be an option. In this chapter we will investigate if the RH neutrino could tick all the boxed and be a promising dark matter candidate.

5.1. Majorana mass scale

Our starting point is the seesaw Lagrangian, which contains the kinetic term for the RH neutrinos, the Yukawa couplings between the neutrinos, leptons and the Higgs boson and the Majorana mass term for the RH neutrinos:

$$\mathcal{L}_\nu = i\,\bar{\nu}_R\,\gamma^\mu\partial_\mu\,\nu_R - \bar{l}\,h\,\tilde{\phi}\,\nu_R - \frac{1}{2}m_R\bar{\nu}_R^c\nu_R + h.c. \tag{5.1}$$

Here, l stands for the $SU(2)_L$ lepton doublet, ϕ is the Higgs boson, and h is the matrix of Yukawa couplings. In general, the number of RH neutrinos is not constrained, but for most of the discussion we are interested in, is suffices to focus only on a single RH neutrino.

After electroweak symmetry breaking, the Higgs relaxes at a non-vanishing vacuum expectation value (VEV) $\langle\phi\rangle = (0, v)^T$, which together with the Yukawa matrix, generates the Dirac mass matrix, $m_D = h\,v$. In the case of only one neutrino generation, m_D would be scalar. As we saw in section 4.3, the smallness of the active neutrino masses can be explained by a very large Majorana mass in the seesaw framework. But how large do we need the Majorana mass m_R to be? Since ν_R is a gauge singlet, the Majorana mass term does not violate gauge invariance and is therefore allowed to exist as a bare mass term. However, it could also be generated by the VEV of another scalar boson similar to the Higgs, conventionally referred to as S (see subsection 5.3.3). In any case, there is no restriction on the scale of the Majorana mass, but there are some ranges which seem better motivated than others. These are the scale of Grand Unified Theories (GUTs) and the electroweak (EW) scale. In the first case, Majorana masses around the GUT scale and active neutrino masses in the sub-eV range, imply a value of order unity for the Yukawa coupling $h \sim \mathcal{O}(1)$, which is very natural for a Yukawa coupling [58]. Also, the Majorana scale could be signalling a relationship between neutrino physics and a GUT theory. Indeed, GUT models, such as those motivated by the $SO(10)$ group, often include ultra heavy RH Majorana neutrinos [59]. On the negative side, if the Majorana scale is this high, it could be impossible to directly produce RH neutrinos in the lab [58]. Moreover, such a high mass scale in combination with a $\mathcal{O}(1)$ Yukawa coupling for the RH neutrino establishes a (strong) hierarchy problem [60]. In the second case, the Majorana mass could be generated by another scalar boson S which has a VEV at the EW scale, just like the Higgs boson [61]. This is attractive because it does not add to the hierarchy problem in the SM and the Majorana scale would be within experimental reach, but also because dark matter production and baryogenesis through leptogenesis is achievable [62]. As a setback, the neutrino Yukawa coupling would have to be much smaller

than the other SM Yukawas in order to generate the right orders of magnitude for the $SU(2)$ neutrino masses [34].

Since our we are interested in dark matter, let us now take a moment to discuss the relevant Majorana mass ranges.

GeV-TeV Majorana Masses

Sterile neutrinos with masses in this range may play different roles depending their other properties, most importantly on their lifetime. Such neutrinos are not entirely stable; depending on their mass, tree level decays of the type $\nu_R \to \phi + l$ are kinematically allowed. For a non-vanishing mixing angle with active neutrinos, decays through loop diagrams are also allowed. If the lifetime of such heavy neutrinos is short, their decays in the early Universe might be responsible the generation of a lepton asymmetry and lead to baryogenesis, if the Sakharov criteria are satisfied [63]. For this to work, the heavy neutrinos would have to decay before the onset of nucleosynthesis in order not to spoil the cosmic chemistry. If they decay while the sphalerons[2] are still in thermal equilibrium with the rest of the plasma, the lepton asymmetry can be transferred to the baryonic sector, thus explaining the baryon asymmetry of the Universe (BAU) [64]. Indeed, this occurs in the neutrino Minimal Standard Model (νMSM), where two heavy RH neutrinos in this mass range decay in the early Universe [65]. If they are degenerate in mass, the right baryon asymmetry can be generated thanks to resonance effects. In other models this can also be achieved without mass degeneracy [66].

If sterile neutrinos with masses in this range are somehow long lived on cosmological timescales, they could potentially contribute to the dark matter density of the Universe. Through the Yukawa interaction in (5.1), sterile neutrinos may decay into a Higgs boson and a lepton, or by its mixing with active neutrinos, it could decay into three active neutrinos or a neutrino and a photon. The requirement of long lifetime for neutrino dark matter implies that the Yukawa coupling (or equivalently, the mixing angle) must be very tiny. This means that sterile neutrinos probably could not reach thermal equilibrium in the early Universe, thus placing constrains on possible production mechanisms, while also making it more challenging to produce them in laboratory experiments. In any case, the decay products should manifest themselves as an excess signal in the cosmic ray background. For a review on the bounds from indirect searches of decaying dark matter with mass in the GeV-TeV range, see reference [67].

keV Majorana Masses

Sterile neutrinos with masses in this range have been intensely studied in recent years because they could be viable dark matter candidates. As we mentioned at the beginning of this chapter, for sterile neutrinos to be dark matter, they have to be long

[2]The sphaleron is a non-perturbative solution to the field equations of the EW theory. In sphaleron processes, the difference between baryon number and lepton number $B - L$ is conserved while their sum $B + L$ is not.

lived, produced to the right amount and agree with experimental constrains. Sterile neutrinos with $m_R \sim$ keV are attractive because they potentially comply with all these conditions. As we will later discuss in detail, there are multiple mechanisms capable of producing this type of dark matter in the correct amount. These involve resonant and non-resonant oscillations, out of equilibrium decays of additional particles coupled to the RH neutrinos, and even thermal production is conciavable [68].

The direct decay to a Higgs boson and a lepton is kinematically forbidden, but one-loop decays into active neutrinos or photons are possible. Also, since the mass would be comparable to that of other SM particles, these RH neutrinos could be observed in accelerators or oscillation experiments. Therefore, this type of dark matter can be potentially discovered or ruled out, making it even more attractive. The νMSM model, also contains a keV sterile neutrino which plays the role of the dark matter while the other two sterile neutrinos have masses in the GeV range and are responsible for baryogenesis through leptogenesis and the masses of the active neutrinos.

In section 3.4 we have briefly discussed the distinction between *cold* dark matter (CDM), which was non-relativistic at the moment of production, and *hot* dark matter (HDM), which was relativistic when produced. Whether the Universe produced CDM or HDM has a noticeable effect on the size (or scale) of structures that were allowed to grow from early on. HDM, by its quality of being relativistic, impedes the growth of structures smaller than a certain scale, called its *free-streaming length* (this process is referred to as *free streaming* or *wash-out*) [22]. On the other hand, CDM supports the growth of density perturbations of all scales. Interestingly, keV sterile neutrinos could be produced as relativistic particles and later slow down to be non-relativistic while still in the radiation dominated era. This type of dark matter is called *warm dark matter* (WDM). It still suppresses the growth of structures on scales below a certain cutoff, however less drastically than HDM, and the dynamics at later times are the same as for CDM. For a long time, cosmological models containing CDM have been favoured because they are better at explaining cosmological structures at large scales. However, recent observations and simulations seem to challenge the CDM model on galactic scales. In short, dark matter simulations disagree with observations at short cosmological scales on the shape of galactic dark matter halos and the density of dwarf satellite galaxies [69, 70, 71]. Even though these discrepancies are controversial and could be the result of imperfections in the simulations [72], if they are real, they could be resolved by keV sterile neutrino WDM [73]. Furthermore, sterile neutrinos in this mass range, if produced out of equilibrium, can have a non-thermal distribution function with large contributions in both the low and high momentum regions, i.e. as a mixture of warm and cold components [68].

As we have seen, there are plenty of reasons for studying keV sterile neutrinos as dark matter. Let us continue by looking into the current bounds in the sterile neutrino parameter space.

5.2. Observational constrains on keV sterile neutrinos

There are multiple astrophysical observations that can be made to constrain the mass and mixing angle parameter space of keV sterile neutrino dark matter. Luckily, the different methods close the parameter space from different directions, thus leaving a well defined window where this dark matter candidate can be searched for.

5.2.1. The Tremaine-Gunn lower mass bound

This bound is obtained by analysing the phase space density for dark matter in compact galaxies. The argument, which holds for any fermionic dark matter candidate χ, is formulated as follows [74].

Since we know that dark matter particles must form halos around galaxies, their velocity distribution should keep them inside the halos (otherwise the halos would disolve). A good approximation is given by a Maxwell distribution

$$F_\chi(\vec{v}) = \frac{1}{(\sqrt{2\pi}\, m_\chi\, \sigma_\chi)^3}\, e^{-\vec{v}^{\,2}/2\sigma_\chi^2}, \tag{5.2}$$

with the dark matter mass m_χ and the dark matter velocity dispersion σ_χ. For dark matter in a galactic halo, the maximum of the phase space density, which is reached at $\vec{v}^{\,2} = 0$, is given by

$$f_\chi^{\max}(\vec{v}, \vec{x}) = \frac{\rho_\chi(\vec{x})}{m_\chi} F_\chi(0), \tag{5.3}$$

where $\rho_\chi(\vec{x})$ stands for the dark matter density in the halo. Because of the fermionic nature of the particles we are considering, the Pauli principle demands that $f_\chi^{\max}$ may not be greater than

$$f_\chi^{\text{crit}} = \frac{g_\chi}{(2\pi)^3}, \tag{5.4}$$

with g_χ the number of internal degrees of freedom. Together with Eq. (5.3), this gives us a model independent lower bound for the mass of a dark matter candidate:

$$\frac{(2\pi)^{3/8}}{g_\chi^{1/4}} \left(\frac{\rho_\chi}{\sigma_\chi^3}\right)^{1/4} \leq m_\chi. \tag{5.5}$$

The largest value for this bound is obtained by applying it to dwarf spheroidal galaxies (dSph), because they have the most compact and homogeneous halos. Ref. [75] concludes that

$$m_\chi \geq 0.4\,\text{keV} \tag{5.6}$$

after analysing multiple dSph galaxies.

If we specify an initial phase space distribution, which is usually determined by the production mechanism, we can improve this bound. The improvement, which comes at the cost of model dependence, is based on the premise that dark matter

particles are collisionless. For them, the Liouville theorem states that the phase space density is constant in time. Therefore, the phase space density today, averaged over a finite macroscopic region (e.g. a galactic center) $\tilde{f}(\vec{p}, \vec{x}, t)$, must not exceed the initial maximal value $f_{0,\max}$. Notice that this improvement on Eq. (5.6) has nothing to do with Fermi statistics or the Pauli exclusion principle, but simply arises from the principle of conservation of the phase space density. For sterile neutrinos, assuming production through non-resonant oscillations (see subsection 5.3.1), the following lower bound has been calculated [76]:

$$m_{\nu_R}^{\mathrm{NRP}} \gtrsim 6\,\mathrm{keV}. \tag{5.7}$$

5.2.2. The Lyman-α forest

As we have already mentioned above, keV sterile neutrinos could constitute WDM, and since WDM impedes the growth of structures at scales below its free streaming length, it should be possible to establish its presence by analysing the matter power spectrum at small scales. The presence of WDM would manifest itself by a suppression of the power spectrum at large momenta k (i.e. at small scales $\lambda \sim k^{-1}$) compared to the expectation for CDM [34]. For the comparison, the *transfer function* $T(k)$ is defined as the ratio of the power spectra for WDM and CDM, so we have

$$T^2(k) = \frac{P_{\mathrm{WDM}}(k)}{P_{\mathrm{CDM}}(k)} < 1 \qquad \text{for large } k. \tag{5.8}$$

The transfer function can be computed from simulations assuming a specific momentum distribution (which means that results are model-dependent), and the result depends on the dark matter particle's mass, as can be seen in Figure 5.1. Upon comparison with observations of the Lyman-α forest, this allows setting a lower bound on the mass m_χ.

The Lyman-α forest is produced when radiation from a source, typically a *quasi-stelar object*, or quasar (QSO), passes through the intergalactic medium, which is mainly neutral hydrogen, and the Lyman-α line of the hydrogen spectrum gets absorbed. Since the wavelength of the line is very precisely known, one can extract the redshift and density of the absorbing material and, with some additional assumptions, compute the power spectrum. With this method, small-to-medium cosmological scales in the range $z = 2 \sim 6$ can be probed, making it ideal to test the WDM hypothesis, because this is the region where it most clearly differs from the expected behaviour of CDM [74].

It is important to note that the Lyman-α forest does not directly place a bound on the dark matter mass, but only on the free streaming length of a dark matter particle. To translate that to a bound on the mass, one must make assumptions about the momentum distribution function of the dark matter. Often, it is assumed that it is proportional to the thermal distribution, which is reasonable depending on the production mechanism.

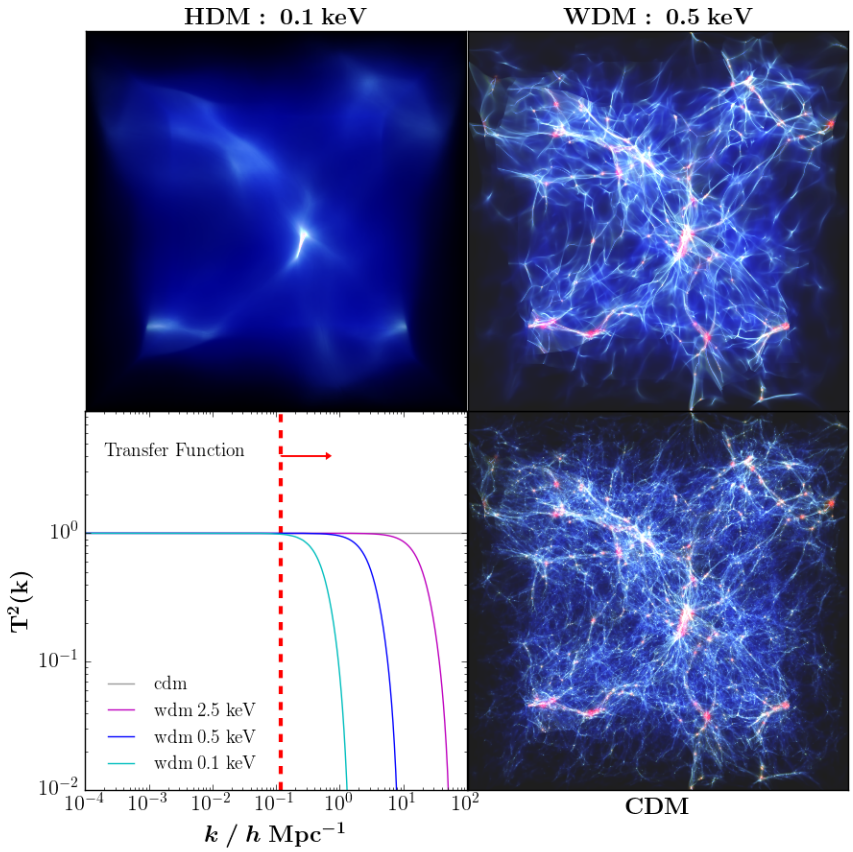

Figure 5.1.: In the lower-left panel, an approximation for the transfer function for different masses is shown. The region to the right of the vertical dashed line is what can be compared to the observed power spectrum by analysing the Lyman-α forest. In the other panels, the baryon density is visualised for $z = 2.5$ and boxes of the size $25\,h^{-1}\,\mathrm{Mpc}$ with 768^3 particles. The different effects from HDM, WDM and CDM (at the infinite mass limit) are evident. Figure from [77].

The most reliable results at the moment conclude that, for non-resonantly produced sterile neutrino dark matter [78],

$$m_\chi \geq 8\,\mathrm{keV} \qquad \text{at } 99.7\%\text{ C.L.}, \tag{5.9}$$

in a purely ΛCDM model, and, for the case in which dark matter is composed of a WDM+CDM mixture, any sterile neutrino mass is allowed if the WDM contribution is less than 60%.

For WDM with a thermal spectrum, Viel et al. report in Ref. [79], with state-of-the-art computations,

$$m_\chi \geq 3.3\,\mathrm{keV} \qquad \text{at } 2\sigma\text{ C.L.} \tag{5.10}$$

Let us conclude by saying that the Lyman-α analysis is still somewhat controversial and the observational and theoretical systematics are not yet fully understood [78].

5.2.3. Radiative decays and X-ray observations

If sterile neutrinos exist as in Equation (5.1) and have a non-zero mixing angle with the active neutrinos, then they are unstable and will decay into three active neutrinos, after transforming into an active neutrino by the active-sterile mixing. The Feynman diagram for this decay is shown in Figure 5.2. The total decay width has been computed in [81]. The result is

$$\Gamma_{\nu_R \to 3\nu_L} = \frac{G_F^2\, m_R^5}{96\pi^3} \sin^2(\theta) = \frac{\mathrm{s}^{-1}}{4.7 \cdot 10^{10}} \left(\frac{m_R}{50\,\mathrm{keV}}\right)^5 \sin^2(\theta), \tag{5.11}$$

with m_R the sterile neutrino's mass and θ the sterile-active mixing angle. For the sterile neutrino to be a serious dark matter candidate, we demand that its lifetime be at least as large as the age of the Universe $t_\mathrm{U} \simeq 4 \cdot 10^{17}\,\mathrm{s}$. This allows one to set a bound on the mixing angle [82],

$$\theta^2 < 1.1 \cdot 10^{-7} \left(\frac{50\,\mathrm{keV}}{m_R}\right)^5. \tag{5.12}$$

As expected, the longevity condition requires that for greater RH neutrino masses, the mixing angle with the active neutrinos be smaller.

However, a much more stringent constraint can be derived by the (non-)observation of the one-loop radiative decay $\nu_R \to \nu_L + \gamma$. The responsible diagrams can be seen in Figure 5.3. Because the propagators are inversely proportional to the masses of the charged leptons in the loops, the main contribution to the processes will be by those diagrams with electrons in the loops. The decay width for the processes in Figure 5.3 is given by [83, 74]

$$\Gamma_{\nu_R \to \gamma + \nu_L} = 5.5 \cdot 10^{-22} \sin^2(2\theta) \left(\frac{m_R}{1\,\mathrm{keV}}\right)^5 \mathrm{s}^{-1} \tag{5.13}$$

Dark matter particles in galactic halos that could decay in these processes are expected to have non-relativistic velocities, so we can approximate $E_{\nu_R} \simeq m_R$. Even

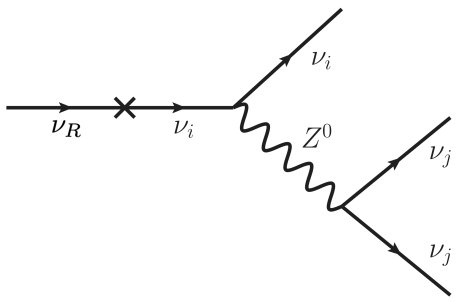

Figure 5.2.: Three body decay of a sterile neutrino [80].

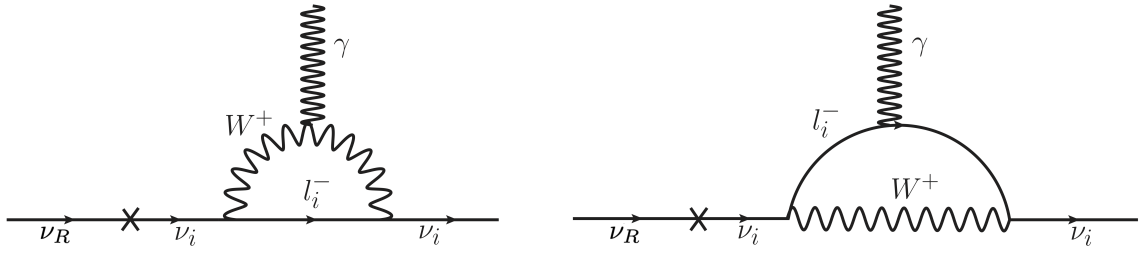

Figure 5.3.: One-loop radiative decays of sterile neutrinos [80].

though the three level decay is roughly 100 times more probable than the radiative decay, $\Gamma_{\nu_R \to 3\nu_L}/\Gamma_{\nu_R \to \gamma + \nu_L} \approx 1.2 \cdot 10^2$, the later is much easier to detect due to the produced photons. Since the active neutrino that is produced in the decay has a very tiny mass, the energy of the sterile neutrino is distributed almost equally among both of the decay products, so that the energy of the photon would be $E_\gamma = m_R/2$. This is potentially a smoking gun for the indirect detection of sterile neutrino dark matter. For keV masses, we expect an excess line in the X-ray portion of the electromagnetic spectrum.

One distinguishes between four different types of sources to look for the X-ray line [74]:

X-ray Background (XRB)
: Decays of keV sterile neutrino dark matter particles throughout the history of the Universe would create a background of redshifted X-ray lines. Because of the redshift effect, the decay line is broad and has a continuous tail.

Galaxy clusters
: Regions with very large dark matter overdensities, such as galaxy clusters would produce a sharp X-ray line at fixed redshift. The flux in this case is similar to that of the XRB.

Milky way halo
: The dark matter halo in our own galaxy would also produce a measurable flux. Since the dark matter density is maximal in the galactic core, this would be the natural place to look. Unfortunately, this is also the region with the greatest background noise.

dSph Galaxies
: Even though having much smaller amounts of dark matter mass, dwarf spheroidal galaxies have are more compact and less active cores. Thanks to their proximity to us, the flux is expected to be similar to that of far away galaxy clusters. Due to the absence of hot, X-ray emitting gas, a signal from a dSph satellite of the milky way would be a promising piece of evidence for dark matter decay.

The X-ray decay line has been searched for in all of these sources by many different and complementary X-ray telescopes, but it has not been convincingly detected. In

recent years, an excess signal at $E = 3.55\,\mathrm{keV}$ has indeed been seen in the spectra of many galaxy clusters, the Andromeda galaxy and our own galactic center [84, 85]. If this line is interpreted as the radiative decay of sterile neutrino dark matter, it would be implying a dark matter mass of $m_R \simeq 7.1\,\mathrm{keV}$. However, whether this interpretation is correct is still very much a matter of ongoing discussion. There are other possible explanations for the signal, e.g. the potassium line K XVIII at 3.51 keV [85]. Systematics, calibration or analysis errors are also possible. Furthermore, it has been reported that in measurements with very long exposure times, no signal is detected from the local galactic group [86]. Even more puzzling is the detection of the line from a supernova remnant, even though one would not have expected a dark matter decay line from it [85]. The fact that no signal has been observed from dSph galaxies is most depressing, as this would have been a clearer indication in favour of the dark matter interpretation.

In sum, Lyman-α and X-ray observations constrain the parameter space of sterile neutrino dark matter as shown in Figure 5.4

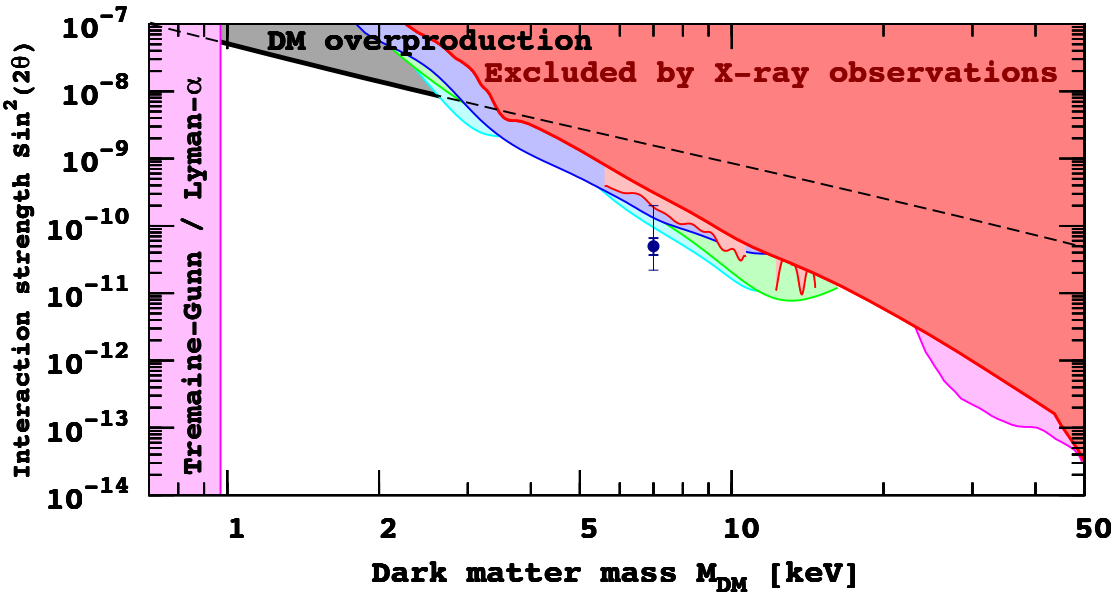

Figure 5.4.: Bounds on the sterile neutrino dark matter parameter space. The upper bound by dark matter overproduction is valid for non resonant production. Lower limits can also be raised by assuming a specific production mechanism. Figure from [74].

5.3. Production mechanisms

Sterile neutrinos are SM-gauge singlets, so the only possible interaction with the rest of the cosmic plasma in the early Universe would be through their Yukawa couplings.

For the masses and mixing angles allowed by the Lyman-α and X-ray bounds in Figure 5.4, and assuming a vanishing initial abundance, the sterile neutrinos are not expected to reach thermal equilibrium in the early Universe. Therefore, production by freeze-out from equilibrium is not considered feasible. In this last section we will comment briefly on the 3 most commonly studied mechanisms for producing keV sterile neutrinos as dark matter.

5.3.1. Non-resonant oscillations - Dodelson-Widrow mechanism

If sterile neutrinos exist and mix with the active neutrinos, as would certainly be the case if the seesaw mechanism is responsible for the masses of the light neutrinos, then they can be produced through non-resonant oscillations (NRP) between active and sterile neutrinos [56]. In fact, if the mixing angle is non-vanishing, then it is unavoidable that this mechanism contributes to the total sterile neutrino abundance. This means that if other mechanism were at work to produce sterile neutrino dark matter, then NRP must be complementary to those mechanisms.

We have discussed the occurrence of oscillations between sterile and active neutrinos in section 4.4. In the early Universe, oscillations occur as in matter with the cosmic plasma as the background medium, but the additional effective potentials are very different. With the effective mixing angle θ_m, the vacuum mixing angle θ and the neutrino momentum p, the oscillation amplitude is expressed as [74]

$$\sin^2(2\theta_m) = \frac{(\Delta m^2/2p)^2 \sin^2(2\theta)}{(\Delta m^2/2p)^2 \sin^2(2\theta) + [(\Delta m^2/2p)\cos(2\theta) - V_D - V_T]}, \tag{5.14}$$

where Δm^2 is the mass squared difference between the active and sterile states, V_T is the finite temperature potential and V_D is the finite density potential, which is $V_D \neq 0$ for a finite matter-antimatter asymmetry. The finite temperature potential is always negative and for $T \lesssim 100\,\mathrm{GeV}$ it can be written as [74]

$$V_T = -G_{\mathrm{eff}}\, p\, T^4, \tag{5.15}$$

with G_{eff} as an effective neutrino coupling constant in the plasma for all flavours. If at the moment of sterile neutrino production the matter-antimatter asymmetry has not yet been generated or is negligible, we can set $V_D = 0$ [87]. Then, the oscillation amplitude reduces to

$$\sin^2(2\theta_m) = \frac{(\Delta m^2/2p)^2 \sin^2(2\theta)}{(\Delta m^2/2p)^2 \sin^2(2\theta) + [(\Delta m^2/2p)\cos(2\theta) + G_{\mathrm{eff}}\, pT^4]} < 1. \tag{5.16}$$

The production rate prior to the EW phase transition is dominated by Higgs decays into a sterile neutrino and a lepton; it is proportional to the Yukawa coupling squared:

$$\Gamma \sim Y_\nu^2\, T \sim \frac{\theta^2 m_R^2}{v^2} T, \tag{5.17}$$

with v the Higgs' vacuum expectation value. Below the EW scale, the production occurs through oscillations; the NRP rate behaves as

$$\Gamma \sim G_F^2\, T^5\, \theta_m^2(T). \tag{5.18}$$

To get the relic abundance, the production rate has to be integrated over the age of the Universe [34]. The relationship between the final abundance, the mass and the Yukawa coupling (which is directly related to the mixing angle) is very different to the case of freeze-out from equilibrium (see section 3.1). Complete computations can be found in the literature, e.g. [88]. Within the relevant range for keV neutrinos, a viable approximation is [87]

$$\Omega_{\nu_R} \sim 0.2 \left(\frac{\sin^2 \theta}{3 \cdot 10^{-9}} \right) \left(\frac{m_R}{3\,\mathrm{keV}} \right)^{1.8}. \tag{5.19}$$

However, the Lyman-α bound (5.10), in combination with the X-ray bounds, have excluded the possibility that 100% of the dark matter was produced in form of sterile neutrinos by this mechanism [74].

5.3.2. Resonant oscillations - Shi-Fuller mechanism

Shi and Fuller showed that, if the lepton asymmetry has a substantial value at the relevant epoch, then resonant oscillations may enhance the sterile neutrino production [57]. This resonant production (RP) is essentially the result of a MSW effect, see subsection 4.4.2. The resonance condition for the density potential is

$$0 \overset{!}{=} (\Delta m^2/2p)\cos(2\theta) - V_D - V_T. \tag{5.20}$$

If this condition is fulfilled, the oscillation amplitude, Equation (5.14), is maximised independently of the value of the vacuum mixing angle θ. By approximating

$$\Delta m^2 \cos(2\theta) \approx m_R^2\,, \tag{5.21}$$

the resonance condition can be written as

$$m_R^2 \overset{!}{\approx} 2p\,V_D + 2p\,V_T. \tag{5.22}$$

For the thermal potential, we can substitute Eq. (5.15). As for the density potential, which is directly related to the asymmetry in the leptonic sector, it can be parametrised in terms of $\mathcal{L}_\alpha$, which quantifies the lepton asymmetry for neutrino production from oscillations between $\nu_\alpha \leftrightharpoons \nu_R$, as follows [74]

$$V_D = \frac{2\sqrt{2}\zeta(3)}{\pi^2}\, G_F\, \mathcal{L}_\alpha\, T^3, \tag{5.23}$$

with $\mathcal{L}_\alpha$ is defined as

$$\mathcal{L}_\alpha = 2L_\alpha + \sum_{\beta\neq\alpha} L_\beta, \qquad \text{with} \qquad L_\alpha = \frac{n_{\nu_\alpha} - n_{\bar{\nu}_\alpha}}{n_\gamma}. \tag{5.24}$$

With this, the resonance condition can be reformulated as

$$m_R^2 \overset{!}{\approx} \frac{4\sqrt{2}\,\zeta(3)}{\pi^2}\, G_F\, \mathcal{L}_\alpha\, p\, T^3 - 2G_{\mathrm{eff}}\, p^2\, T^4 =: m_{\mathrm{eff}}^2, \tag{5.25}$$

where we have defined the effective neutrino mass in the cosmic plasma m_{eff}. If we consider the effective neutrino mass in Eq. (5.25) as a function of temperature, then it is clear that the resonance condition can be interpreted as the crossing point of the effective mass and the mass of the sterile neutrino. This is visualised for different neutrino energies in Figure 5.5.

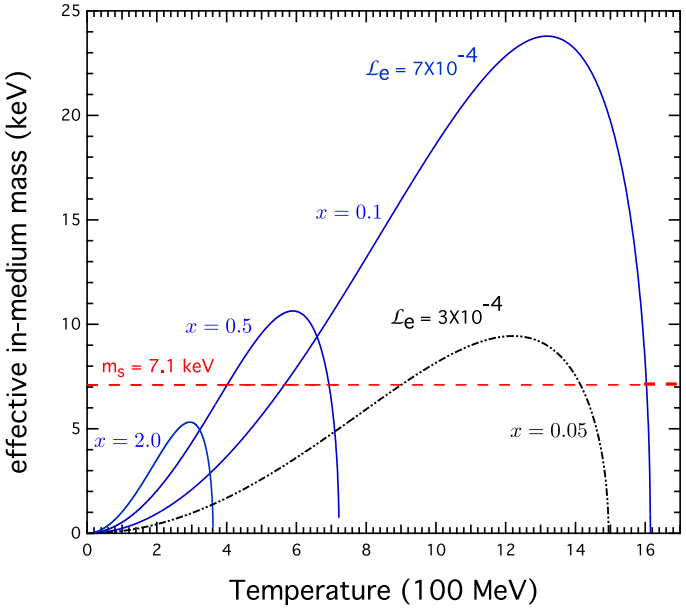

Figure 5.5.: The effective neutrino mass in the cosmic plasma as defined in Eq. (5.25) for different values of $x = E_\nu/T$ and for an electron lepton number of $\mathcal{L}_e = 7 \cdot 10^{-4}$, assuming that the sterile neutrinos are produced in oscillation with electron neutrinos $\nu_e \leftrightharpoons \nu_R$. At temperatures at which the effective mass crosses with the sterile neutrino's mass, which in this example is set to $m_s = 7.1\,\text{keV}$, resonant production may occur. Plot from [74].

For the RP to be possible, the lepton asymmetry has to be much larger than the baryon asymmetry ($\eta_B \sim 10^{-10}$) and the mass of the sterile neutrino must be smaller than the maximum of m_{eff}. This is achieved (for example) within the νMSM, which contains 3 heavy sterile neutrinos, the lightest of which is the dark matter [88]. The lepton asymmetry is generated at temperatures above the EW scale by oscillations involving the heavier sterile neutrinos and transferred to the baryon sector by sphalerons. After the sphalerons have frozen out, the two heavier sterile neutrinos may decay and generate additional lepton asymmetry without modifying the baryon number, thus making the RP of dark matter possible [89].

By this mechanism the oscillation amplitude is maximised regardless of the value of the vacuum mixing angle θ, which means that the bounds on θ by the non-observation of X-ray decay signals are relaxed. Furthermore, due to the momentum and temperature dependence of the resonance condition, the resulting energy distribution of the sterile neutrinos could be highly non-thermal. Particularly, the spectrum may have

a spike at lower energies than the corresponding thermal spectrum. This means that the dark matter produced this in way is potentially colder than in the non-resonant scenario and could thus evade the Lyman-α bounds for small masses [68].

5.3.3. Production by scalar decay

If we allow for the existence of a new real scalar field S that is also a $SU(2)_L$ singlet, and has a Yukawa coupling to the RH neutrinos and a non-vanishing VEV, then a new production mechanism is possible. Consider the following Lagrangian,

$$\mathcal{L} = \mathcal{L}_{\mathrm{SM}} + i\,\bar{\nu}_R\,\gamma^\mu \partial_\mu\,\nu_R - \bar{l}\,h\,\tilde{\phi}\,\nu_R - \frac{f}{2} S\,\bar{\nu}_R^c \nu_R + V(\phi, S) + h.c. \tag{5.26}$$

Here, f is the Yukawa coupling between S and the sterile neutrinos and the Majorana mass is generated when the scalar field relaxes into its VEV,

$$m_R = f \cdot \langle S \rangle. \tag{5.27}$$

The masses of both scalars are contained in the scalar potential $V(\phi, S)$.

The presence of the term $S\,\bar{\nu}_R^c \nu_R$ allows for the decay of S into RH neutrinos,

$$S \to \bar{\nu}_R + \nu_R, \tag{5.28}$$

which is a new production mechanism for dark matter. The scalar field would be in thermal equilibrium and decay into sterile neutrinos at a rate

$$\Gamma_{S \to 2\nu_R} \sim f^2\, m_S, \tag{5.29}$$

where m_S stands for the mass of the scalar field. The dark matter production keeps going until the number density of S starts being negligible at $T \approx m_s$. Detailed calculations for the number density of the dark matter produced in this mechanism can be found in [90]. The case in which the scalar has a mass in the EW scale is particularly interesting, because it would not add to the hierarchy problem und could be pointing to an extended Higgs sector at the EW scale. Furthermore, the dark matter is produced at temperatures $T \gtrsim 100\,\mathrm{GeV}$ and its density is diluted by the entropy production that occurs between $T \sim 100\,\mathrm{GeV}$ and $T \sim 1\,\mathrm{MeV}$. This would also redshift the momentum distribution, making the dark matter colder, which is favoured by the Lyman-α bounds. Interestingly, Alanne et al. have shown that in this scenario it is also possible to successfully implement leptogenesis by the CP violating decays of the RH neutrino [62]. For $m_S \gtrsim 100\,\mathrm{GeV}$, the dark matter abundance can be approximated as [87]

$$\Omega_{\nu_R} \sim 0.2 \left(\frac{f}{10^{-8}}\right)^3 \left(\frac{\langle S \rangle}{m_S}\right). \tag{5.30}$$

If the mass and VEV of the scalar are in the EW scale and the Yukawa coupling is such that the right amount of dark matter is produced, then the corresponding Majorana mass for the sterile neutrinos is [87]

$$m_R \sim f \cdot \langle S \rangle \sim 10^{-8} \cdot (10^2 - 10^3)\,\mathrm{GeV} \sim (1 - 10)\mathrm{keV}. \tag{5.31}$$

As we have seen in this chapter, keV sterile neutrinos can potentially comply with all requirements to be appealing dark matter candidates. They can be made to be very long lived, produced in the right quantities and maybe even be part of the solution to other problems at the frontier of fundamental physics.

6. A new production mechanism for sterile neutrino Dark Matter

Inspired by two of the most promising dark matter candidates, the WIMP and the sterile neutrino, we propose a *new* way to produce sterile neutrino dark matter. We will merge some of the characteristics of WIMPs, which were originally conceived as particles produced from a thermal bath in equilibrium, and sterile neutrinos, whose existence is also motivated by other problems in the frontier of fundamental physics.

Concretely, we will investigate the conditions under which it could be possible to produce the right amount of sterile neutrinos by freeze-out from thermal equilibrium to account for the observed dark matter mass density in the Universe. Previously, this possibility had been ruled out for the sterile neutrinos introduced in the minimal seesaw type I framework, for reasons which we will discuss in the first section of this chapter.

As a first study, this work focuses on the general concept of sterile neutrino production by freeze-out. Therefore, we will avoid the complications related to flavour physics and only consider one neutrino generation. The results presented here should be taken as a proof of concept; more detailed studies are left for future work.

6.1. The problem: why there is no freeze-out in the minimal seesaw framework

As we discussed at length in chapter 5, the production mechanisms for sterile neutrinos as dark matter candidates involving neutrino oscillations and the decays of additional SM singlet scalars have been throughly investigated and are well understood. However, the very simple and attractive mechanism of production by freeze-out from thermal equilibrium, which we reviewed in chapter 3, has been deemed unsuitable for sterile neutrinos within the seesaw extension of the SM. To understand why, and for future reference in this chapter, let us remind ourselves of the seesaw Lagrangian:

$$\mathcal{L}_\nu = i\,\bar{\nu}_R\,\gamma^\mu\partial_\mu\,\nu_R - \bar{l}\,h\,\tilde{\phi}\,\nu_R - \frac{1}{2}m_R\bar{\nu}_R^c\nu_R + h.c., \tag{6.1}$$

where h is the neutrino Yukawa coupling.

The only type of interaction allowed for the RH neutrinos by this Lagrangian is the Yukawa interaction with Higgs bosons and leptons. In order for the RH neutrinos to reach thermal equilibrium, they must have interactions with the rest of the thermal bath at a rate Γ_{ν_R} larger than the expansion rate of the Universe,

$$\Gamma_{\nu_R}(T) \geq H(T). \tag{6.2}$$

Unfortunately, the longevity condition and the non-observation of X-ray signals from decays (see subsection 5.2.3) demand that the mixing angle between sterile and active neutrinos be very small (see Eq. (4.25)). Upon EW symmetry breaking, the VEV v of the Higgs boson generates a Dirac mass for the neutrinos, which is given by

$$m_D = v \cdot h, \tag{6.3}$$

The mixing angle is related to the Yukawa coupling as in Eq. (4.25). For small mixing angles we can write

$$\theta \simeq \frac{m_D}{m_R} = \frac{v \cdot h}{m_R}. \tag{6.4}$$

As an example, the mixing angle for a sterile neutrinos with $m_R = 7.1\,\mathrm{keV}$ is bounded through the radiative decay by the X-ray constrains to be $\sin^2(2\theta) \lesssim 10^{-10}$, see Figure 5.4. Since the Yukawa coupling enters the rate Γ_{ν_R} as h^2, the reaction rate would be very small. If the sterile neutrinos start their existence out of thermal equilibrium, regardless what their assumed initial abundance is, they are never able to reach equilibrium because the condition (6.2) simply cannot be satisfied due to the smallness of the Yukawa coupling.

Another challenge is to achieve freeze-out itself. This occurs when a species is kept in thermal equilibrium at high temperatures but the equilibrium condition (6.2) is violated for $T < T_{\mathrm{fo}}$. The only interactions that are relevant for freeze-out and are included in the Boltzmann equation, are those which change the number of particles that undergo freeze-out, e.g. annihilations. Indeed, in chapter 3 we calculated an approximate solution to the Boltzmann equation for WIMPs considering only annihilations into fermions, $\chi\overline{\chi} \leftrightharpoons f\bar{f}$. In the case of sterile neutrinos, an annihilation process into active neutrinos through the t-channel exchange of a Higgs boson is conceivable,

$$\nu_R\,\bar{\nu}_R \overset{\phi}{\leftrightharpoons} \nu_\alpha\,\bar{\nu}_\alpha, \tag{6.5}$$

however, the cross section would behave as $\sigma_{\mathrm{ann}} \propto h^4$, such that the rate would be even more drastically suppressed by a small Yukawa coupling.

In the following section, we will offer a simple solution to this challenges.

6.2. How to maintain thermal equilibrium

We start by assuming an initial thermal distribution for sterile neutrinos in the early Universe, i.e. the neutrinos start out being in thermal equilibrium. This is reasonable if we assume that they were copiously produced in the last reheating phase of the Universe. Then the initial abundance would have been large and the sterile neutrinos could have quickly thermalised.

It is vital that the sterile neutrinos are kept in thermal equilibrium long enough for their density to decrease to acceptable levels; if freeze-out occurs too early we

might end up with a Universe overclosed by the huge sterile neutrino density. On the other side, if they stay in equilibrium for too long, their density will be exponentially depleted and we will have no neutrinos left to explain the dark matter. The question is then, which interactions are available to maintain the thermal equilibrium. Up to three level, the Yukawa term in Eq. (6.1) allows for the following (sterile neutrino) number changing processes:

1. Decay and inverse decay

$$\nu_R \leftrightharpoons \phi\, l \tag{6.6}$$

2. Quark scattering

$$l\,\nu_R \leftrightharpoons q_3\,\bar{u}_3, \qquad q_3\,\bar{l} \leftrightharpoons \nu_R\,\bar{u}_3, \qquad u_3\,\bar{l} \leftrightharpoons \nu_R\,\bar{q}_3 \tag{6.7}$$

3. Higgs and gauge boson (A) scattering

$$l\,\nu_R \leftrightharpoons \bar{\phi}\,A, \qquad \nu_R\,\phi \leftrightharpoons A\,\bar{l}, \qquad \nu_R\,A \leftrightharpoons \bar{\phi}\,\bar{l} \tag{6.8}$$

4. Annihilations to active neutrinos

$$\nu_R\nu_R \leftrightharpoons \nu_\alpha\,\bar{\nu}_\alpha \tag{6.9}$$

The fist three types of processes (along with other processes where the sterile neutrino is involved as the virtual exchange particle) violate lepton number conservation and have been widely studied in the context of thermal leptogenesis [91, 92]. There, a vanishing initial abundance of sterile neutrinos is assumed, so that they are produced out of equilibrium in the reactions above.

Depending on the behaviour of the neutrino Yukawa coupling, it is possible that these reactions are capable of keeping the sterile neutrinos in equilibrium long enough for them not to overclose the Universe. The decay process, however, has the potential to spoil our efforts to construct a (near) constant, frozen-out relic density, because even if the rates of the reactions (6.7) - (6.9) fall below the Hubble rate and freeze-out, there is nothing to stop the decays from completely decimating all of the sterile neutrinos; we will deal with this problem in the next section.

The Feynman diagrams for the scattering processes can be seen in Figure 6.1.

6.3. How to achieve freeze-out

We are interested in the scenario in which the sterile neutrinos have an initial thermal distribution and are in equilibrium with the plasma at an early stage of high temperature. In order for the sterile neutrino density to freeze-out from thermal equilibrium with the correct relic abundance, the rate of its interactions with the plasma must fall below the Hubble rate at the right time. It is easy to intuitively understand that, with a large enough Yukawa coupling, this is possible for the scattering interactions in

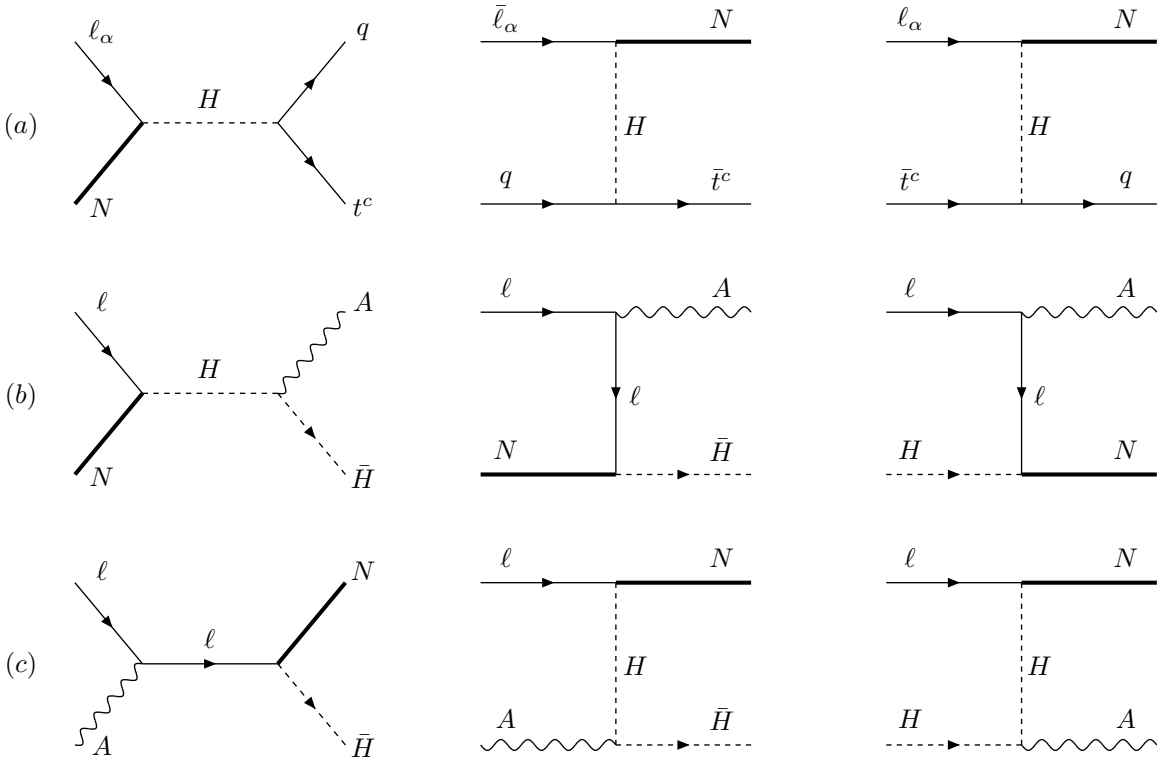

Figure 6.1.: Diagrams of the $2 \leftrightharpoons 2$ scatterings in Eqs. (6.7) - (6.9), with a slightly different nomenclature for the fields. The diagrams in (a) are the scatterings eith top quarks, the diagrams in (b) and (c) are the Higgs and gauge boson scatterings. Diagrams from [93].

Figure 6.1: if the sterile neutrinos are heavier than the quarks and bosons, the reactions that create the neutrinos will be kinematically forbidden once the temperature of the plasma has dropped below m_R; on the other direction, the Hubble expansion will eventually have diluted the densities of the particles such that the reactions that consume the sterile neutrinos will be very rare.

However, the decays are more problematic. The decay channel is always open to heavy sterile neutrinos, either as in Eq. (6.6) when the temperature is high, or through the mixing with active neutrinos after EW symmetry breaking, see Eq. (5.11). The decay rate, which is approximately given by

$$\Gamma_D \simeq \frac{h^2\, m_R}{8\pi}, \tag{6.10}$$

is not influenced by the Hubble rate; regardless of how diluted their density has become, sterile neutrinos will still decay. Remember that RH neutrino decays are also responsible for the stringent X-ray bounds on the parameter space in Figure 5.4. Those constrains become even stronger for larger masses in the γ-ray portion of the spectrum [67].

How can we evade this problem? One simple yet powerful solution is the introduction of a varying neutrino Yukawa coupling. The possibility of varying Yukawa couplings is well motivated by other problems in particle physics. The Yukawa couplings are responsible for the flavour hierarchy in the SM; in the limit of vanishing masses, the related fermions of different flavours are indistinguishable. If the Yukawa couplings have a dynamical nature at some scale, it is conceivable that this is the origin of the flavour hierarchy [94, 95]. Varying Yukawas have also been proposed in relation to the values of the CKM matrix [96], baryogenesis at the EW scale [97], and the EW phase transition [98], among others.

We propose a varying neutrino Yukawa coupling which goes from a sizeable initial value while the neutrinos are in equilibrium at some high scale and decreases with time (or equivalently, with decreasing temperature). This effectively shuts down the the decay of sterile neutrinos making freeze-out feasible and helps us evade the X-ray and γ-ray constrains on the mixing angle. We conveniently parametrize the varying Yukawa in terms of $z = m_R/T$ by

$$h = \frac{Y_\nu}{z^2}. \tag{6.11}$$

In the remainder of this chapter, we will solve the Boltzmann equation under this assumption and show that there exists a non-zero region in the parameter space where sterile neutrinos with a varying Yukawa can be produced by freeze-out from equilibrium to yield the correct dark matter abundance.

6.4. The Boltzmann equation for sterile neutrinos

In chapter 3 we derived the Boltzmann equation for a generic WIMP χ with annihilation interactions to the SM fermions. With $z = m_\chi/T$ we arrived at Eq. (3.35)

$$\begin{aligned} \frac{dy_\chi}{dz} &= -\frac{s}{H\,z}\langle\sigma_{\rm ann}v\rangle\left(y_\chi^2 - y_{\chi,\rm eq}^2\right) \\ &= -\sqrt{\frac{8\pi^2}{45}}\, g_*^{1/2}\, M_{\rm Pl}\, m_\chi\, z^{-2}\,\langle\sigma_{\rm ann}v\rangle\left(y_\chi^2 - y_{\chi,\rm eq}^2\right), \end{aligned} \tag{6.12}$$

where s is the entropy density and $\langle\sigma_{\rm ann}v\rangle$ the thermally averaged annihilation cross section. For a general $2 \to 2$ process, it is formally defined as

$$\langle\sigma_{ab\to cd}\,v\rangle = -\frac{\int d\pi_a d\pi_b f_a^{\rm eq} f_b^{\rm eq} \int d\pi_c d\pi_d (2\pi)^4\delta^{(4)}(p_a + p_b - p_c - p_d)|\mathcal{M}|^2}{n_a^{\rm eq}\, n_b^{\rm eq}}, \tag{6.13}$$

with all symbols as defined in section 3.3. For annihilation processes, where the masses of the initial states are identical, one can approximate the center of mass energy in terms of the relative velocity and use a partial wave expansion for $\langle\sigma_{\rm ann}v\rangle$.

In the case of sterile neutrinos, The Boltzmann equation would include all of the processes in Figure 6.1 plus the decay. This equation has been studied in the context of thermal leptogenesis and lepton asymmetry. Here, the Boltzmann equation is

usually given in a slightly different notation, namely in terms of reaction rates $\gamma^{\rm eq}$ instead of thermally averaged cross sections. The relationship is [92]

$$\gamma^{\rm eq}_{ab\to cd} = \langle \sigma_{ab\to cd}\, v\rangle \cdot n_a^{\rm eq}\, n_b^{\rm eq}. \tag{6.14}$$

For the $2 \to 2$ scatterings, three of the integrals in Eq. (6.13) can be done analytically, so that we are left with

$$\gamma^{\rm eq}_{ab\to cd} = \frac{T}{64\pi^4}\int_{s_{\rm min}}^{\infty} ds\,\sqrt{s}\,\hat{\sigma}(s)\,{\rm K}_1(\sqrt{s}/T), \tag{6.15}$$

where s stands for the center of mass energy squared (and is not to be confused with the entropy density in the Boltzmann equation), $\rm K_1$ is the modified Bessel function of the second kind, and $\hat{\sigma}(s)$ is the reduced cross section for the process $ab \to cd$, defined in terms of the full cross section σ as

$$\hat{\sigma}(s) := 2s\lambda(1, m_a^2/s, m_b^2/s)\,\sigma(s), \tag{6.16}$$

with

$$\lambda(u,v,w) := (u-v-w)^2 - 4vw. \tag{6.17}$$

Also, the lower integration bound is $s_{\rm min} = \max[(m_a+m_b)^2, (m_c+m_d)^2]$. For a single scattering process $\nu\, a \leftrightharpoons c\, d$ in which the sterile neutrino is the only particle departing from equilibrium, the Boltzmann equation is written as [99]

$$zHs\frac{dy_{\nu_R}}{dz} = -\gamma^{\rm eq}_{\nu a\to cd}\left(\frac{y_{\nu_R}}{y^{\rm eq}_{\nu_R}} - 1\right). \tag{6.18}$$

One can easily verify with Eq. (6.14) that this is equivalent the form we studied in (3.35). Going from here to the full Boltzmann equation only requires replacing $\gamma^{\rm eq}_{\nu a\to cd}$ by the full reaction rate containing all relevant interactions,

$$\gamma^{\rm eq}_{\rm full} = \gamma^{\rm eq}_{\rm quarks} + \gamma^{\rm eq}_{\rm bosons} + \gamma^{\rm eq}_{\rm decay}, \tag{6.19}$$

where the first two terms get contributions from all the diagrams in Figure 6.1 and

$$\gamma^{\rm eq}_{\rm decay} = n^{\rm eq}_{\nu_R}\,\frac{{\rm K}_1(z)}{{\rm K}_2(z)}\,\Gamma_D, \tag{6.20}$$

with the decay width Γ_D [92]. Since we will only be tracking the density of sterile neutrinos, from now on we will suppress the index ν_R in y_{ν_R}, as there is no risk of confusion. Thus, the Boltzmann equation we want to solve is

$$zHs\frac{dy}{dz} = -\left(\gamma^{\rm eq}_{\rm quarks} + \gamma^{\rm eq}_{\rm bosons} + \gamma^{\rm eq}_{\rm decay}\right)\left(\frac{y}{y_{\rm eq}} - 1\right). \tag{6.21}$$

To solve this differential equation numerically, we have to compute the reaction rates using Eq. (6.15), for which we need the cross sections for the diagrams in Figure 6.1.

Since the setting of our considerations is the early Universe at temperatures above the EW scale, we choose to use the thermal masses[1] for all particles involved except for the sterile neutrino, whose bare mass is approximately the Majorana mass (see Eq. (4.28)) and has a different origin as the masses of the SM particles. Thermal corrections to the Majorana mass are negligible because they would be generated by the Yukawa coupling to the Higgs, which is much smaller than all other SM couplings [101]. The thermal masses of the particles involved are given by [102]

$$\frac{m_\phi^2}{T^2} = \frac{3}{16}g_2^2 + \frac{1}{16}g_Y^2 + \frac{1}{4}y_t^2 + \frac{1}{2}\lambda =: a_\phi, \tag{6.22}$$

$$\frac{m_l^2}{T^2} = \frac{3}{32}g_2^2 + \frac{1}{32}g_Y^2, =: a_l \tag{6.23}$$

$$\frac{m_{q_3}^2}{T^2} = \frac{1}{6}g_3^2 + \frac{3}{32}g_2^2 + \frac{1}{288}g_Y^2 + \frac{1}{16}y_t^2, =: a_q \tag{6.24}$$

$$\frac{m_{u_3}^2}{T^2} = \frac{1}{6}g_3^2 + \frac{1}{18}g_Y^2 + \frac{1}{8}y_t^2, =: a_u \tag{6.25}$$

$$\frac{m_W^2}{T^2} = \frac{11}{12}g_2^2, =: a_W \qquad \frac{m_B^2}{T^2} = \frac{11}{12}g_Y^2 =: a_B, \tag{6.26}$$

with the gauge couplings g_3, g_2 and g_Y, the top quark Yukawa coupling y_t and the Higgs quartic coupling λ. Notice that we have given the polynomials in the couplings names, which we will refer to in the appendix. Using the thermal masses has the additional benefit of evading IR divergencies in the cross sections.

6.5. Results: solving the Boltzmann equation for sterile neutrinos

In order to compute the reaction rates in Eq. (6.19) and solve the Boltzmann equation (6.21), we use the cross section found in Ref. [101]. More details about the computation can be found in the appendix.

We parametrise the varying Yukawa coupling by $h = Y_\nu/z^2$, where Y_ν is the value of the Yukawa at $T = m_R$, and compute the solution to Eq. (6.21) for a wide range of combinations of masses and Y_ν's. With the value of the comoving density today, y_0, we compute the sterile neutrino's relic abundance as

$$\Omega_{\nu_R} h^2 = \frac{s_0\, y_0\, m_R}{\rho_{\text{crit}}}, \tag{6.27}$$

with the entorpy density today s_0, the critical density ρ_{crit}, and h defined by the Hubble parameter as $H = h \cdot 100\,\text{km}\,\text{s}^{-1}\,\text{Mpc}^{-1}$. The resulting parameter plot is shown in Figure 6.2. We recognise that there is a seemingly tight stripe extending diagonally through the whole parameter space, in which sterile neutrino freeze-out is

[1] Prior to EW symmetry breaking, the SM particles have no bare masses, but since they find themselves in a hot plasma of other particles with which they interact, the particles *experience* an effective mass as a result of the frequent interactions. For more details, see Ref. [100].

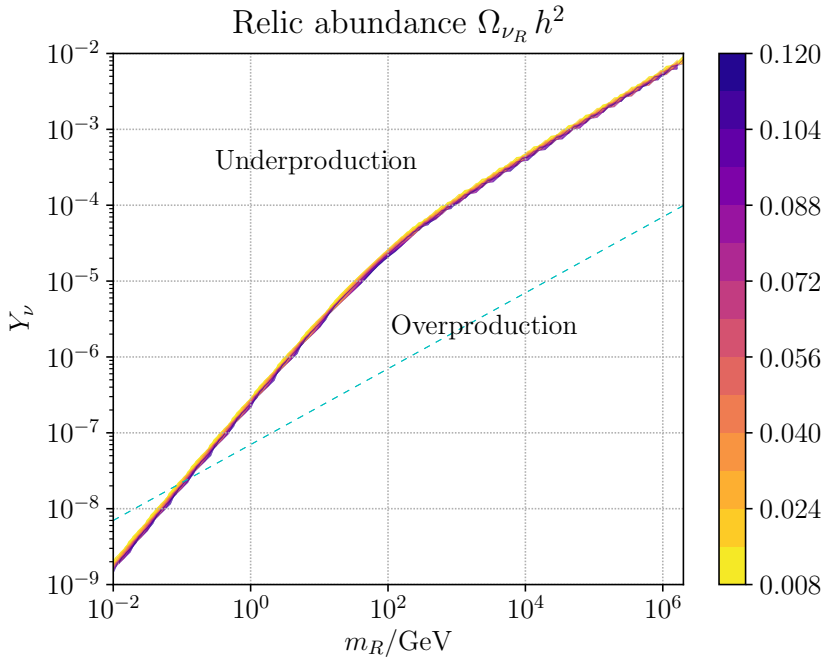

Figure 6.2.: Parameter scan showing in color the region of the parameter space in which a varying Yukawa coupling $h = Y_\nu/z^2$ leads to the freezing-out of the sterile neutrino yield, such that its relic abundance is compatible with the dark matter hypothesis. Below the diagonal dashed line, the seesaw mechanisms also generates an active neutrino mass compatible with the cosmological bound $\sum m_\alpha \lesssim 0.3\,\text{eV}$ [103]; the line is calculated by solving for Y_ν in $(Y_\nu\, v)^2/m_R \lesssim 0.3\,\text{eV}$. This shows that, in principle, this production mechanism for sterile neutrino dark matter is also compatible with the mass generating mechanism for active neutrinos by the type I seesaw framework. Further studies are necessary to investigate the consequences of a varying Yukawa on the masses of active neutrinos.

not only possible, but it also yields the correct contribution to the energy density of the Universe to be either 100% of the dark matter, or a component thereof.

Notice that, even though the mass range spreads for over 6 orders of magnitude, for every mass there is Yukawa Y_ν that yields just the right dark matter abundance through freeze-out. The fact that for increasing values of m_R, Y_ν is required to increase as well, has to do with the fact that Ω_{ν_R} is proportional to m_R. In order to keep Ω_{ν_R} constant for ever larger values of m_R, one needs a larger Y_ν in order to keep the neutrinos longer in equilibrium so that their yield is further depleted for a longer period.

The relative thinness of the allowed stripe in the parameter space is related to the fact that m_R and Y_ν are not only required to achieve thermal equilibrium and then freeze-out, but also deliver a relic abundance in the range $0.008 \lesssim \Omega_{\nu_R} h^2 \lesssim 0.12$ to contribute meaningfully to the dark matter density. This requirement is independent

from achieving freeze-out. Indeed, freeze-out is realised bellow the allowed stripe in Figure 6.2, but the abundance obtained grossly overcloses the Universe. Examples of the evolution of the comoving density with randomly chosen parameters m_R and Y_ν are shown below for four different cases:

(a) Moderate Overproduction, Figure 6.3,

(b) Gross Overproduction, Figure 6.4,

(c) Underproduction, Figure 6.5,

(d) Freeze-out compatible with dark matter, Figure 6.6.

6.6. Final remarks

Over the course of this thesis we have seen that there is solid evidence from many different sources for the existence of dark matter. We have discussed the basic properties of two of the most important dark matter candidates. We studied neutrinos and understood how neutrino flavour oscillations require that the mass of the neutrinos be non-vanishing. The introduction of RH sterile neutrinos not only explains how the masses of the active neutrinos are generated, but might also be involved in the solution to the problem of the matter-antimatter asymmetry of the Universe and in some circumstances provide a plausible dark matter candidate. The most favoured production mechanisms for sterile neutrino dark matter in the literature employ resonant neutrino oscillations in the primordial plasma or decays from other BSM particles.

On the other Hand, in the classical WIMP scenario the dark matter particles are produced in a very natural manner by thermal freeze-out, assuming that they couple weakly with the plasma and have an initial thermal distribution.

In this thesis we have shown that, by introducing a varying neutrino Yukawa coupling that decreases in value as the Universe cools down (which has also be proposed elsewhere, e.g. Ref. [98]), the interactions within the minimal seesaw framework allow the production of sterile neutrinos by freeze-out from thermal equilibrium if we only assume that the initial density was comparable to that of other particles in equilibrium. By choosing the parameters Y_ν and m_R appropriately, the final relic abundance of sterile neutrinos is compatible with the observed dark matter abundance.

This result is encouraging, but should only be taken as an indication that the concept of thermal freeze-out might be applicable to sterile neutrinos after all. Further studies are necessary to investigate the mechanisms that could be responsible for a dynamical Yukawa coupling, and also to look into flavour effects and the role that other sterile neutrinos might play in this picture. Hopefully, the scientific community will be able to find conclusive answers to the questions about the nature of neutrinos and dark matter in the near future.

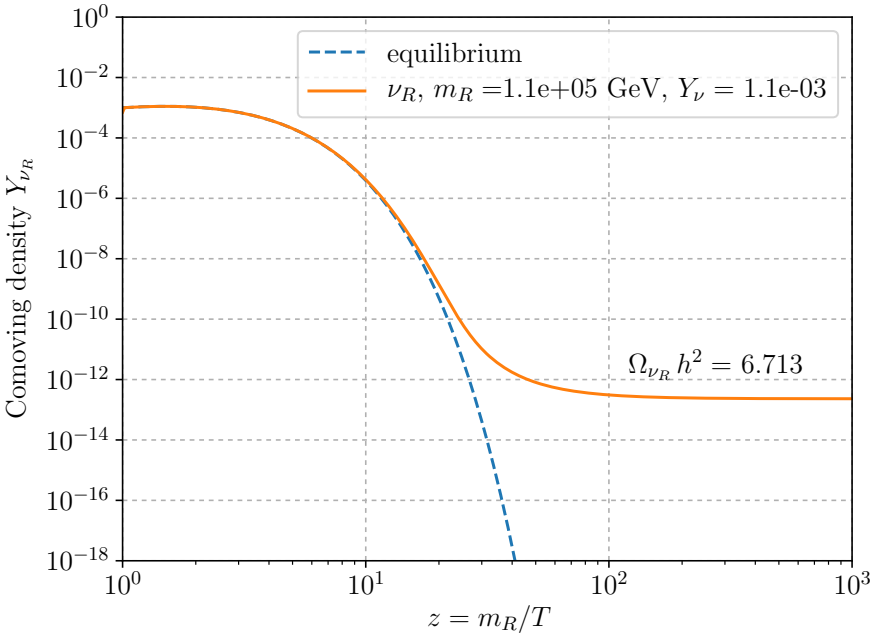

Figure 6.3.: Moderate overproduction. Although the sterile neutrinos are able to perform freeze-out, the resulting abundance is well above the observed dark matter abundance.

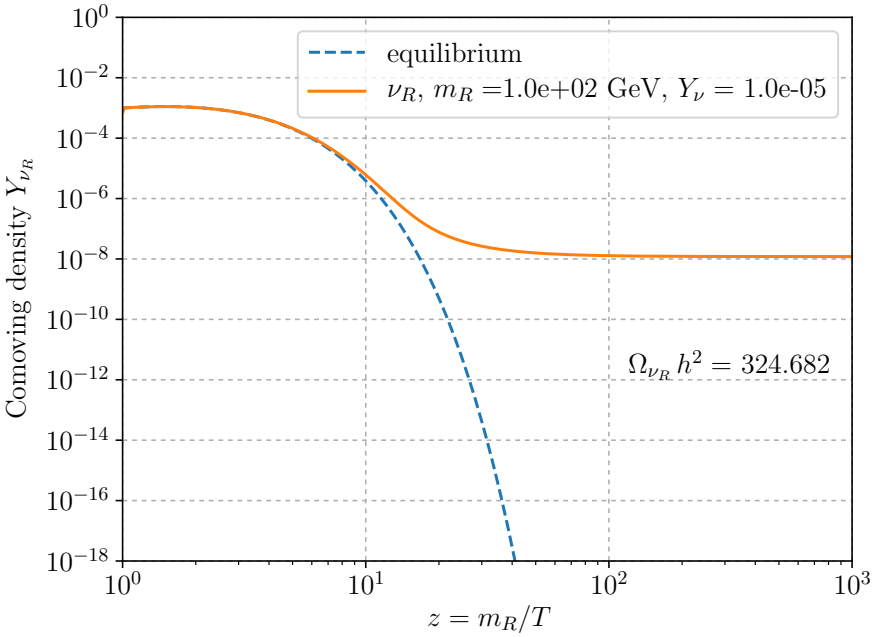

Figure 6.4.: Gross overproduction. Freeze-out is accomplished, yet the resulting abundance is badly beyond anything acceptable.

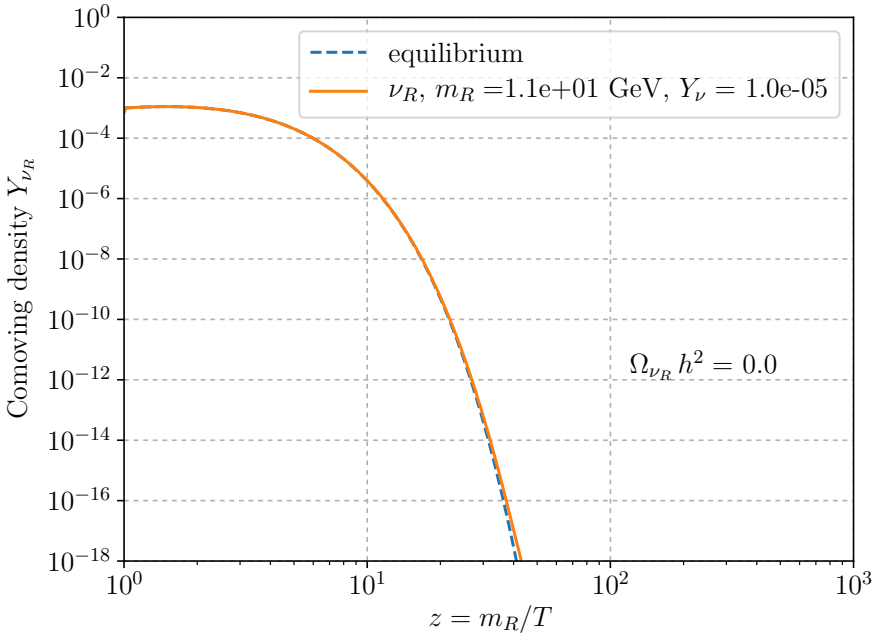

Figure 6.5.: Underproduction. In this case the sterile neutrinos almost do not decouple at all from equilibrium. Their density is completely depleted.

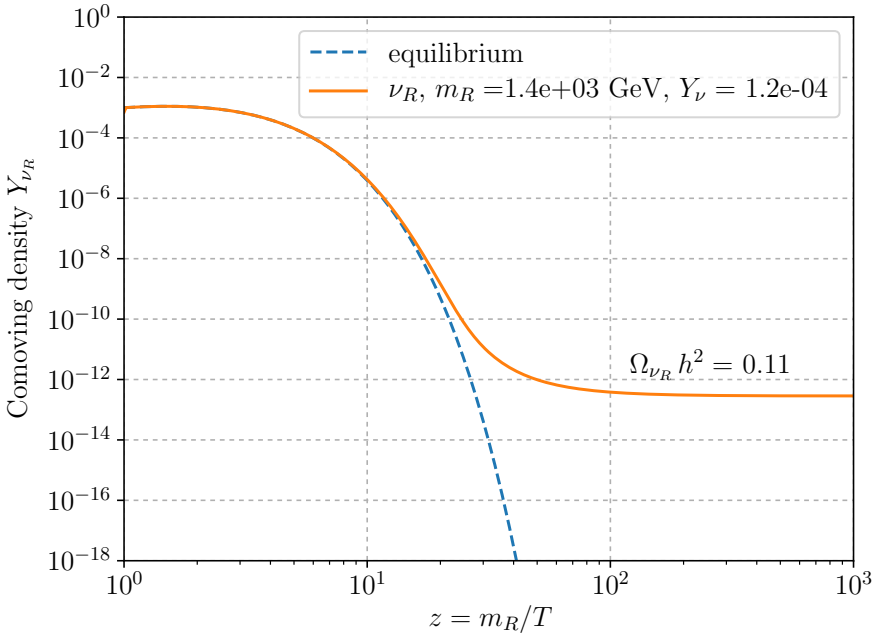

Figure 6.6.: Freeze-out is realised and the relic abundance is compatible with a 100% dark matter hypothesis.

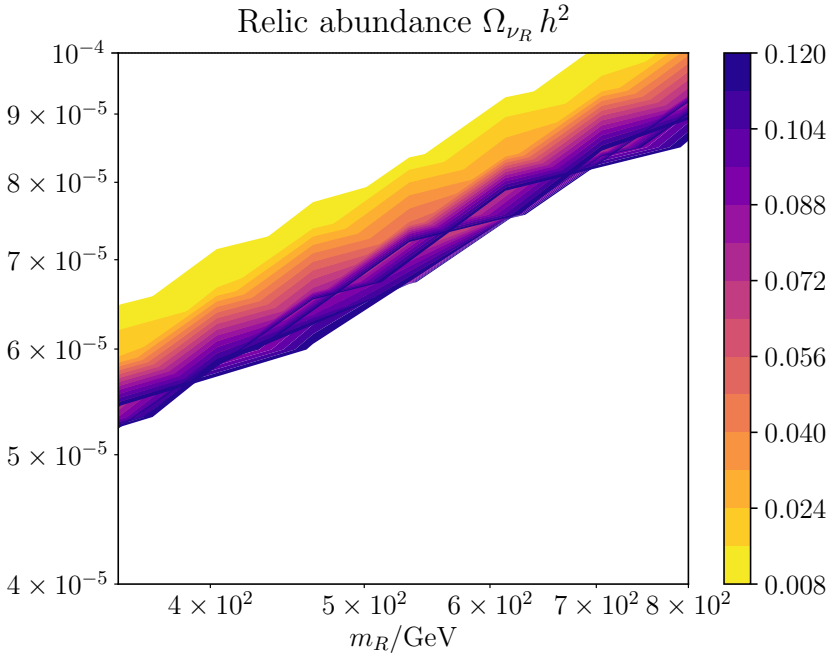

Figure 6.7.: Zoom in a portion of the region of the parameter space from Figure 6.2 where freeze-out succeeds in producing the right amount of sterile neutrinos for the dark matter hypothesis.

Bibliography

[1] F. Zwicky. "Die Rotverschiebung von extragalaktischen Nebeln". In: *Helvetica Physica Acta* 6 (1933), pp. 110–127.

[2] F. Zwicky. "On the Masses of Nebulae and of Clusters of Nebulae". In: *Astrophys. J.* 86 (1937), pp. 217–246. DOI: 10.1086/143864.

[3] R. Herman R. A. Alpher. "Evolution of the Universe". In: *Nature* 162 (Nov. 1948), p. 774.

[4] R. Wilson A. Penzias. "A Measurement of excess antenna temperature at 4080 Mc/s". In: *Astrophysical Journal* 142 (May 1965), p. 419.

[5] N. Jarosik et al. "Seven-year Wilkinson Microwave Anisotropy Probe (WMAP) Observations: Sky Maps, Systematic Errors, and Basic Results". In: 192, 14 (Feb. 2011), p. 14. DOI: 10.1088/0067-0049/192/2/14. arXiv: 1001.4744.

[6] N. Aghanim et al. "Planck 2018 results. VI. Cosmological parameters". In: (2018). arXiv: 1807.06209 [astro-ph.CO].

[7] *10 years of Large Hadron Collider discoveries*. https://earthsky.org/human-world/large-hadron-collider-lhc-discoveries. Accessed: 2019-02-12.

[8] The ATLAS Collaboration. "Observation of a new particle in the search for the Standard Model Higgs boson with the ATLAS detector at the LHC". In: *Physics Letters B* 716.1 (2012), pp. 1–29. ISSN: 0370-2693. DOI: https://doi.org/10.1016/j.physletb.2012.08.020.

[9] The CMS Collaboration. "Observation of a new boson at a mass of 125 GeV with the CMS experiment at the LHC". In: *Physics Letters B* 716.1 (2012), pp. 30–61. ISSN: 0370-2693. DOI: https://doi.org/10.1016/j.physletb.2012.08.021.

[10] E. Aprile et al. "Dark Matter Search Results from a One Ton-Year Exposure of XENON1T". In: *Phys. Rev. Lett.* 121.11 (2018), p. 111302. DOI: 10.1103/PhysRevLett.121.111302. arXiv: 1805.12562 [astro-ph.CO].

[11] LIGO Scientific Collaboration and Virgo Collaboration. "Observation of Gravitational Waves from a Binary Black Hole Merger". In: *Physical Review Letters* 116.6 (Feb. 2016). DOI: 10.1103/physrevlett.116.061102.

[12] Douglas Clowe et al. "A direct empirical proof of the existence of dark matter". In: *Astrophys. J.* 648 (2006), pp. L109–L113. DOI: 10.1086/508162. arXiv: astro-ph/0608407 [astro-ph].

[13] Glenn D. Starkman. "Modifying gravity: you cannot always get what you want". In: *Philosophical Transactions of the Royal Society of London A: Mathematical, Physical and Engineering Sciences* 369.1957 (2011), pp. 5018–5041. ISSN: 1364-503X. DOI: 10.1098/rsta.2011.0292.

[14] Stacy S. McGaugh. "A tale of two paradigms: the mutual incommensurability of ΛCDM and MOND". In: *Canadian Journal of Physics* 93.2 (2015), pp. 250–259. DOI: 10.1139/cjp-2014-0203. eprint: https://doi.org/10.1139/cjp-2014-0203. URL: https://doi.org/10.1139/cjp-2014-0203.

[15] Jaan Einasto. "Dark Matter". In: *Astronomy and Astrophysics 2010* (Jan. 6, 2009). arXiv: http://arxiv.org/abs/0901.0632v2 [astro-ph.CO].

[16] Stefano Profumo. *An Introduction to Particle Dark Matter*. WORLD SCIENTIFIC (EUROPE), Nov. 2015. DOI: 10.1142/q0001.

[17] T. S. van Albada et al. "Distribution of dark matter in the spiral galaxy NGC 3198". In: *The Astrophysical Journal* 295 (Aug. 1985), p. 305. DOI: 10.1086/163375.

[18] F. W. Dyson, A. S. Eddington, and C. Davidson. "A Determination of the Deflection of Light by the Sun's Gravitational Field, from Observations Made at the Total Eclipse of May 29, 1919". In: *Philosophical Transactions of the Royal Society A: Mathematical, Physical and Engineering Sciences* 220.571-581 (Jan. 1920), pp. 291–333. DOI: 10.1098/rsta.1920.0009.

[19] Richard Massey, Thomas Kitching, and Johan Richard. "The dark matter of gravitational lensing". In: *Rept. Prog. Phys.* 73 (2010), p. 086901. DOI: 10.1088/0034-4885/73/8/086901. arXiv: 1001.1739 [astro-ph.CO].

[20] M. Oguri et al. "Combined strong and weak lensing analysis of 28 clusters from the Sloan Giant Arcs Survey". In: *Mon. Not. R. Astron. Soc.* 420 (Mar. 2012), pp. 3213–3239. DOI: 10.1111/j.1365-2966.2011.20248.x. arXiv: 1109.2594.

[21] Scott Dodelson. *Modern cosmology*. San Diego, CA: Academic Press, 2003. URL: https://cds.cern.ch/record/1282338.

[22] Edward W. Kolb and Michael S. Turner. "The Early Universe". In: *Front. Phys.* 69 (1990), pp. 1–547.

[23] Bradley W. Carroll and Dale A. Ostlie. *An Introduction to Modern Astrophysics*. Ed. by San Francisco: Pearson Addison-Wesley. 2nd (International). 2007.

[24] Jacob D. Bekenstein. "Relativistic gravitation theory for the modified Newtonian dynamics paradigm". In: *Phys. Rev. D* 70 (8 Oct. 2004), p. 083509. DOI: 10.1103/PhysRevD.70.083509. URL: https://link.aps.org/doi/10.1103/PhysRevD.70.083509.

[25] Scott Dodelson. "The Real Problem with MOND". In: *Int. J. Mod. Phys.* D20 (2011), pp. 2749–2753. DOI: 10.1142/S0218271811020561. arXiv: 1112.1320 [astro-ph.CO].

[26] Will J. Percival et al. “The shape of the SDSS DR5 galaxy power spectrum”. In: *Astrophys. J.* 657 (2007), pp. 645–663. DOI: 10.1086/510615. arXiv: astro-ph/0608636 [astro-ph].

[27] J. Einasto. “Dark Matter and Large Scale Structure”. In: (Dec. 7, 2000). arXiv: http://arxiv.org/abs/astro-ph/0012161v1 [astro-ph].

[28] John A. Peacock et al. “A Measurement of the cosmological mass density from clustering in the 2dF Galaxy Redshift Survey”. In: *Nature* 410 (2001), pp. 169–173. DOI: 10.1038/35065528. arXiv: astro-ph/0103143 [astro-ph].

[29] Will J. Percival et al. “The 2dF Galaxy Redshift Survey: The Power spectrum and the matter content of the Universe”. In: *Mon. Not. Roy. Astron. Soc.* 327 (2001), p. 1297. DOI: 10.1046/j.1365-8711.2001.04827.x. arXiv: astro-ph/0105252 [astro-ph].

[30] Springel, Volker and Frenk, Carlos S. and White, Simon D. M. “The large-scale structure of the Universe”. In: *Nature* 440 (2006). URL: http://dx.doi.org/10.1038/nature04805.

[31] G. Gamow. “The Evolution of the Universe”. In: *Nature* 162 (Oct. 1948), p. 680.

[32] G. Gamow. “Expanding Universe and the Origin of Elements”. In: *Phys. Rev.* 70 (Oct. 1946), p. 572.

[33] H. Bethe R. A. Alpher and G. Gamow. “The Origin of Chemical Elements”. In: *Phys. Rev.* 73 (Apr. 1948), p. 803.

[34] J. Silk et al. *Particle Dark Matter: Observations, Models and Searches*. Ed. by Gianfranco Bertone. Cambridge Univ. Press, 2010. ISBN: 9781107653924. DOI: 10.1017/CBO9780511770739.

[35] Benjamin W. Lee and Steven Weinberg. “Cosmological Lower Bound on Heavy Neutrino Masses”. In: *Phys. Rev. Lett.* 39 (1977). [,183(1977)], pp. 165–168. DOI: 10.1103/PhysRevLett.39.165.

[36] R. Cowsik and J. McClelland. “An Upper Limit on the Neutrino Rest Mass”. In: *Physical Review Letters* 29.10 (Sept. 1972), pp. 669–670. DOI: 10.1103/physrevlett.29.669.

[37] Paolo Gondolo and Graciela Gelmini. “Cosmic abundances of stable particles: Improved analysis”. In: *Nucl. Phys.* B360 (1991), pp. 145–179. DOI: 10.1016/0550-3213(91)90438-4.

[38] Lars Husdal. “On Effective Degrees of Freedom in the Early Universe”. In: *Galaxies* 4.4 (2016), p. 78. DOI: 10.3390/galaxies4040078. arXiv: 1609.04979 [astro-ph.CO].

[39] Robert J. Scherrer and Michael S. Turner. “On the Relic, Cosmic Abundance of Stable Weakly Interacting Massive Particles”. In: *Phys. Rev.* D33 (1986). [Erratum: Phys. Rev.D34,3263(1986)], p. 1585. DOI: 10.1103/PhysRevD.33.1585,10.1103/PhysRevD.34.3263.

[40] Peter J. Mohr, David B. Newell, and Barry N. Taylor. "CODATA recommended values of the fundamental physical constants: 2014". In: *Reviews of Modern Physics* 88.3 (Sept. 2016). DOI: 10.1103/revmodphys.88.035009.

[41] Gary Steigman, Basudeb Dasgupta, and John F. Beacom. "Precise relic WIMP abundance and its impact on searches for dark matter annihilation". In: *Physical Review D* 86.2 (July 2012). DOI: 10.1103/physrevd.86.023506.

[42] G. G. Raffelt. "Dark matter: Motivation, candidates and searches". In: *1997 European School of High-energy physics, Menstrup, Denmark, 25 May-7 Jun, 1997: Proceedings*. 1997, pp. 235–278. arXiv: hep-ph/9712538 [hep-ph].

[43] Kim Griest and Marc Kamionkowski. "Unitarity Limits on the Mass and Radius of Dark Matter Particles". In: *Phys. Rev. Lett.* 64 (1990), p. 615. DOI: 10.1103/PhysRevLett.64.615.

[44] Wolfgang Pauli. *Aufsaetze und Vortraege ueber Physik und Erkenntnistheorie*. Vieweg Teubner Verlag, 1961. DOI: 10.1007/978-3-663-07092-4.

[45] C. L. Cowan et al. "Detection of the Free Neutrino: a Confirmation". In: *Science* 124.3212 (July 1956), pp. 103–104. DOI: 10.1126/science.124.3212.103.

[46] Thomas Peters. "Quantum Field Theory and the Standard Model, by Matthew D. Schwartz". In: *Contemporary Physics* (Oct. 2014), pp. 1–1. DOI: 10.1080/00107514.2014.970232.

[47] The Super-Kamiokande Collaboration. "Neutrino-induced upward stopping muons in Super Kamiokande". In: *Phys.Lett.B467:185-193,1999* (Aug. 11, 1999). DOI: 10.1016/S0370-2693(99)01188-0. arXiv: http://arxiv.org/abs/hep-ex/9908049v3 [hep-ex].

[48] SNO Collaboration. "Direct Evidence for Neutrino Flavor Transformation from Neutral-Current Interactions in the Sudbury Neutrino Observatory". In: *Phys. Rev. Lett. 89: 011301, 2002* (Apr. 21, 2002). DOI: 10.1103/PhysRevLett.89.011301. arXiv: http://arxiv.org/abs/nucl-ex/0204008v2 [nucl-ex].

[49] N. Schmitz. *Neutrinophysik*. Vieweg + Teubner V., 1997. ISBN: 9783519032366.

[50] E. Kh. Akhmedov. "Neutrino physics". In: (Jan. 25, 2000). arXiv: http://arxiv.org/abs/hep-ph/0001264v2 [hep-ph].

[51] *Proton proton cycle, Wikimedia Commons*. http://commons.wikimedia.org/wiki/File:Proton_proton_cycle.svg. Accessed: 2018-12-27.

[52] Evgeny Kh. Akhmedov and Joachim Kopp. "Neutrino oscillations: Quantum mechanics vs. quantum field theory". In: *JHEP* 04 (2010). [Erratum: JHEP10, 052(2013)], p. 008. DOI: 10.1007/JHEP04(2010)008,10.1007/JHEP10(2013)052. arXiv: 1001.4815 [hep-ph].

[53] Kai Zuber. *Neutrino Physics, Second Edition*. Taylor and Francis, Aug. 2011. DOI: 10.1201/b11065.

[54] L. Wolfenstein. "Neutrino Oscillations in Matter". In: *Phys. Rev.* D17 (1978), pp. 2369–2374. DOI: 10.1103/PhysRevD.17.2369.

[55] S. P. Mikheyev and A. Yu. Smirnov. "Resonance Amplification of Oscillations in Matter and Spectroscopy of Solar Neutrinos". In: *Sov. J. Nucl. Phys.* 42 (1985), pp. 913–917.

[56] Scott Dodelson and Lawrence M. Widrow. "Sterile neutrinos as dark matter". In: *Physical Review Letters* 72.1 (Jan. 1994), pp. 17–20. DOI: 10.1103/physrevlett.72.17. URL: https://arxiv.org/abs/hep-ph/9303287.

[57] Xiang-Dong Shi and George M. Fuller. "A New dark matter candidate: Nonthermal sterile neutrinos". In: *Phys. Rev. Lett.* 82 (1999), pp. 2832–2835. DOI: 10.1103/PhysRevLett.82.2832. arXiv: astro-ph/9810076 [astro-ph].

[58] Marco Drewes. "Heavy neutrinos in particle physics and cosmology". In: *PoS* EPS-HEP2015 (2015), p. 075. DOI: 10.22323/1.234.0075. arXiv: 1510.07883 [hep-ph].

[59] S. F. King. "Neutrino mass models". In: *Rept. Prog. Phys.* 67 (2004), pp. 107–158. DOI: 10.1088/0034-4885/67/2/R01. arXiv: hep-ph/0310204 [hep-ph].

[60] F. Vissani. "Do experiments suggest a hierarchy problem?" In: *Phys.Rev. D57 (1998) 7027-7030* (Sept. 19, 1997). DOI: 10.1103/PhysRevD.57.7027. arXiv: http://arxiv.org/abs/hep-ph/9709409v1 [hep-ph].

[61] Alexey Boyarsky, Oleg Ruchayskiy, and Mikhail Shaposhnikov. "The Role of sterile neutrinos in cosmology and astrophysics". In: *Ann. Rev. Nucl. Part. Sci.* 59 (2009), pp. 191–214. DOI: 10.1146/annurev.nucl.010909.083654. arXiv: 0901.0011 [hep-ph].

[62] Tommi Alanne et al. "Low-scale leptogenesis assisted by a real scalar singlet". In: (Dec. 11, 2018). arXiv: http://arxiv.org/abs/1812.04421v1 [hep-ph].

[63] Andrei D Sakharov. "Violation of CP invariance, C asymmetry, and baryon asymmetry of the Universe". In: *Soviet Physics Uspekhi* 34.5 (May 1991), pp. 392–393. DOI: 10.1070/pu1991v034n05abeh002497.

[64] F. R. Klinkhamer and N. S. Manton. "A saddle-point solution in the Weinberg-Salam theory". In: *Phys. Rev. D* 30 (10 Nov. 1984), pp. 2212–2220. DOI: 10.1103/PhysRevD.30.2212. URL: https://link.aps.org/doi/10.1103/PhysRevD.30.2212.

[65] Takehiko Asaka and Mikhail Shaposhnikov. "The nuMSM, dark matter and baryon asymmetry of the Universe". In: *Phys. Lett.* B620 (2005), pp. 17–26. DOI: 10.1016/j.physletb.2005.06.020. arXiv: hep-ph/0505013 [hep-ph].

[66] Marco Drewes and Bjorn Garbrecht. "Leptogenesis from a GeV Seesaw without Mass Degeneracy". In: (June 24, 2012). DOI: 10.1007/JHEP03(2013)096. arXiv: http://arxiv.org/abs/1206.5537v1 [hep-ph].

[67] Alejandro Ibarra, David Tran, and Christoph Weniger. "Indirect Searches for Decaying Dark Matter". In: *Int. J. Mod. Phys.* (July 24, 2013). DOI: 10.1142/S0217751X13300408. arXiv: http://arxiv.org/abs/1307.6434v2 [hep-ph].

[68] Alexander Merle. "keV sterile neutrino Dark Matter". In: (Feb. 27, 2017). arXiv: http://arxiv.org/abs/1702.08430v1 [hep-ph].

[69] Michael Boylan Kolchin, James S. Bullock, and Manoj Kaplinghat. "Too big to fail? The puzzling darkness of massive Milky Way subhaloes". In: *Monthly Notices of the Royal Astronomical Society: Letters* 415.1 (June 2011), pp. L40–L44. DOI: 10.1111/j.1745-3933.2011.01074.x.

[70] W. J. G. de Blok. "The Core Cusp Problem". In: (Oct. 19, 2009). DOI: 10.1155/2010/789293. arXiv: http://arxiv.org/abs/0910.3538v1 [astro-ph.CO].

[71] Anatoly A. Klypin et al. "Where are the missing galactic satellites?" In: *Astrophys. J. 522:82-92, 1999* (Jan. 19, 1999). DOI: 10.1086/307643. arXiv: http://arxiv.org/abs/astro-ph/9901240v2 [astro-ph].

[72] Anna Genina et al. "The core-cusp problem: a matter of perspective". In: *Monthly Notices of the Royal Astronomical Society* 474.1 (Nov. 2017), pp. 1398–1411. DOI: 10.1093/mnras/stx2855.

[73] Mark R. Lovell et al. "Addressing the too big to fail problem with baryon physics and sterile neutrino dark matter". In: *Monthly Notices of the Royal Astronomical Society* 468.3 (Mar. 2017), pp. 2836–2849. DOI: 10.1093/mnras/stx621.

[74] M. Drewes et al. "A White Paper on keV Sterile Neutrino Dark Matter". In: *JCAP* 1701.01 (2017), p. 025. DOI: 10.1088/1475-7516/2017/01/025. arXiv: 1602.04816 [hep-ph]. URL: https://arxiv.org/pdf/1602.04816.pdf.

[75] Alexey Boyarsky, Oleg Ruchayskiy, and Dmytro Iakubovskyi. "A lower bound on the mass of Dark Matter particles". In: *JCAP 0903:005,2009* (Aug. 28, 2008). DOI: 10.1088/1475-7516/2009/03/005. arXiv: http://arxiv.org/abs/0808.3902v2 [hep-ph].

[76] D. Gorbunov, A. Khmelnitsky, and V. Rubakov. "Constraining sterile neutrino dark matter by phase-space density observations". In: *JCAP 0810:041,2008* (Aug. 28, 2008). DOI: 10.1088/1475-7516/2008/10/041. arXiv: http://arxiv.org/abs/0808.3910v2 [hep-ph].

[77] Julien Baur et al. "Lyman-alpha Forests cool Warm Dark Matter". In: (Dec. 7, 2015). DOI: 10.1088/1475-7516/2016/08/012. arXiv: http://arxiv.org/abs/1512.01981v2 [astro-ph.CO].

[78] Alexey Boyarsky et al. "Lyman-alpha constraints on warm and on warm-plus-cold dark matter models". In: *JCAP* 0905 (2009), p. 012. DOI: 10.1088/1475-7516/2009/05/012. arXiv: 0812.0010 [astro-ph].

[79] Matteo Viel et al. "Warm dark matter as a solution to the small scale crisis: New constraints from high redshift Lyman-alpha forest data". In: *Phys. Rev.* D88 (2013), p. 043502. DOI: 10.1103/PhysRevD.88.043502. arXiv: 1306.2314 [astro-ph.CO].

[80] Sin Kyu Kang and Ayon Patra. "keV Sterile Neutrino Dark Matter and Low Scale Leptogenesis". In: *J. Korean Phys. Soc.* 69.8 (2016), pp. 1375–1382. DOI: 10.3938/jkps.69.1375. arXiv: 1412.4899 [hep-ph].

[81] Vernon D. Barger, R. J. N. Phillips, and Subir Sarkar. "Remarks on the KARMEN anomaly". In: *Phys. Lett.* B352 (1995). [Erratum: Phys. Lett. B 356, 617(1995)], pp. 365–371. DOI: 10.1016/0370-2693(95)00486-5,10.1016/0370-2693(95)00831-5. arXiv: hep-ph/9503295 [hep-ph].

[82] A. D. Dolgov and S. H. Hansen. "Massive sterile neutrinos as warm dark matter". In: *Astropart. Phys.* 16 (2002), pp. 339–344. DOI: 10.1016/S0927-6505(01)00115-3. arXiv: hep-ph/0009083 [hep-ph].

[83] Robert E. Shrock. "Electromagnetic properties and decays of Dirac and Majorana neutrinos in a general class of gauge theories". In: *Nuclear Physics B* 206.3 (Oct. 1982), pp. 359–379. DOI: 10.1016/0550-3213(82)90273-5.

[84] Alexey Boyarsky et al. "Unidentified Line in X-ray Spectra of the Andromeda Galaxy and Perseus Galaxy Cluster". In: *Phys. Rev. Lett.* 113 (2014), p. 251301. DOI: 10.1103/PhysRevLett.113.251301. arXiv: 1402.4119 [astro-ph.CO].

[85] Tesla E. Jeltema and Stefano Profumo. "Discovery of a 3.5 keV line in the Galactic Centre and a critical look at the origin of the line across astronomical targets". In: *Mon. Not. Roy. Astron. Soc.* 450.2 (2015), pp. 2143–2152. DOI: 10.1093/mnras/stv768. arXiv: 1408.1699 [astro-ph.HE].

[86] Shunsaku Horiuchi et al. "Sterile neutrino dark matter bounds from galaxies of the Local Group". In: *Phys. Rev.* D89.2 (2014), p. 025017. DOI: 10.1103/PhysRevD.89.025017. arXiv: 1311.0282 [astro-ph.CO].

[87] Alexander Kusenko. "Sterile neutrinos: The Dark side of the light fermions". In: *Phys. Rept.* 481 (2009), pp. 1–28. DOI: 10.1016/j.physrep.2009.07.004. arXiv: 0906.2968 [hep-ph].

[88] Takehiko Asaka, Mikhail Shaposhnikov, and Alexander Kusenko. "Opening a new window for warm dark matter". In: *Phys. Lett.* B638 (2006), pp. 401–406. DOI: 10.1016/j.physletb.2006.05.067. arXiv: hep-ph/0602150 [hep-ph].

[89] M. Laine and M. Shaposhnikov. "Sterile neutrino dark matter as a consequence of nuMSM-induced lepton asymmetry". In: *JCAP 0806:031,2008* (Apr. 29, 2008). DOI: 10.1088/1475-7516/2008/06/031. arXiv: http://arxiv.org/abs/0804.4543v2 [hep-ph].

[90] Kalliopi Petraki and Alexander Kusenko. "Dark-matter sterile neutrinos in models with a gauge singlet in the Higgs sector". In: *Physical Review D* 77.6 (Mar. 2008). DOI: 10.1103/physrevd.77.065014. arXiv: 0711.4646.

[91] W. Buchmueller and C. Greub. "Heavy Majorana neutrinos in electron-positron and electron-proton collisions". In: *Nuclear Physics B* 363.2-3 (Oct. 1991), pp. 345–368. DOI: 10.1016/0550-3213(91)80024-g.

[92] Alessandro Strumia. "Baryogenesis via leptogenesis". In: (Aug. 31, 2006). arXiv: http://arxiv.org/abs/hep-ph/0608347v1 [hep-ph].

[93] Chee Sheng Fong, Enrico Nardi, and Antonio Riotto. "Leptogenesis in the Universe". In: *Advances in High Energy Physics, vol. 2012, Article ID 158303, 59 pages, 2012* (Jan. 14, 2013). DOI: 10.1155/2012/158303. arXiv: http://arxiv.org/abs/1301.3062v1 [hep-ph].

[94] R. Alonso et al. "On the Potential of Leptonic Minimal Flavour Violation". In: *Phys. Lett.* B715 (2012), pp. 194–198. DOI: 10.1016/j.physletb.2012.07.056. arXiv: 1206.3167 [hep-ph].

[95] R. Alonso et al. "Leptonic Dynamical Yukawa Couplings". In: *JHEP* 08 (2013), p. 069. DOI: 10.1007/JHEP08(2013)069. arXiv: 1306.5922 [hep-ph].

[96] Iason Baldes, Thomas Konstandin, and Geraldine Servant. "Flavor Cosmology: Dynamical Yukawas in the Froggatt-Nielsen Mechanism". In: *JHEP* 12 (2016), p. 073. DOI: 10.1007/JHEP12(2016)073. arXiv: 1608.03254 [hep-ph].

[97] Benedict v. Harling and Geraldine Servant. "Cosmological evolution of Yukawa couplings: the 5D perspective". In: *JHEP* 05 (2017), p. 077. DOI: 10.1007/JHEP05(2017)077. arXiv: 1612.02447 [hep-ph].

[98] Iason Baldes, Thomas Konstandin, and Geraldine Servant. "A first-order electroweak phase transition from varying Yukawas". In: *Phys. Lett.* B786 (2018), pp. 373–377. DOI: 10.1016/j.physletb.2018.10.015. arXiv: 1604.04526 [hep-ph].

[99] W. Buchmüller, P. Di Bari, and M. Plümacher. "Leptogenesis for pedestrians". In: *Annals of Physics* 315.2 (Feb. 2005), pp. 305–351.

[100] Michel Le Bellac. *Thermal Field Theory*. Cambridge Monographs on Mathematical Physics. Cambridge U. Press, 1996. DOI: 10.1017/CBO9780511721700.

[101] G. F. Giudice et al. "Towards a complete theory of thermal leptogenesis in the SM and MSSM". In: *Nucl. Phys.* B685 (2004), pp. 89–149. DOI: 10.1016/j.nuclphysb.2004.02.019. arXiv: hep-ph/0310123 [hep-ph].

[102] D. Comelli and J. R. Espinosa. "Bosonic thermal masses in supersymmetry". In: *Phys. Rev.* D55 (1997), pp. 6253–6263. DOI: 10.1103/PhysRevD.55.6253. arXiv: hep-ph/9606438 [hep-ph].

[103] Shaun A. Thomas, Filipe B. Abdalla, and Ofer Lahav. "Upper Bound of 0.28 eV on the Neutrino Masses from the Largest Photometric Redshift Survey". In: *Phys.Rev.Lett.105:031301,2010* (Nov. 27, 2009). DOI: 10.1103/PhysRevLett.105.031301. arXiv: http://arxiv.org/abs/0911.5291v2 [astro-ph.CO].

A. Appendix

A.1. Solving the Boltzmann equation for sterile neutrinos

In order to actually solve Eq. (6.21), it is best to introduce dimensionless variables. We define

$$z := \frac{m_R}{T}, \qquad x := \frac{s}{m_R^2}, \qquad \frac{m_I^2(T)}{m_R^2} := \frac{a_I}{z^2}, \tag{A.1}$$

where s is the CM energy squared and m_I stands for any of the thermal masses given in Eq. (6.22)-(6.26). In terms of these new variables, Eq. (6.15) reads

$$\gamma_i^{\mathrm{eq}} = \frac{m_R^4\, h^2}{64\pi^4\, z} \int_{x_{\min}}^{\infty} dx \sqrt{x}\, \tilde{\sigma}_i(x)\, \mathrm{K}_1(z\sqrt{x}) \tag{A.2}$$

$$=: h^2 \cdot \frac{m_R^4}{64\pi^4\, z} \hat{\gamma}_i^{\mathrm{eq}} \tag{A.3}$$

Here, we have extracted the neutrino Yukawa coupling from the cross section by defining $\hat{\sigma}_i(x) = h^2 \tilde{\sigma}_i(x)$. Furthermore, for the decay width we have

$$\Gamma_D = \frac{h^2}{8\pi\, z^4} \sqrt{(z^2 - a_\phi - a_L)^2 - 4 a_\phi a_L} \cdot (z^2 - a_\phi + a_L) \cdot m_R, \tag{A.4}$$

where a_I stands for the polynomials defined in Eq. (6.22)-(6.26). Assuming the sterile neutrinos are non-relativistic near freeze-out, their number density is given by $n_{\nu_R}^{\mathrm{eq}} = 2 m_R^3\, (2\pi)^{-3/2}\, z^{-3/2}\, e^{-z}$. With this, the decay rate is written as

$$\gamma_{\mathrm{decay}}^{\mathrm{eq}} = h^2 \cdot \frac{2 m_R^3}{(2\pi)^{3/2}} z^{-3/2}\, e^{-z} \frac{\mathrm{K}_1(z)}{\mathrm{K}_2(z)}\, \tilde{\Gamma}_D \tag{A.5}$$

$$=: h^2 \cdot m_R^3\, \hat{\gamma}_{\mathrm{decay}}^{\mathrm{eq}} \tag{A.6}$$

where, again, we have extracted the Yukawa coupling by defining $\Gamma_D = h^2 \tilde{\Gamma}_D$. In Eqs. (A.6) and (A.3) we have defined the reduced rates $\hat{\gamma}^{\mathrm{eq}}$. Also, the product of the entropy density and the Hubble parameter results in

$$s \cdot H = \frac{2\pi^3}{45\sqrt{90}}\, g_\rho \sqrt{g_s} \frac{m_R^5}{M_{\mathrm{Pl}}}. \tag{A.7}$$

Altogether, the Boltzmann equation (6.21) is written as

$$\frac{dy}{dz} = -\xi(Y_\nu, m_R)\, z^{-1} \left(\hat{\gamma}_{\mathrm{quarks}}^{\mathrm{eq}} + \hat{\gamma}_{\mathrm{bosons}}^{\mathrm{eq}} + 32\pi^4 \frac{z}{m_R} \hat{\gamma}_{\mathrm{decay}}^{\mathrm{eq}} \right) \left(\frac{y}{y_{\mathrm{eq}}} - 1 \right). \tag{A.8}$$

The reduced reaction rates depend solely on z. All other constants and parameters (with the exception of z/m_R in front of $\hat{\gamma}^{\rm eq}_{\rm decay}$) are contained in the function ξ, which we define as

$$\xi(Y_\nu, m_R) = \frac{45\sqrt{90}}{64\pi^7} \frac{M_{\rm Pl}}{g_\rho \sqrt{g_s}} \frac{Y_\nu^2}{m_R}, \tag{A.9}$$

where we have already inserted the parametrization of the varying Yukawa. With the help of the cross sections found in Ref. [101], we solve this differential equation numerically using the *python* code provided below.

A.2. Numerical code

```
import numpy as np
from scipy.special import kn as BesselK
from scipy.integrate import odeint
from scipy.integrate import quad
import time
import matplotlib.pyplot as plt
from matplotlib.ticker import MaxNLocator
from matplotlib import ticker, cm
plt.rc('text', usetex=True)
plt.rc('font', size=14)
plt.rc('font', family='serif')

# ========================================
#        some important numbers
# ========================================

# ====== the degrees of freedom
g = 106.75
gs = 106.75
gsToday = 3.91
# =========== The CMB temperature today
T0 = 2.7255*4.34 # in cm^-1
# =========== Planck mass in GeV
Mpl = 2.435E18
# =========== entropy density today
s0 = ((2*np.pi**2)/45.)*gsToday*T0**3
# =========== the critical density in units of h^2 GeV cm^-3
rho_crit = 1.05e-5
# =========== Prefactor to the equilibrium distribution y_eq = Alpha *
    ↪ x^(3/2)*exp(-x)
Alpha = 45/(np.pi**2*(2*np.pi)**(3./2)*gs)

```

```
# ====================================================================
#        SM gauge couplings - renormalization scheme (point): muMS = mZ
#        cite: (maybe)   isbn = 9781107292543
# ====================================================================

g3 = 1.221
g2 = 0.652
gY = 0.357
Yt = 0.989
LH = 0.129

# ====================================================================
#        Thermanl masses
#        The polynomials in the couplings between the thermal masses
#        squared and T^2: mX^2/T^2 = aX
#        cite hep-ph/0310123v2 or hep-ph/9606438
# ====================================================================

aH = (3./16)*g2**2 + (1./16)*gY**2 + (1./4)*Yt**2 + (1./2)*LH
aL = (3./32)*g2**2 + (1./32)*gY**2
aQ = (1./6) *g3**2 + (3./32)*g2**2 + (1./288)*gY**2 + (1./16)*Yt**2
at = (1./6) *g3**2 + (1./18)*gY**2 + (1./8)*Yt**2
aW = (11./12)*g2**2
aB = (11./12)*gY**2

# ====================================================================
#        The cross sections
#        cite hep-ph/0310123v2
# ====================================================================

# Decay
def gammaD(m,z,Ynu):

        def BesselRatio12(z):
                if BesselK(1,z) == 0.0:
                        return 1.0
                else:
                        return BesselK(1,z)/BesselK(2,z)

        n_eq = lambda m,z: 2*m**3/(2*np.pi) * z**(-3./2)*np.exp(-z)
        DecayWidth = lambda m,z,Ynu: Ynu**2/(z**4 *8*np.pi)*np.sqrt((z**2
            ↪  -aH -aL)**2 -4*aH*aL)*(z**2 -aH +aL)*m

        return n_eq(m,z)*BesselRatio12(z)*DecayWidth(m,z,Ynu)

```

```
76 # The cross sections for top quark scattering
77
78 # ***** top quarks. s channel. LN <--> QU
79 sigma_H_s = lambda x,z,Ynu: 3/(4*np.pi)*Ynu**2*Yt**2 *(x -1 -aL/z**2)*(x
       ↪  -2*aQ/z**2)/(x*(x-aH/z**2)**2)*np.sqrt(((1 +aL/z**2-x)**2
       ↪  -4*aL/z**2)*(1 -4*aQ/z**2*1/x))
80
81 # ***** top quarks. t channel. QN <--> UL
82 # ----- def. Hilfsfunktion t+ bzw t-
83 tp = lambda x,z: 1/(2*x)*(aQ/z**2 +x -(aQ/z**2 -x)**2 +aL/z**2*(x +aQ/z**2
       ↪  -1) +np.sqrt(( (aQ/z**2)**2 +(x -1)**2 -2*aQ/z**2 *(1 +x) )*(
       ↪  (aL/z**2)**2 +(x -aQ/z**2)**2 -2*aL/z**2 *(x +aQ/z**2))))
84 tm = lambda x,z: 1/(2*x)*(aQ/z**2 +x -(aQ/z**2 -x)**2 +aL/z**2*(x +aQ/z**2
       ↪  -1)-np.sqrt(( (aQ/z**2)**2 +(x -1)**2 -2*aQ/z**2*(1 +x) )*(
       ↪  (aL/z**2)**2 +(x -aQ/z**2)**2 -2*aL/z**2*(x +aQ/z**2))))
85
86 # now the cross section itself
87 sigma_H_t = lambda x,z,Ynu: 3/(4*np.pi) *Ynu**2 *Yt**2 *1./x
       ↪  *(tp(x,z)-tm(x,z) -(1 -aH/z**2 +aL/z**2)*(aH/z**2
       ↪  -2*aQ/z**2)*(1/(aH/z**2 -tp(x,z)) -1/(aH/z**2 -tm(x,z))) -(1
       ↪  -2*aH/z**2 +aL/z**2 +2*aQ/z**2)*np.log((tp(x,z) -aH/z**2)/(tm(x,z)
       ↪  -aH/z**2)))
88
89 # The cross sections for Higgs and Gauge Boson scattering
90
91 # ----- def. Hilfsfunktion r+ bzw r-
92 rp = lambda a1,a2,a3,a4,x,z: (a1-a2-a3+a4)**2/(4*x*z**4)-(np.sqrt(((x*z**2 +
       ↪  a1-a2)**2/(4*x*z**4)) - a1/z**2)+ np.sqrt(((x*z**2 +
       ↪  a3-a4)**2/(4*x*z**4)) - a3/z**2))**2
93 rm = lambda a1,a2,a3,a4,x,z: (a1-a2-a3+a4)**2/(4*x*z**4)-(np.sqrt(((x*z**2 +
       ↪  a1-a2)**2/(4*x*z**4)) - a1/z**2) - np.sqrt(((x*z**2 +
       ↪  a3-a4)**2/(4*x*z**4)) - a3/z**2))**2
94
95 # ***** gauge bosons. NL <--> HA . LN-HA actually
```

```
96  sigmaNL_HA = lambda x,z,Ynu,eps: (3*g2**2 *Ynu**2)/(16*np.pi*x**2)
        ↪  *((2*rp(aL,z**2,aH,aW,x,z)*(x-2) +
        ↪  (2-2*x+x**2)*np.log((aL/z**2-rp(aL,z**2,aH,aW,x,z))**2+eps) +
        ↪  2*(x*(aL/z**2-rp(aL,z**2,aH,aW,x,z))*(aL/z**2+aL/z**2*x-aW/z**2) +
        ↪  eps*(2-2*x+x**2))/((aL/z**2-rp(aL,z**2,aH,aW,x,z))**2+eps))-
        ↪  (2*rm(aL,z**2,aH,aW,x,z)*(x-2) +
        ↪  (2-2*x+x**2)*np.log((aL/z**2-rm(aL,z**2,aH,aW,x,z))**2+eps) +
        ↪  2*(x*(aL/z**2-rm(aL,z**2,aH,aW,x,z))*(aL/z**2+aL/z**2*x-aW/z**2) +
        ↪  eps*(2-2*x+x**2))/((aL/z**2-rm(aL,z**2,aH,aW,x,z))**2+eps))) + (gY**2
        ↪  * Ynu**2)/(32*np.pi*x**2) *((2*rp(aL,z**2,aH,aB,x,z)*(x-2) +
        ↪  (2-2*x+x**2)* np.log((aL/z**2-rp(aL,z**2,aH,aB,x,z))**2 + eps) +
        ↪  2*(x*(aL/z**2-rp(aL,z**2,aH,aB,x,z))*(aL/z**2+aL/z**2*x-aB/z**2) +
        ↪  eps*(2-2*x+x**2))/((aL/z**2-rp(aL,z**2,aH,aB,x,z))**2 + eps)) -
        ↪  (2*rm(aL,z**2,aH,aB,x,z)*(x-2) +
        ↪  (2-2*x+x**2)*np.log((aL/z**2-rm(aL,z**2,aH,aB,x,z))**2+eps) +
        ↪  2*(x*(aL/z**2-rm(aL,z**2,aH,aB,x,z))*(aL/z**2+aL/z**2*x-aB/z**2) +
        ↪  eps*(2-2*x+x**2))/((aL/z**2-rm(aL,z**2,aH,aB,x,z))**2+eps)))
97
98  # ***** gauge bosons. LH <--> NA . HL-NA actually
99  sigmaLH_NA = lambda x,z,Ynu: (3*g2**2
        ↪  *Ynu**2)/(8*np.pi*x*(1-x))*((2*x*np.log(abs(rp(aH,aL,z**2,aW,x,z)
        ↪  -aH/z**2))-(1+x**2)*np.log(abs(rp(aH,aL,z**2,aW,x,z)
        ↪  +x-1-aW/z**2-aH/z**2))) - (2*x*
        ↪  np.log(abs(rm(aH,aL,z**2,aW,x,z)-aH/z**2))-(1+x**2)*
        ↪  np.log(abs(rm(aH,aL,z**2,aW,x,z) +x-1-aW/z**2-aH/z**2)))) + (gY**2 *
        ↪  Ynu**2)/(16*np.pi*x*(1-x))*
        ↪  ((2*x*np.log(abs(rp(aH,aL,z**2,aB,x,z)-aH/z**2))-(1+x**2)
        ↪  *np.log(abs(rp(aH,aL,z**2,aB,x,z) +x-1-aB/z**2-aH/z**2))) -
        ↪  (2*x*np.log(abs(rm(aH,aL,z**2,aB,x,z)-aH/z**2))-(1+x**2)*
        ↪  np.log(abs(rm(aH,aL,z**2,aB,x,z) +x-1-aB/z**2-aH/z**2))))
100
101 # ***** gauge bosons. LA <--> NH
```

```
102 sigmaAL_NH = lambda x,z,Ynu: (3*g2**2 *Ynu**2)/(16*np.pi*x**2)*((
    ↪  rp(aW,aL,z**2,aH,x,z)**2 +2* rp(aW,aL,z**2,aH,x,z) *(x-2)-4*(x-1)*
    ↪  np.log( abs(rp(aW,aL,z**2,aH,x,z) -aH/z**2))+ x*(aW/z**2-4*aH/z**2)
    ↪  /(aH/z**2-rp(aW,aL,z**2,aH,x,z)) -(rm(aW,aL,z**2,aH,x,z)**2 +2*
    ↪  rm(aW,aL,z**2,aH,x,z) *(x-2)-4*(x-1)* np.log(
    ↪  abs(rm(aW,aL,z**2,aH,x,z) -aH/z**2))+
    ↪  x*(aW/z**2-4*aH/z**2)/(aH/z**2-rm(aW,aL,z**2,aH,x,z)))) + (gY**2
    ↪  *Ynu**2)/(32*np.pi*x**2) *(( rp(aB,aL,z**2,aH,x,z)**2 +2*
    ↪  rp(aB,aL,z**2,aH,x,z) *(x-2)-4*(x-1)* np.log(
    ↪  abs(rp(aB,aL,z**2,aH,x,z)
    ↪  -aH/z**2))+x*(aB/z**2-4*aH/z**2)/(aH/z**2-rp(aB,aL,z**2,aH,x,z)))-
    ↪  (rm(aB,aL,z**2,aH,x,z)**2 +2* rm(aB,aL,z**2,aH,x,z) *(x-2)-4*(x-1)
    ↪  *np.log( abs(rm(aB,aL,z**2,aH,x,z)
    ↪  -aH/z**2))+x*(aB/z**2-4*aH/z**2)/(aH/z**2-rm(aB,aL,z**2,aH,x,z))))
103
104 # ========================================================================
105 #        Other auxiliary functions for the Boltzmann equation
106 # ========================================================================
107
108 # ========== The equilibrium yield
109
110 Yeq = lambda z : Alpha*z**(3./2)*np.exp(-z)#/xi(m,Ynu)
111
112 # ========== The relic abundance
113
114 def Omegah2(yToday, m):
115     if yToday < 0.0:
116         return 0.0
117     else:
118         return m*s0*yToday/rho_crit
119
120 def xi(z,m,Ynu):
121         '''
122         xi is the prefactor to the differential equation
123         it contains M_pl, m_R and the neutrino Yukawa Y_nu
124         here, the neutrino Yukawa has been multiplied by a factor of
               ↪  $1/z**2$,
125         so that it decreases with falling temperature.
126         '''
127         return 45*np.sqrt(90)/64/np.pi**7 *
               ↪  (Ynu/(1.0*z**2))**2/(np.sqrt(g)*gs) * Mpl/m
128
129 # ========================================================================
130 #        The integrands for the reaction rates
131 # ========================================================================
```

```
132
133 # here we compute the normalized reaction rates for a process
    ↪ $12\leftrightarrow34$, defined as <br>
134 # $ \hat{\gamma}^{\rm eq}(z) = \int_{x_{\rm min}}^\infty
    ↪ \sqrt{x}\,\hat{\sigma}(s)\,K_1(z\,\sqrt{x}) $, <br>
135 # with $x_{\rm min} = m_\nu^{-2}\max[(m_1+m_2)^2,(m_3+m_4)^2] =
    ↪ \max[(\sqrt{a_1}/z+\sqrt{a_2}/z)^2,(\sqrt{a_3}/z+\sqrt{a_4}/z)^2]$,
    ↪ and with $a_\nu=z$. <br>
136 # Notice the additional argument of epsilon in Integrand_A_1, which is
    ↪ necessary to avoid the resonance and get a smooth reaction rate
    ↪ curve. <br>
137 # The Yukawa couplings and the mass of the RH neutrinos are set here to 1,
    ↪ which is equivalent to extranting them and from the rates and
    ↪ reinserting them in the Boltzmann equation later.
138
139 Integrand_H_s = lambda x,z,Ynu:
    ↪ np.sqrt(x)*sigma_H_s(x,z,Ynu)*BesselK(1,z*np.sqrt(x))
140 Integrand_H_t = lambda x,z,Ynu:
    ↪ np.sqrt(x)*sigma_H_t(x,z,Ynu)*BesselK(1,z*np.sqrt(x))
141 Integrand_A_1 = lambda x,z,Ynu:
    ↪ np.sqrt(x)*sigmaNL_HA(x,z,Ynu,0.0001*aL**2)*BesselK(1,z*np.sqrt(x)) #
    ↪ notice the arg of epsilon, which is necessary to avoid the resonance
    ↪ and get a smooth reaction rate curve
142 Integrand_A_2 = lambda x,z,Ynu:
    ↪ np.sqrt(x)*sigmaLH_NA(x,z,Ynu)*BesselK(1,z*np.sqrt(x))
143 Integrand_A_3 = lambda x,z,Ynu:
    ↪ np.sqrt(x)*sigmaAL_NH(x,z,Ynu)*BesselK(1,z*np.sqrt(x))
144
145 # ======================================================================
146 #  THE FULL BOLTZMANN EQN FOR RH NEUTRINO DECAY AND SCATTERING
147 # ======================================================================
148
149 def Boltzmann_N_RH(Y,z,m,Ynu): # Bolzmann eq. in hep-ph/0310123v2 form eq.
    ↪ (75)
150
151     x_min_H_s = max((1+np.sqrt(aL)/z)**2,4*aQ/z**2)
152     x_min_H_t = max((1+np.sqrt(aQ)/z)**2,(np.sqrt(aQ)/z+np.sqrt(aL)/z)**2)
153     x_min_A_1 = max((1+np.sqrt(aL)/z)**2,(np.sqrt(aH)/z+np.sqrt(aW)/z)**2)
154     x_min_A_2 = max((np.sqrt(aL)/z+np.sqrt(aH)/z)**2,(1+np.sqrt(aW)/z)**2)
155     x_min_A_3 = max((np.sqrt(aW)/z+np.sqrt(aL)/z)**2,(1+np.sqrt(aH)/z)**2)
156
157     ScatterRate_H_s = lambda z : abs(quad(Integrand_H_s, x_min_H_s, np.inf,
        ↪ args=(z,1))[0])#,epsabs=1E-28,epsrel=1E-16)[0])
158     ScatterRate_H_t = lambda z : abs(quad(Integrand_H_t, x_min_H_t, np.inf,
        ↪ args=(z,1))[0])#,epsabs=1E-28,epsrel=1E-16)[0])
```

```
159     ScatterRate_A_1 = lambda z : abs(quad(Integrand_A_1, x_min_A_1, np.inf,
            ↪  args=(z,1))[0])#,epsabs=1E-28,epsrel=1E-16)[0])
160     ScatterRate_A_2 = lambda z : abs(quad(Integrand_A_2, x_min_A_2, np.inf,
            ↪  args=(z,1))[0])#,epsabs=1E-28,epsrel=1E-16)[0])
161     ScatterRate_A_3 = lambda z : abs(quad(Integrand_A_3, x_min_A_3, np.inf,
            ↪  args=(z,1))[0])#,epsabs=1E-28,epsrel=1E-16)[0])
162     DecayRate = lambda z : gammaD(1,z,1)
163
164     if Yeq(z)==0.0:
165         print('setting dY/dz = 0, as Yeq('+str(round(z,5))+') = 0')
166         return 0
167     else:
168         dYdz = -z**3 *xi(z,m,Ynu)*(ScatterRate_H_s(z) + 2*ScatterRate_H_t(z)
                ↪  + ScatterRate_A_1(z) + ScatterRate_A_2(z) +
                ↪  ScatterRate_A_1(z) +32.*np.pi**4 *z/m *DecayRate(z)) *
                ↪  (Y*np.nan_to_num(1/Yeq(z)) - 1)
169     return dYdz
170
171 # ====================================================================
172 #        SOLVE THE BOLTZMANN EQ. OR MAKE A PARAMETER PLOT
173 # ====================================================================
174
175 def Yield(m,Ynu):
176   start_time = time.time()
177   sol = odeint(Boltzmann_N_RH,Yeq(3),z,args=(m,Ynu),atol=1.E-36)#
          ↪  rtol=1.E-23,
178   computing_time = time.time() - start_time
179   print("--- %s seconds ---" % (time.time() - start_time))
180   #return np.concatenate(np.array([m,Ynu,Omegah2(sol[-1,0],m)]),sol[:,0]))
181   #print("--- final yield: %s ---" % (sol[-1,0])
182   return sol[:,0]
183
184 ###        MAKE A PLOT of the comoving density
185
186 def plotYield(z,m,Ynu,sol,save=False,name='Yield_plot.pdf'):
187
188   fig = plt.figure(0)
189   ax0 = plt.subplot(111)
190
191   plt.loglog(z,Yeq(z),label='equilibrium',linestyle='--')
192   plt.loglog(z,sol,label=r'$\nu_R$, $m_R = $'+'{:.1e}'.format(m)+r' GeV,
          ↪  $Y_\nu = $ '+'{:.1e}'.format(Ynu))
193
194   ax0.set_xlim(z[0],z[-1])
195   ax0.set_ylim(1E-18,1E0)
```

```
196
197   ax0.grid(ls='--', dashes=(3,3))
198   ax0.legend()#loc='center right', bbox_to_anchor=(1.0, 0.5))
199   #fig.subplots_adjust(right=.6)
200
201   ax0.set_xlabel(r'$z = m_R/T$')
202   ax0.set_ylabel('Comoving density  '+r'$Y_{\nu_R}$')
203   ax0.text(1.2E2,1.E-12,r'$\Omega_{\nu_R}\,h^2 =$
          ↪  '+str(round(Omegah2(sol[-1],m), 3)))
204
205   plt.tight_layout()
206   if save == True:
207       plt.savefig(path+name)
208   plt.show()
209   return
210
211 # ======================================================================
212 #        MAKE A PARAMETER PLOT after solving many times the Boltzmann eqn.
213 # ======================================================================
214
215 def ParamScan(m,Ynu,Omegah2,save=False):
216     fig, ax1 = plt.subplots()
217
218     cmap = plt.get_cmap('plasma_r')
219     levels = MaxNLocator(nbins=18).tick_values(0.01, 1.2e-1)
220
221     ax1.set_xscale('log')
222     ax1.set_yscale('log')
223     #ax1.set_xlim(1.e4,4.e4)
224     ax1.set_ylim(1.e-7,4.e-3)
225     ax1.set_xlabel(r'$m_R/$GeV')
226     ax1.set_ylabel(r'$Y_\nu$')
227     ax1.set_title('Relic abundance '+r'$\Omega_{\nu_R} \, h^2$')
228     ax1.text(3.e3,3.e-6,'Overproduction')
229     ax1.text(0.5e1,3.e-4,'Underproduction')
230     ax1.grid(ls='--', dashes=(1,1))
231
232     cf = ax1.contourf(m,Ynu,Omegah2, levels=levels,cmap=cmap)
233     cbar = fig.colorbar(cf)
234
235     # bellow this line, generation of active neutrino masses are possible
236     #plt.loglog(m,7.e-8 * m**(0.5),'-k')
237
238     plt.tight_layout
239     if save == True:
```

```
240         plt.savefig('RN-nu-Param-scan-plasma.pdf')
241     plt.show()
242 
243     return
244 
245 # ======================================================================
246 # Identify individual solutions and parameters from the parameter plot
247 # ======================================================================
248 
249 def GetParamIndex(data,mApprox,Yapprox):
250     new_data = data.reshape(10000,1,603)
251     Indexes = []
252     for i in range(10000):
253         if new_data[i,0,0] >= mApprox and new_data[i,0,0] <=
            ↪  10**(np.log10(mApprox)+0.06):
254             if new_data[i,0,1] >= Yapprox and new_data[i,0,1] <=
                ↪  10**(np.log10(Yapprox)+0.05):
255                 Indexes.append(i)
256                 print(i)
257     if len(Indexes)>1:
258         print('**** many solutions in range ****')
259     else:
260         return np.array(new_data[Indexes[0],0,:])
261 
262 def readData(path):
263     return np.load(path)
264 
265 def prepareData(data):
266     data = data.reshape(100,100,603)
267     for i in range(100):
268         for j in range(100):
269             if data[i,j,2]<1.e-8:
270                 data[i,j,2] = None # extract divergent/unstable solutions
271     return data
272 
273 path =
    ↪  '/Users/charlie/ownCloud/MPIK/00_Masterarbeit/computations/Boltzmann-eqn-python/'
274 data = readData(path+'RH_freeze-out-v2.npy')
275 data = prepareData(data)
276 ParamScan(data[:,:,0],data[:,:,1],data[:,:,2],save=False)
277 
278 z1 = np.logspace(0,0.8,100)
279 z2 = np.logspace(0.81,1.5,400)
280 z3 = np.logspace(1.51,3,100)
281 z = np.concatenate((z1,z2,z3))
```

```
282
283 #over = GetParamIndex(data,1e2,1e-5)
284 #under = GetParamIndex(data,1.e1,1e-5)
285 right = GetParamIndex(data,1.3e3,1.1e-4)
286 #
287 #plotYield(z,over[0],over[1],over[3:],True,'overproduction_badly.pdf')
288 #plotYield(z,under[0],under[1],under[3:],False,'underproduction.pdf')
289 plotYield(z,right[0],right[1],right[3:],False,'freeze-out-production.pdf')
```

Aknowledgements

First and foremost, I want to thank Prof. Dr. Dr. h.c. Manfred Lindner, Prof. Dr. Thomas Schwetz-Mangold and Dr. Werner Rodejohann for giving me the opportunity to work under their supervision on one of the most interesting topics in theoretical physics. Prof. Schwetz-Mangolds lectures on dark matter at the Karlsruhe Institute of Technology triggered my fascination for the research in this field. My time at the Max-Planck Institute for Nuclear Physics has been truly wonderful and remarkable. The contact with world class scientists and students at the institute has been inspiring. Prof. Lindner and Dr. Rodejohann were excellent scientific mentors, who always had the ability to steer me in the right direction even in difficult times. I sincerely thank Prof. Lindner for the opportunity to continue doing research as a member of his group and look forward to the coming years.

A special thanks goes to Dr. Moritz Platscher and Thomas Rink, whose scientific support and help in times of despair were essential to the completion of this thesis, but also to my colleagues Christian Döring, Ingolf Bischer and Thomas Hugle for many fruitful discussion not only about physics, but also about the rewards of a scientific career and the dangers of communism.

I also thank Dr. Stefan Vogl and PD Dr. Giorgio Arcadi for their availability to answer quick questions and provide me with useful literature references.

I thank Julia Schäfer, who has been with me since the very beginning of my journey through physics and whose support is largely responsible for any accomplishment I might have achieved. And finally, I thank my parents in Ecuador; thank you for everything.